Charles University in Prague

Faculty of Mathematics and Physics

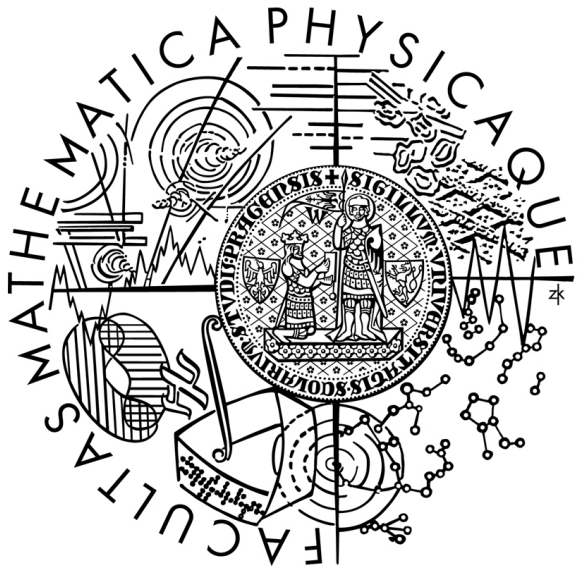

Doctoral Thesis

Neutron diffraction studies of martensitic transformation and deformation processes in shape memory alloys

Peter Molnár

Supervisor: Prof. RNDr. Vladimír Sechovský DrSc.
Consultants: RNDr. Petr Šittner CSc., RNDr. Petr Lukáš CSc.,
RNDr. Václav Novák CSc.

Branch: F3 – Physics of condensed matter and material research

Prague, 2008

Contents

Motivation

Shape memory alloys (SMA) belong to a class of so-called functional materials. These materials are more important for what they do than for what they are. The unique functional properties of SMAs are basically nonlinear stress-strain-temperature hysteretic responses originating from reversible martensitic transformation (MT) in solid state. The product phase of the martensitic transformation - martensite - contains large number of twin interfaces which, in particular case of SMAs, can easily move under the variation of applied stress, temperature or magnetic field and bring about reversible strain changes. From the microstructural point of view, the twin interfaces separate regions of different orientation but same crystal structure (martensitic variant). In addition to twin interface, there exist also interfaces separating the austenite and martensite phases and between various martensitic phases which are highly mobile as well. The structure, properties and mobility of all mentioned interfaces are of essential importance for the functional properties of SMAs - shape memory effects. While the austenite-martensite interfaces have already been thoroughly investigated in the literature and their properties are known for most of currently developed SMAs, much less is known about the intramartensitic twin interfaces. Though it has been evident for sometime that much more experimental data on twin interfaces are needed in order to further develop SMAs, SMA models and engineering applications, such data are scarce in the literature due to the experimental difficulties with preparation of good martensite single crystals.

In order to evaluate the elementary properties of martensitic phases and twin interfaces of different shape memory alloys, single crystalline samples in martensitic state are indispensable. A technology to prepare them has been developed at IP ASCR. However, there was no method allowing for inspection of the quality of such prepared martensite single crystal (meaning to identify which martensitic variant exist in the sample and whether the crystal is indeed interface free). Such experimental method must be a non-interfering method and must provide integral structural sensitive information over bulk volume of ~1cm^3. Single crystal neutron diffraction is in principle capable of that, but no such method has existed before.

The goal of this thesis was to develop such single crystal neutron diffraction method for characterization of the quality of martensite single crystals and in-situ investigation of twinning processes in the martensite phase. The method was developed using CuAlNi single crystals as a model material, for which production of good quality martensite crystals was

already mastered and later applied to NiMnGa and CoNiAl single crystals, which are currently of application interest as magnetic shape memory alloy actuators.

Acknowledgements

I would like to express my gratitude to my supervisor Prof. Vladimír Sechovský for his help and encouragement during my PhD study. I am also thankful to my consultants Dr. Petr Šittner and Dr. Václav Novák for their advice, ideas and comments to my work during my stay at Institute of Physics in Prague. I would also thank them for the intensive discussion about the shape memory alloys. Moreover, I would like to express my thanks to my consultant Dr. Petr Lukáš from Nuclear Physics Institute in Řež, who introduced me to the field of neutron diffraction and for his advice and comments during my work.

I also would like to thank to whole team of scientific workers of the Department of neutron physics in Řež. Many thanks also to the technicians Mr. Pavel Hyka and Mrs. Božena Michalcová.

I would like to thank to Miroslav Vrána from the Nuclear Physics Institute in Řež for the intensive discussion during my work.

I also would like to thank to whole team of scientific workers of the Department of Metals at Institute of Physics and, first of all to Prof. Pavel Lejček. Many thanks also to the technicians Mr. Vladimir Novák and Ing. Jaroslav Bradler.

I would like to thank to Doc. Pavel Svoboda from Charles University for the help and discussion about single crystal neutron diffraction.

1. Shape memory effects and martensitic transformation

The term “shape memory” describes the unusual ability to remember shape, which can be initiated in certain materials thermally, mechanically or magnetically. Even after heavy deformation, materials with shape memory are able to recover a previously memorized shape [1]. This phenomenon was first found in Au-47.5 at % Cd alloy in 1951 [2]. The real importance of the shape memory effect has become obvious only since its discovery in a NiTi alloy [3]. Nowadays the most important materials of commercial significance with shape memory properties can be classified either as metal alloys or as polymers. Furthermore, there are ceramics and biological systems in which shape memory properties are observed as well [1]. Table 1.1 lists a number of alloy systems, which possess shape memory effect.

Table 1.1: Shape memory alloy systems

Alloy	Composition [at%]	Temperature hysteresis [K]	Structure change
Ag-Cd	44 – 49Cd	15	B2-2H
Cu-Zn-X (X=Al, Si, Sn, Ga)	38,5-41,5Zn few at%X	<10	B2-9R, B2-M9R DO_3 –18R, DO_3-M18R
Cu-Al-Ni	13,5-14,5Al 3-4,5Ni	35	DO_3-2H
Ni-Ti	49 – 51 Ni	30 1-2	B2 – monoclinic B2 - rhombohedral
Ni-Al	36-38 Al	10	B2 – 3R
Ni-Mn-Ga	49.7 Ni 29.3 Mn 21Ga	10	$L2_1$ – 5M tetragonal
Fe-Pd	~30 Pd	Small	$L1_2$ – ordered BCT

Underlying mechanism of shape memory effect is crystallographically reversible *martensitic transformation* between *austenite* (high-temperature phase, usually cubic symmetry) and *martensite* (a low-temperature phase with lower symmetry). Martensitic transformation is a first-order, difussionless, solid to solid phase transformation. The change of the structure is diffusionless it means that there is no rearrangement of atoms and one can obtain one structure from a deformation of the other [4].

Martensitic transformation is associated with hysteresis. As a consequence, four temperatures are generally required for characterization. Transformation to austenite begins at the austenite

start temperature – A_S and ends at the austenite finish temperature – A_f. Accordingly, transformation into martensite begins at the martensite start temperature – M_S and finishes at the temperature M_f. Since the austenite has the higher symmetry than the martensitic phase, multiple formation of martensite with the same structure in different orientation is possible. These are called variants of martensite. The two neighboring variants of martensite are twin related to each other and may contribute to deformation if the interface is mobile under external force (stress, magnetic field) [5]. The number of the variants of martensite depends on the symmetry of the martensitic phase and it starts from three for tetragonal martensite, six for orthorhombic martensite, twelve for monoclinic martensite, etc. (see chapter 2.5).

The key effects of shape memory alloys associated with martensitic transformation are: one-way shape memory effect, two-way shape memory effect, pseudoelasticity and pseudoplasticity. They are explained in more details in next paragraphs.

1.1 One-way shape memory effect

If shape memory alloy is deformed in its lower temperature form (martensite), it will return to its original shape when heated above the temperature A_f. This process is known as the *one – way shape memory effect*, because the shape change occurs only upon heating. If the shape recovery during reverse transformation to austenite is hindered, high forces occur that can be used to perfom work. This is the basis of SMA actuators [1]. The changes of the microstructure during the one-way shape memory effect are schematically shown in Fig.1.1. The parent austenitic phase will transform upon cooling to multiple martensitic lattice correspondence variants (same martensitic structure but different orientation with respect to austenite lattice) shown in blue and yellow in Fig. 1.1 [6].

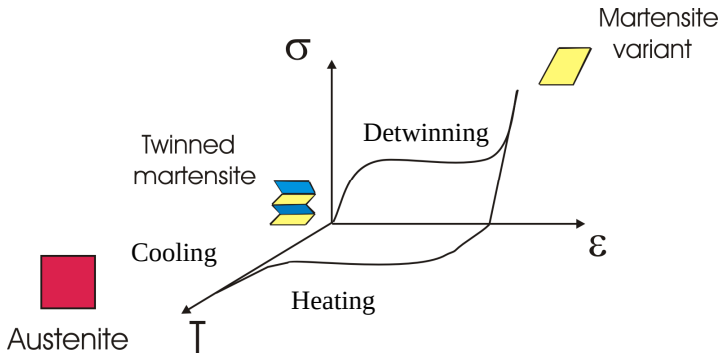

Fig. 1.1: Microscopic changes during the shape memory effect.

The stress-free cooling of austenite produces a complex arrangement of several variants of martensite in such a way that the final macroscopic strain equals zero for the polycrystalline sample without texture. This is called the *self-accommodation*. SMA sample have the same shape as in austenite but now it contains twin interfaces, which separate individual martensitic variants. These twin interfaces can move under the different values (0.1 MPa up to 100 MPa) of the applied stress (stress plateau) and the large deformations can be produced. Martensitic variant, which gives the largest transformation strain with respect to the applied stress is produced (in our case the yellow one in Fig. 1.1). After unloading there is no change of the shape of the sample. Upon heating the reverse martensitic transformation occurs and the original shape of the sample is recovered (sample recovers back to the austenitic structure).

1.2 Pseudoelasticity

The pseudoelastic behavior is observed during loading and unloading above A_f temperature. Three distinct stages are observed on the uniaxial stress-strain curve representing the pseudoelastic behaviour of SMA (Fig. 1.2).

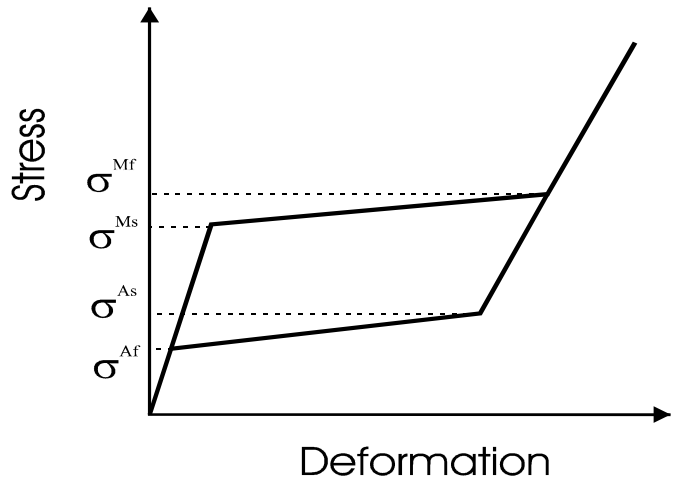

Fig. 1.2: Pseudoelastic behavior of shape memory alloy

For stresses below σ^{Ms}, the material behaves in a purely elastic way. As soon as the critical stress is reached, forward transformation (austenite to martensite) initiates and *stress-induced martensite* starts forming. During the formation of stress induced martensite large transformation strains are generated (upper plateau of stress-strain curve in Fig. 1.2). When the applied stress reaches the σ^{Mf} the forward transformation is completed and the SMA is in the martensitic phase. For further loading above σ^{Mf} the elastic deformation of martensite is

observed. Upon unloading, the reverse transformation initiates at a stress σ^{As} and completes at a stress σ^{Af}. Increasing the test temperature results in an increase of the values of critical transformation stresses. This is well described by the Clausius-Clapeyron equation (see section 3).

Reversible deformation which can be obtained due to the pseudoelastic behavior of the shape memory alloys is in the range of ~8%. The classical metallic material e.g. steel has approximately 0.2% of the elastic deformation.

For the stress-induced formation of martensite there is an upper temperature limit, M_d, above which irreversible processes such as formation of dislocations and slipping are thermodynamically favored [1]. Between the M_d and A_f there is so called pseudoelastic window. Above M_d, SMAs behave like conventional materials with elastic strain characteristic and subsequent plasticity up to the fracture.

1.3 Pseudoplasticity

Deforming the SMA material in martensitic state will deform easily in the range of 8 %. At the end of the plateau the sample is mainly in martensitic variant (M_T), which is the favorable one with respect to the applied tension stress direction. Behind this plateau and during the unloading the elastic deformation of martensite occurs.

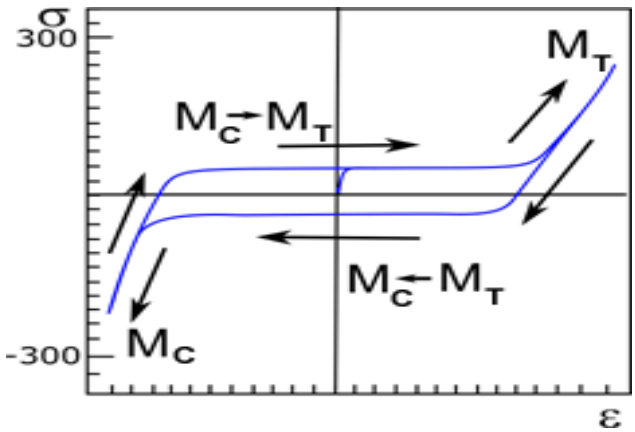

Fig. 1.3: Pseudoplastic behaviour of SMA

Applying the compressive deformation on such a sample in martensitic variant M_T will leads to the twin boundary movements and at the end of the plateau different martensitic variant (M_C) is created, which gives the largest transformation strain with respect to applied compressive stress. In such a way by applying the tensile deformation and then the compressive deformation we can observe the large deformations (shape changes). During the compressive or tensile deformation the dislocations do not move, only twin interfaces move.

After heating such a martensitic sample in one martensitic variant the reverse martensitic transformation occurs, the strain is recovered and the material returns to its original shape and structure (cubic austenite).

1.4 Two-way shape memory effect

Shape memory alloys can be trained to memorize two configurations in both the martensitic state and austenitic state. This phenomenon is known as the *two-way shape memory effect (TWSME)* [2]. It means that the shape change occurs upon heating and upon cooling, without application of external stress. The amount of this shape change is always significantly less than obtained with one-way shape memory effect. The reason why specimen remembers the martensitic state is in the introduction of dislocations, which stabilize the configuration of martensites [7]. These dislocations exist even in the parent phase after reverse transformation upon heating, and the stress field around them induces particular martensitic variants upon cooling. There are several thermomechanical treatments, such as the introduction of plastic deformation, constraint ageing, thermal cycling, utilization of precipitation etc., which results to the development of TWSME.

2. Crystallography of shape memory alloys

2.1 Crystal structures of austenite

Typical shape memory alloys as CuAlNi, CuZnAl, are ordered intermetallic alloys. They are thermodynamically metastable at room temperature and have to be quenched from the high temperature regions of phase stability to achieve optimum properties. The atomic order is essential for the necessary resistance of the crystal lattice again dislocation glide as well for the shape memory effect itself [2].

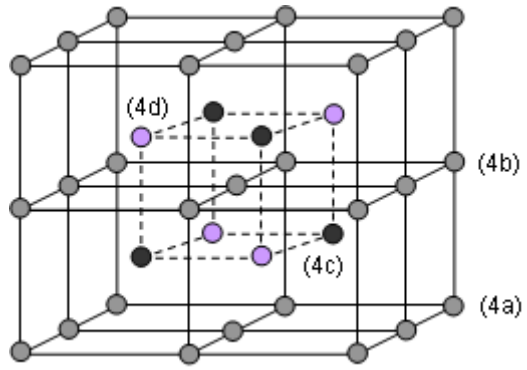

occ (4a) = occ (4b)
= occ (4c) = occ (4d) : 2A structure
= occ (4c) ≠ occ (4d) : DO_3 structure
≠ occ (4c) = occ (4d) : B_2 structure
≠ occ (4c) ≠ occ (4d) : and also
occ (4a) ≠ occ (4d) : $L2_1$ structure

Fig. 2.1: Possible site ordering of Cu – based shape memory alloys

Atomic arrangement of Cu – based shape memory alloys varies between A2, B2, DO_3 or $L2_1$ structures upon cooling (Fig. 2.1). All these structures originate from high temperature parent disordered bcc structure (A2) in which all sites have the same population. By cooling the site reordering usually occurs. If the population becomes the same for all Wyckoff positions except (4d), the structure is ordered DO_3 (Fe_3Al type). If the populations of both (4c) and (4d) positions are different, the structure is $L2_1$ (Cu_2MnAl type, Heusler). In the case when the population of (4c) equals the population of (4d) but differs from the population of (4a) and (4b) which remains equal, then the structure becomes B2 (CsCl type) and effectively the dimensions of the unit cell are halved.

2.2 Closed – packed layered structures of Cu-based martensites

Among many structural changes in various martensitic transformations, those in β alloys (Cu-Al-Ni, Cu-Zn-Al, etc.) are important. Other important phases in phase diagram are α and γ phases. The ordered BCC structures (austenite) of β phase are usually B2 type or DO_3 type. With lowering temperature this BCC ordered structures change martensitically into closed-packed structures, which are called long period stacking order structures [2]. The closed packed layer is transformed from a $\{110\}_{BCC}$ plane, that is, the transformation shear plane [8]. For shear direction there are two possibilities, $\pm[1\bar{1}0]$, on each plane. In the case that plus and minus shears occur periodically, this is referred to as *shuffling*.

The structure of B2 type parent phase is shown in Fig. 2.2a this structure may be viewed as that in which the $(110)_{B2}$ plane is stacked in $A_1B_1A_1B_1$ … order, as shown in Fig. 2.2b [2]. Upon martensitic transformation, the $(110)_{B2}$ plane changes into a more close-packed plane $(001)_M$ in Fig. 2.2c, by contracting along $[001]_{B2}$, and elongating along $[\bar{1}10]_{B2}$, so that the indicated angle changes from 70.32° to close to 60°. Once the plane becomes a close-packed one as shown in Fig. 2.2c, we have three stacking positions A, B, C shown in Fig. 2.2c along the *a* - axis of the martensite. Then we can create various stacking order structures.

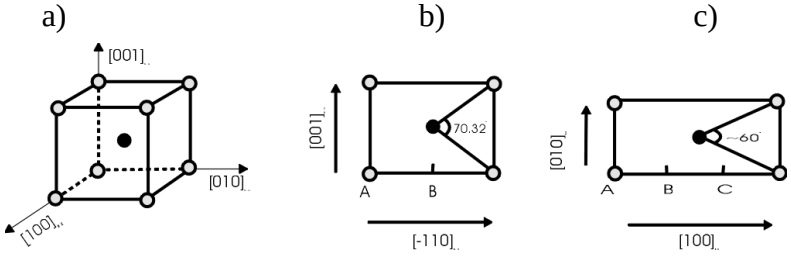

Fig. 2.2: Atomic arrangement in B2 type parent phase (b) and close-packed plane in martensite (c).

Otsuka [2] observed various martensites ($\gamma`_1$(2H), $\beta`_1$(9R), $\alpha`_1$(6R)…) during stress-induced transformation in Cu-Al-Ni single crystal alloy. The examples of two of them are shown in Fig. 2.3. Using the Ramsdel notation [9] the 2H $\gamma`_1$ martensite means that the period along the c-axis is 2, and the symmetry is hexagonal, when ordering is disregarded. In the case of the $\beta`_1$ martensite the 9R structure is observed, it means that one period contains 9 layers and the symmetry is rhomhohedral when ordering is disregarded.

The structures determined by the diffraction techniques shows the long period stacking order but the intensity distribution did not fit to the above schemes [10]. Tadaki [11] found that the $\beta`_1$ martensite is monoclinic and that the monoclinicity originates from the displacement of the stacking positions from the ideal a/3 positions.

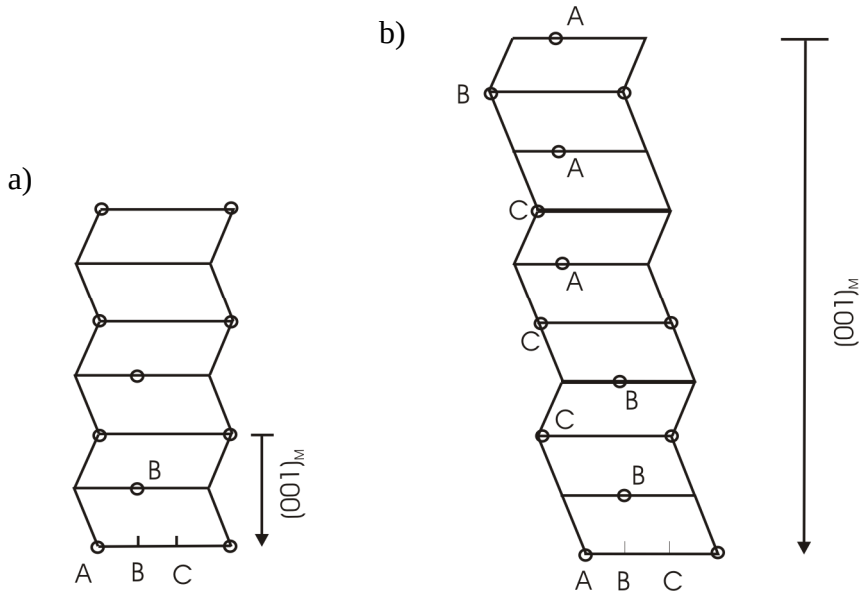

Fig. 2.3: Close-packed layered structures of 2H $\gamma`_1$ martensite (a) and 9R $\beta`_1$ martensite (b)

Ye et al [12] studied the structure of $\gamma`_1$ martensite and they came with the orthorhombic structure. Because the basal plane is a close-packed plane it may be expected that the second layer sits at the center of the triangular atom configuration, *i.e.* the a/3 position. However, Ye et al found that there were considerable atom displacements from the ideal position. They used Tadaki`s model to explain this displacements and from the least squares refinements they concluded that the structure is orthorhombic.

2.3 Lattice correspondence and lattice correspondence variant of martensite

Since the martensitic transformation occurs diffusionlessly, the lattice of the parent phase deform to that of the martensite phase maintaining one-to-one correspondence called a lattice correspondence. *Lattice correspondence* means that any vector x_0 (u_0, v_0, w_0) in the parent

phase has the following correspondence with vector *x (u, v, w)* in the martensite phase, although the length of the vector x_0 is different from that of the vector *x* according to the lattice distortion associated with the transformation [13].

The coordinate transformation $x_0 \rightarrow x$ is described by the transformation matrix ***R*** with dimensions 3x3:

$$\mathbf{x = R^{-1}. x_0} \qquad (1)$$

where *x* and x_0 are the coordinate vectors in new (martensite) and old system (austenite), respectively.

Miller indexes of planes in the new *(H,K,L)* and old system *(h,k,l)* transform according the formula:

$$\mathbf{(H, K, L) = R^{T} . (h, k, l)} \qquad (2)$$

From the difference of crystal symmetry between the parent phase-austenite (cubic structure DO_3) and product phase-martensite (orthorhombic structure 2H) there are six martensite lattices which can be formed from DO_3 crystal lattice. It means that *a, b, c* axes in the 2H lattice can originate from six different crystal directions in the DO_3 lattice. Each such a correspondence is called *lattice correspondence variant (LCV).* The number of lattice correspondence variants corresponds to the number of the lattice correspondences. Schematic example of one lattice correspondence variant for CuAlNi shape memory alloy is depicted in Fig. 2.4.

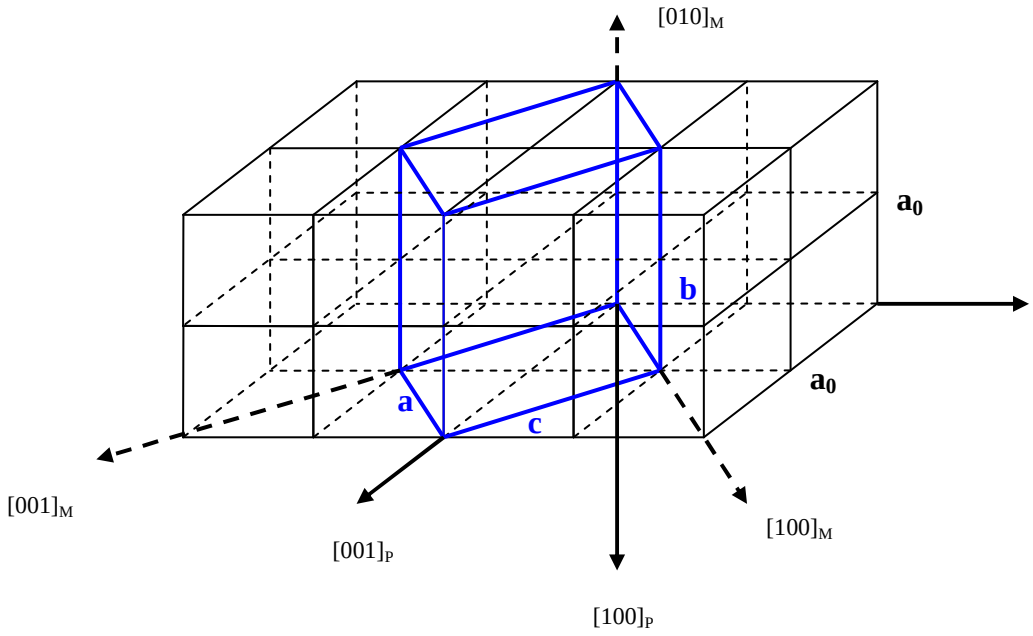

Fig. 2.4: Crystal structure of parent phase DO_3 structure showing a lattice correspondence between parent phase (***P***) and martensite (***M***).

Lattice correspondences for Cu-Al-Ni shape memory alloy are shown in Table 2.1.

Table 2.1: Lattice correspondence between cubic (austenite) and orthorhombic (martensite) lattices in Cu-Al-Ni.

Martensitic variant	**[100]m**	**[010]m**	**[001]m**
1	$\frac{1}{2}[011]_A$	$[\bar{1}00]_A$	$\frac{1}{2}[0\bar{1}1]_A$
2	$\frac{1}{2}[0\bar{1}1]_A$	$[100]_A$	$\frac{1}{2}[0\bar{1}\bar{1}]_A$
3	$\frac{1}{2}[101]_A$	$[0\bar{1}0]_A$	$\frac{1}{2}[10\bar{1}]_A$
4	$\frac{1}{2}[10\bar{1}]_A$	$[010]_A$	$\frac{1}{2}[\bar{1}0\bar{1}]_A$
5	$\frac{1}{2}[110]_A$	$[00\bar{1}]_A$	$\frac{1}{2}[\bar{1}10]_A$
6	$\frac{1}{2}[\bar{1}10]_A$	$[001]_A$	$\frac{1}{2}[\bar{1}\bar{1}0]_A$

2.4 Martensitic transformation and transformation matrix

The transformation from the austenite lattice to the martensite lattice can be described as a deformation because there is no diffusion. For lattice correspondence variant depicted on Fig. 2.4 we can express the lattice distortion ***B*** in the coordinate system of the martensite lattice by the following matrix when the structure of the martensite is tetragonal or orthorhombic [13]:

$$B=\begin{pmatrix} \alpha & 0 & 0 \\ 0 & \beta & 0 \\ 0 & 0 & \gamma \end{pmatrix} \qquad (3)$$

Where $\alpha=(\sqrt{2}\,a)/a_0$, $\beta=b/a_0$, $\gamma=(\sqrt{2}\,c)/a_0$ are the strain components of the lattice distortion along the crystal axes of the martensite phase, and the *a*, *b*, *c* are the lattice constants of the martensite and a_0 is lattice constant of cubic austenite.

In order to consider the deformation $\boldsymbol{U_1}$ in the coordinate system of the parent lattice, it is necessary to introduce the coordinate transformation ***R*** from the coordinate system of the martensite lattice to that of the parent lattice. $\boldsymbol{U_1}$ is expressed in the following equation:

$$\mathbf{U_1=RBR^T} \qquad (4)$$

where $\boldsymbol{R^T}$ is the transpose of ***R***.

According to the first lattice correspondence from Table 2.1 the coordinate transformation $\boldsymbol{R}$ and its transpose $\boldsymbol{R^T}$ is expressed as follows:

$$R= \begin{pmatrix} 0 & -1 & 0 \\ \frac{1}{\sqrt{2}} & 0 & \frac{-1}{\sqrt{2}} \\ \frac{1}{\sqrt{2}} & 0 & \frac{1}{\sqrt{2}} \end{pmatrix} \qquad (5)$$

$$R^T= \begin{pmatrix} 0 & \frac{1}{\sqrt{2}} & \frac{1}{\sqrt{2}} \\ -1 & 0 & 0 \\ 0 & \frac{-1}{\sqrt{2}} & \frac{1}{\sqrt{2}} \end{pmatrix} \qquad (6)$$

Than the $\boldsymbol{U_1}$ is expressed as:

$$U_1= RBR^T = \begin{pmatrix} \frac{-b}{a_0} & 0 & 0 \\ 0 & \frac{a+c}{\sqrt{2}\,a_0} & \frac{a-c}{\sqrt{2}\,a_0} \\ 0 & \frac{a-c}{\sqrt{2}\,a_0} & \frac{a+c}{\sqrt{2}\,a_0} \end{pmatrix} \qquad (7)$$

$\boldsymbol{U_1}$ represents the homogeneous deformation that takes the lattice of the austenite to that of the martensite. This is called the *Bain matrix* or the *transformation matrix*. $\boldsymbol{U_1}$ is transformation matrix for the first lattice correspondence variant of orthorhombic martensite (table 2.1) depicted in Fig. 2.4. We have six such a transformation matrices for every lattice correspondence variant of orthorhombic martensite, see appendix 1.

2.5 General consideration for creation of martensite variants

In genereal, the way how the lattice correspondence variants are created can be explained as follows [4]. We rotate the austenite lattice through rotation $\boldsymbol{Q}$ in its point group P_a and then transform it. This gives us a lattice correspondence variant of martensite. The transformation matrix of this lattice correspondence variant is $\boldsymbol{QU_1Q^T}$. Doing this for all rotations $\boldsymbol{Q}$ in P_a we

obtain all the different lattice correspondence variants of martensite. However for some rotations $\boldsymbol{Q}$ in P_a, it may turn out that $\boldsymbol{QU_1Q^T=U_1}$. This happens if $\boldsymbol{Q}$ is also in the point group of the martensite P_m. In such a case we do not obtain a different lattice correspondence variant. Thus the number ($\boldsymbol{N}$) of lattice correspondence variants of martensite is:

$$\boldsymbol{N} = \frac{\text{the number of rotations in } P_a}{\text{the number of rotations in } P_m}$$

In the example of the cubic to orthorhombic transformation, $\boldsymbol{N}$ = 24/4 = 6. Point groups of the seven symmetry types and rotations $\boldsymbol{Q}$ are listed in [4].

2.6 The phenomenological theory of martensitic transformation

The basis of the phenomenological theory of the crystallography of martensitic transformation is that the overall macroscopic strain associated with the transformed region (the shape strain) must be an invariant plane (a strain which leaves one particular plane in the two phases undistorted and unrotated) [14]. Such a particular plane which is common for parent phase and martensite is called *habit plane*. The existence of the habit plane is a characteristic of the first order transformation, which occurs by nucleation and following growth of transformed area.

The phenomenological theory of the crystallography of the martensitic transformation was developed by Wechsler, Lieberman and Read (W-L-R) [15, 16].

In more mathematical term, to ensure that the shape strain is an invariant plane strain, one of its principal strains must be zero and the other two must be of opposite sign. In general, the strain required to convert the crystal structure of the parent phase to that of the martensite (the Bain strain *B*) will not satisfy these conditions. Bain strain is not itself an invariant plane strain. Hence, in order to ensure that the final, overall strain, is an invariant plane strain, another strain is required. This strain must not alter the crystal structure of the new product phase resulting from the Bain strain *B*, but it must change the shape of the transformed volume in such a way that it satisfies the conditions for an invariant plane strain. This additional strain *P* is known as the lattice invariant shear (*LIS*). It is inhomogeneous on macroscopic scale, but has no effect on the crystal structure on a microscopic or atomic scale – it is lattice invariant. Typical examples of a lattice invariant shear are slip and twinning, both which leave the structure of the crystalline material subjected to shears unaltered. In the

thermoelastic martensitic transformation in many shape memory alloys, the lattice invariant shear is twinning deformation by introducing twin planes, which move easily upon loading and disappear after reverse transformation.

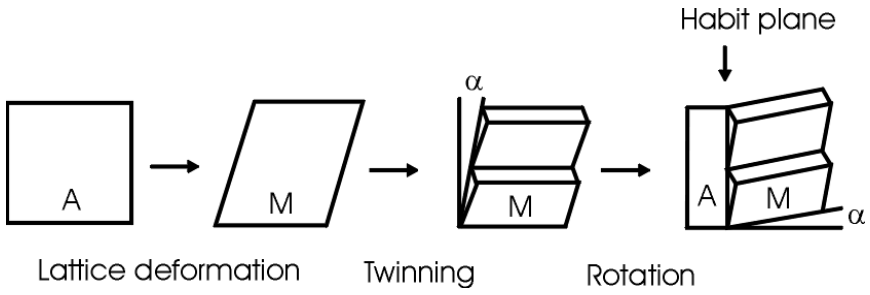

Fig. 2.5: Two - dimensional schematic diagram of processes during the martensitic transformation

Finally, after combining the Bain strain *B* and the lattice invariant shear *P*, a rotation *R* will be required to ensure that the undistorted plane is also unrotated (Fig. 2.5).

Thus, the shape strain (total strain) associated with the transformation is written in the following matrix form [2]:

$$P_1 = RP_2B \qquad (8)$$

where B is the lattice deformation matrix, P_2 lattice invariant shear and R a lattice rotation matrix. When equation (8) is solved for an invariant plane strain, P_1 becomes

$$P_1 = I + m_1 d_1 p^T_1 \qquad (9)$$

where, d_1 : a unit column vector in the direction of the shape strain

I: the (3x3) identity matrix

m_1: the magnitude of the shape strain

p^T_1: a unit row vector in the direction normal to the invariant plane, see Fig. 2.6.

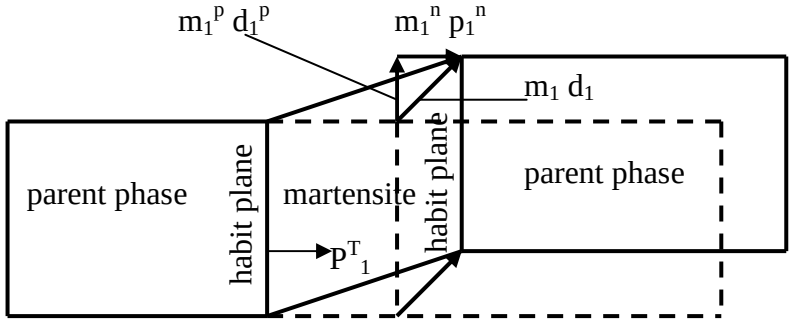

Fig. 2.6: Schematic illustration of the martensitic transformation, where m_1 is the magnitude of the shape strain, d_1 is a unit vector in the direction of the shape strain, and $p`_1$ is a unit vector in the direction normal to habit plane.

The inputs required by the phenomenological theory are:

1. The lattice parameter of parent phase and martensite
2. The lattice correspondence between parent phase and martensite
3. The lattice invariant shear

By giving only three input data, we can calculate all crystallographic parameters, such as habit plane, orientation relationship between the parent and product phase, shape strain and twin width ratio.

2.7 Twinning as a lattice invariant shear

In shape memory alloys the lattice invariant shear is twinning. *Twinning* is said to be any region of a parent phase, which has undergone a homogeneous shear to give a reoriented region with the same crystal structure. Two twin crystals are generally related by a symmetry operation with respect to a mirror plane or a rotation axis. A description of twins are characterized by five crystallographic elements: K_1 – twinning plane, η_1 - twinning shear direction, K_2 – another undistorted plane, η_2 - intersection of K_2 and the plane of shear, s – magnitude of twinning shear. K_1 and η_2, or K_2 and η_1 are sufficient to determine twinning completely [2]. All crystallographic elements are schematically shown in Fig. 2.7. The open circles are the lattice points before the shear while the filled circles are the lattice points after the shear. Further, the dashed line shows two unit cells of the original lattice before the shear while the solid line indicates a unit cell for each of the lattices after the shear [17].

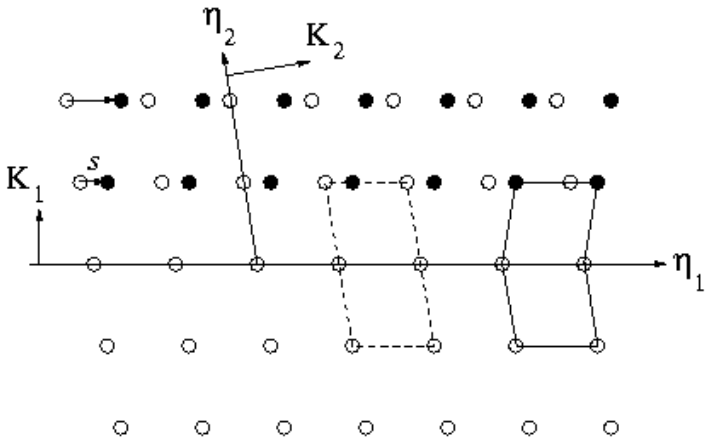

Fig. 2.7: Schematic view of twinning and twinning elements K_1, η_2, K_2 and η_1.

In order to create the twin by the shearing process the original lattice must be restored by this process. To satisfy the condition there are two cases. In case I, two lattice vectors lie on the K_1 plane, and the third lattice vector is parallel to the η_2 direction. In this case K_1 and η_2 are represented by rational indices, and the two crystals are related by mirror symmetry with respect to K_1 plane. This is called *type I twinning*. In case II, two lattice vectors lie on the K_2 plane, and the third lattice vector is parallel to the η_1 direction. In this case, K_2 and $\eta_1$are represented by rational indices, K_1 and η_2 being irrational, and the two twins are related by the rotation by π around the η_1 axis. This is called *type II twinning*. In some crystal systems K_1, η_2, K_2 and η_1 may all become rational indices. This is called *compound twinning* and the two twin crystals have both symmetry characteristics. With respect to the transformation twins as a lattice invariant strain, the K_1 for type I twinning must originate from the mirror plane in parent phase, while η_1 for type II twinning must originate from the two-fold axis in the parent phase. Different types of twinning for CuAlNi SMA are shown in Table 2.4 [18].

Table 2.4: Types of twinning for γ'_1 martensite in CuAlNi SMA

Type of twinning	**K_1**	**η_1**	**K_2**	**η_2**
Type I	{121}	<-1, 0.7953, -0.5907>	{-1, 1.5036, -0.5036}	<111>
Type II	{-1, 1.5036, -0.5036}	<111>	{121}	<-1, -0.7953, -0.5907>
Compound	{101}	$<\bar{1}01>$	$\{\bar{1}01\}$	<101>

Two variants of martensite can form the twin when they satisfy the following twinning equation [19]:

$$R_{ij}\, U_i - U_j = a \otimes n \qquad (10)$$

where the R_{ij} is the relative rotation between the two variants, $\boldsymbol{U_i}$ and $\boldsymbol{U_j}$ are the transformation matrices of the two variants, $\boldsymbol{n}$ is the twinning plane normal, $\boldsymbol{a}$ is the twinning shear direction. Using the equation (10) the all twinning systems for an individual material can be calculated.

In particular, there are thirty possible variant pairs between six orthorhombic variants of CuAlNi, and these variants can be segregated into two sets [20]:

$$S_1 = \begin{pmatrix} (1:2) \\ (3:4) \\ (5:6) \end{pmatrix} \quad \text{and} \quad S_2 = \begin{pmatrix} (1:3) & (1:4) & (1:5) & (1:6) \\ (2:3) & (2:4) & (2:5) & (2:6) \\ (3:5) & (3:6) & (4:5) & (4:6) \end{pmatrix}$$

where it is to be understood that if the variant pair (i : j) is contained in a particular set, then so is the variant pair (j : i). The Variants in set S_1 are joint through the compound type twinning and the variants in set S_2 are joint through the type I or type II twinning.

2.8 Habit plane variant, detwinning and maximum recoverable strain in SMA

From phenomenological theory of crystallography of martensitic transformation, an interface between martensite and parent phase is necessary to be formed. It is also necessary to induce lattice invariant shear and rigid rotation in order to make the habit plane undistorted and unrotated. Therefore, a unit of martensite is a martensite variant including the lattice invariant shear and rigid body rotation. Since the lattice invariant shear is twinning in shape memory alloys, the unit martensite consists of the two layers of martensite variants, which have a twinning relationship. The unit martensite, which has a habit plane is especially called *habit plane variant*, while each component martensite in the habit plane martensite variant is lattice correspondence variant. The number of the habit plane variants depends on the symmetry of the martensite [4]. For the cubic to tetragonal transformation there are 24 habit plane variants, 96 for cubic to orthorhombic and 192 habit plane variants for the cubic to monoclinic transformation. The scheme of the habit plane variant is shown in Fig. 2.8, where we can see deformation induced by habit plane variant and two twin related lattice correspondence variants M_1 and M_2.

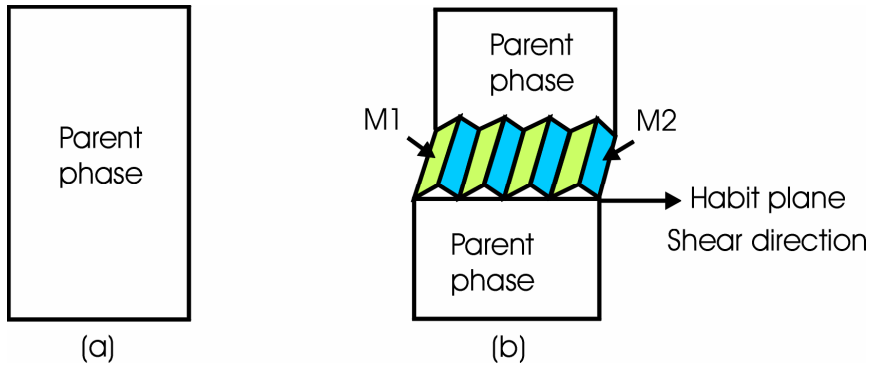

Fig. 2.8: Scheme of untransformed specimen (a) and deformation induced by habit plane variant of martensite (b).

Austenite-twinned orthorhombic martensite interfaces (habit planes) for the CuAlNi are listed in table 2.5 [21]. It can be seen that there does not exist an austenite-orthorhombic twinned martensite interface for compound type twins in CuAlNi SMA.

Table 2.5: Comparison of calculations and experimental data for a CuAlNi alloy [21].

Twin type	Predicted by theory	Observed in experiment	Number
Compound twins			
Twin plane normal (K_1)	{100}	{100}[a,b]	12
Twin shear direction (η_1)	<010>	(see text)	12
Twin shear magnitude *(s)*	0.0747	(see text)	
Austenite-martensite interface	Does not exist	Not observed	0
Type I twins			
Twin plane normal (K_1)	{110}	{110}[b, c, d]	24
Twin shear direction (η_1)	<0.696, 0.696, 0.180>	(see text)	24
Twin shear magnitude *(s)*	0.261	(see text)	
Habit plane normal ***(m)***	{0.749, 0.635, 0.191}	{331}	
		With scatter[c, e, f]	24
Shape-strain direction $(\boldsymbol{b}/\lvert\boldsymbol{b}\rvert)$	<0.685, 0.684, 0.249>	Not available	24
Habit plane normal ***(m)***	{0.715, 0.650, 0.258}	Not available	24
Shape-strain direction $(\boldsymbol{b}/\lvert\boldsymbol{b}\rvert)$	<0.780, 0.601, 0.178>	Not available	24
Magnitude of shape strain ***(b)***	0.0959	Not available	
Twin volume fraction (λ)	0.290	~0.36[e]	
Type II twins			
Twin plane normal (K_1)	{0.688, 0.688, 0.228}	(see text)	24
Twin shear direction (η_1)	<110>	(see text)	24
Twin shear magnitude *(s)*	0.261	(see text)	
Habit plane normal ***(m)***	{0.728, 0.635, 0.261}	{0.725, 0.234, 0.648}[(f) g, h]	24
Shape-strain direction $(\boldsymbol{b}/\lvert\boldsymbol{b}\rvert)$	<0.702, 0.701, 0.131>	[-0.684, 0.214, 0.698][g]	24
Habit plane normal ***(m)***	{0.730, 0.668, 0.143}	(0.651, 0.153, 0.744)[h]	24
Shape-strain direction $(\boldsymbol{b}/\lvert\boldsymbol{b}\rvert)$	<0.758, 0.600, 0.254>	Not available	24
Magnitude of shape strain ***(b)***	0.0932	0.096[g]	
Twin volume fraction (λ)	0.301	Not available	

[a] Otsuka & Shimizu(1970); [b] Otani et al. (1983); [c] Otsuka & Shimizu (1969); [d] Otsuka (1971); [e] Otsuka & Shimizu (1974a); [f] Kurdyumov et al. (1961); [g] Okamoto et al. (1986); [h] Morii & Otsuka (1990)

The total deformation P_1 induced by the habit plane martensite variant is described in a matrix form with equation (8). After fully transformed the specimen, there is no parent phase remained so that the twin planes (lattice invariant shear) are not necessary to exist, because the habit plane (interface between the martensite and parent phase) does not exist. By further applying stress, detwinning deformation occurs. *Detwinning* means that the one lattice correspondence variant of martensite (M_1 or M_2 from Fig. 2.8b), which is the most preferable variant for the applied stress will growth. And as a result we obtain single crystal lattice correspondence variant of martensite (single crystal of martensite). Detwinning process occurs at the stress plateau on stress strain curve. This detwinning will induce further deformation from the deformation of Equation (8) and the maximum recoverable strain will be achieved. The lattice distortion *B* for the maximum recoverable deformation is expressed

by the equation (3). We consider the coordinate transformation as we did in equation (4). After the deformation U any vector of austenite in parent phase (austenitic) basis $x_0 = (u_0, v_0, w_0)$ change to martensite vector in austenitic basis $x = (u, v, w)$ as follows:

$$\boldsymbol{x = U_i\, x_0} \qquad (11)$$

where U_i is the transformation matrix and $i = 1, \ldots, 6$ for orthorhombic martensite and $i = 1,..,3$ for tetragonal martensite.

Therefore, the strain ε induced by the deformation U along the direction of the vector x_0 in the parent phase (austenite) can be calculated by the following equation:

$$\varepsilon = \frac{|x|}{|x_0|} - 1 = \sqrt{\frac{u^2 + v^2 + w^2}{u_0^2 + v_0^2 + w_0^2}} - 1 \qquad (12)$$

Transformation strains along some typical directions in austenite calculated for the CuAlNi single crystal when deformed in γ'_1 martensite are shown in Table 2.6:

Table 2.6: Transformations strains for CuAlNi orthorhombic martensite for variant 1.

Direction in austenite	Transformation strain ε_{tr} [%]
[100]	8.22
[010]	4.27
[001]	4.27
[110]	1.78
[101]	1.78
[011]	6.19
[111]	1.61
[210]	5.59
[211]	3.18

3. Thermodynamics of the martensitic transformation

The martensitic transformation is a diffusionless transformation, hence there is no associated chemical composition change. The transforming system can thermodynamically be considered as a single component system [22, 23]. In such a way the free energy curves of both parent and martensite phases as a function of temperature may be represented as schematically show in Fig. 3.1, where T_0 represents the thermodynamic equilibrium

temperature between the two phases, and $\Delta G^{p-m}|M^s = G^m - G^p$ represents the driving force for the nucleation of martensite, where the G^m and G^p represents the Gibbs free energy of martensite and parent phase respectively.

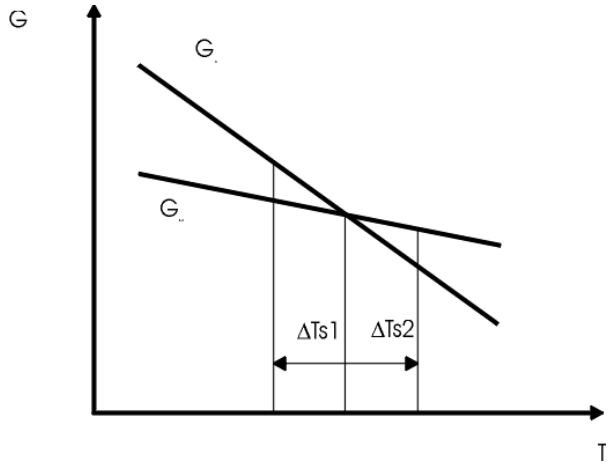

Fig. 3.1: Schematic diagram of Gibbs potentials for martensitic and austenitic phases

The Gibbs free energy change of a system upon martensitic transformation may be written as follows [2]:

$$\Delta G = \Delta G_c + \Delta G_s + \Delta G_e = \Delta G_c + \Delta G_{nc} \qquad (13)$$

where ΔG_c is a chemicall energy term originating in the structural change from parent to martensite, ΔG_s is a surface energy term between parent and martensite, ΔG_e is an elastic energy term around the martensite, and $\Delta G_{nc} = \Delta G_s + \Delta G_e$ is a nonchemical energy term. In most martensitic transformations ΔG_{nc} is equally as large as ΔG_c. Because of this supercooling of ΔT_s is necessary for nucleation of a martensite and superheating is necessary for the reverse transformation.

The equilibrium temperature can be approximated using the temperatures A_s and M_f as :

$$T_0 = (M_s + A_f)/2 \qquad (14)$$

Martensitic transformation may be induced by external stress. To analyze the effect of the stress on the martensitic transformation Clausius-Clapeyron equation can be used:

$$d\sigma/dT = - \Delta S/\varepsilon_{tr} = - \Delta H/ \varepsilon T \qquad (15)$$

where σ is a uniaxial stress, ε_{tr} a transformation strain, ΔS the entropy of transformation per unit volume, and ΔH the enthalpy of the transformation per unit volume.

Schematically the stress-temperature ($\sigma - T$) dependence is shown in Fig. 3.1. The $\sigma - T$ diagram shows the regions of the stability for individual phases (austenite and martensite) [24, 25].

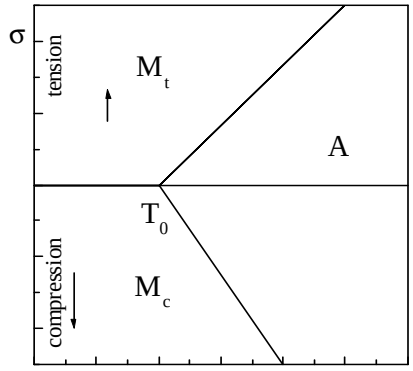

Fig. 3.1: $\sigma - T$ diagram in equilibrium (T_0) showing austenite phase A, tensile M_t and compressive martensite M_c, respectively.

4. Ferromagnetic NiMnGa shape memory alloys

The principle of the magnetic shape memory (MSM) alloys, also referred as a ferromagnetic shape memory alloys (FSMA), was presented by Ullakko [26, 27], who observed a large 0.2% magnetic field induced strain (MFIS) in an unstressed [001] martensite single crystal of Ni_2MnGa in $800kAm^{-1}$ magnetic field at 265 K. MFIS in MSM alloys is based on the rearrangement of the martensite twin variants by the twin boundary motion. Magnetic shape memory effect (MSME) works best in a NiMnGa alloys having a modulated five-layered tetragonal martensite structure (5M) and it is possible also in the modulated seven-layered orthorhombic martensite (7M). Other alloys which posses the MSME are Fe-31.2at%Pd (~ 3% MFIS [28]) and Fe_3Pt (~ 0.2 % MFIS [29]).

MSM materials have potential for actuator and sensor applications since they combine a large strain (~ 6 % for 5M martensite) with rather high frequencies without a temperature change [30]. Main limiting factor in currently available MSM alloys is the low actuation stress levels of usually less than 3 MPa [31, 32]. Recently a one-way shape memory effect due to stress-assisted magnetic field induced martensitic phase transformation has been observed in Ni_2MnGa single crystal [33]. The single crystal is loaded under zero magnetic field to a stress level above critical stress for the forward transformation allowing forward transformation to occur and than unloaded to a stress level between the critical stress for the reverse transformation in the presence of magnetic field and critical stress for the forward transformation. When the magnetic field is applied the reverse transformation occurs since the martensite is unstable at that stress level under the magnetic field. In such a way it is possible

to obtain larger actuation stresses (~ 24 MPa) induced by magnetic field. However, the MSME based on the reorientation of martensite induced by magnetic field is only used in practical applications in present.

4.1 Magnetic shape memory effect

The magnetic shape memory effect is demonstrated with a Ni-Mn-Ga MSM alloy in the magnetic field (Fig. 4.1). Applying the magnetic field H to the single variant material (single crystal of tetragonal Ni-Mn-Ga martensite) causes the other twin variant to appear and grow [34]. These tetragonal martensitic variants have different magnetic and crystallographic orientations. When magnetic field increases the boundaries between twins move, as amount of preferentially oriented twin variants grow at the expense of the other twin variant. The inset on the left in Fig. 4.1a presents a crystal lattice orientation of tetragonal martensite variant. The *c*-axis, *i.e*. the shorter lattice axis of the martensitic variant is aligned along the longest edge of the MSM material. In other martensitic variant, the *c*-axis is perpendicular to the previous variant`s *c*-axis (Fig. 4.1a, right). *C*-axis is the easy direction of magnetization of the material [34]. MSME is possible only if the energy required to rotate the magnetization out of the easy direction, the magnetic anisotropy energy MAE, is higher than the energy required to move a twin than, it is energetically more favorable to move the twin boundaries instead of rotating the magnetization [35]. As a result of the interaction between the magnetic field and twins, the length of the sample contracts in the direction of applied field and increases in the direction perpendicular to the applied magnetic field by the amount of the ratio *a/c* (Fig. 4.1a). This holds for the sample in essential orientation {100}. Fig. 4.1b shows the deformation induced by magnetic field and corresponding changes of magnetization [36].

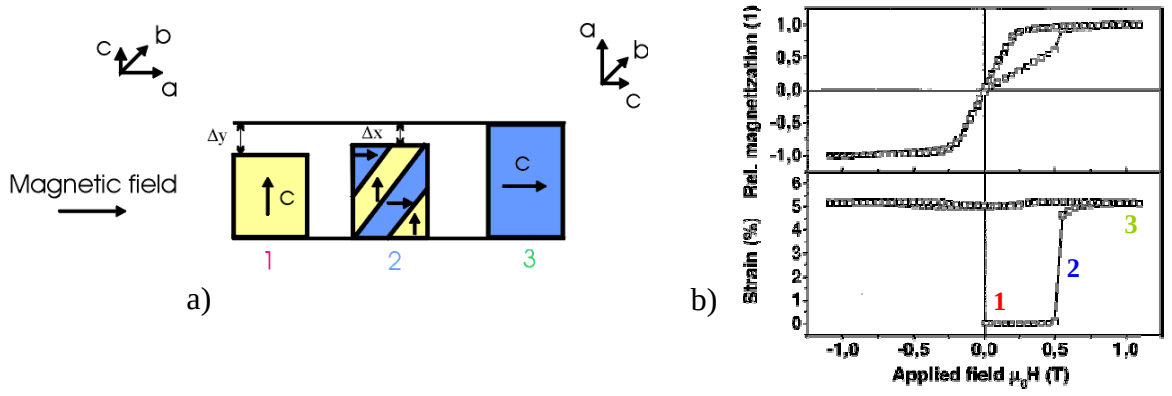

Fig. 4.1: Schematic diagram of MSME (a) together with the measured deformation induced by magnetic field (b).

This shape change remains after removing the magnetic field [37]. In order to obtain the MSM actuation, the single variant state created by the magnetic field should be changed to another single variant martensitic state. This is possible either by rotating the magnetic field perpendicular to its original orientation or with an external spring-back load. The actuation applies usually the axial movement. Other potential applications of NiMnGa magnetic shape memory alloys are different couplers, positioning devices, sensors [38].

Based on the above discussion the basic requirements for the appearance of the MSME are:

- Mobile twin boundaries
- The material should be ferromagnetic and exhibit a martensitic transformation
- The magnetic anisotropy energy must be higher than the energy required to move a twin boundary

4.2 Crystallographic characteristic of NiMnGa SMA

The high temperature parent phase of near-stoichiometric Ni_2MnGa alloys has the highly ordered $L2_1$ cubic structure with lattice parameter a = 0.576-0.597 nm depending on the alloy composition and the external temperature [39-42]. The degree of atomic order affects the structure and the magnetic properties. The ordering can be changed, for example, by fast cooling from homogenization temperature resulting in 100 K lower martensitic transformation temperature [43].

A variety of martensite crystal structures have been observed in Ni-Mn-Ga: Non-modulated (NM) and modulated 5-layered (5M), 7-layered (7M), 8-layered (8M) or 10-layered (10M) [44, 45]. Modulation is observed as extra diffraction peaks between the fundamental spots in <110> direction of reciprocal space and the crystal structure can be interpreted either as a long period stacking of closed-packed planes (110) [46] or a periodic shuffling of basal planes (110) along $[1\bar{1}0]$ direction [44]. The structure of 5M martensite is tetragonal with lattice parameters $a = b$ = 0.5945 nm and c = 0.5610nm [42]. Possible twinning planes between all three martensite variants pairs are listed in Table 4.1.

Table 4.1: A complete list of all twinning planes with all tetragonal variants pairs of NiMnGa [47].

Variant pair	Twinning plane
(1 : 2)	$(1\bar{1}0)$
(1 : 2)	(110)
(1 : 3)	$(10\bar{1})$
(1 : 3)	(101)
(2 : 3)	$(0\bar{1}1)$
(2 : 3)	(011)

The stoichiometric Ni_2MnGa alloy transforms from $L2_1$ phase into a martensite structure approximately at 200K [39, 48]. In the off-stoichiometric Ni-Mn-Ga alloys the transformation is highly composition dependent and occurs below 630 K [40, 49, 50]. The Curie point of ternary Ni-Mn-Ga alloys is at 370 K and they transform to the 5M martensite structure at 343 K at the highest [50].

Lattice correspondence variants of 5M tetragonal martensite are schematically shown in Fig. 4.2.

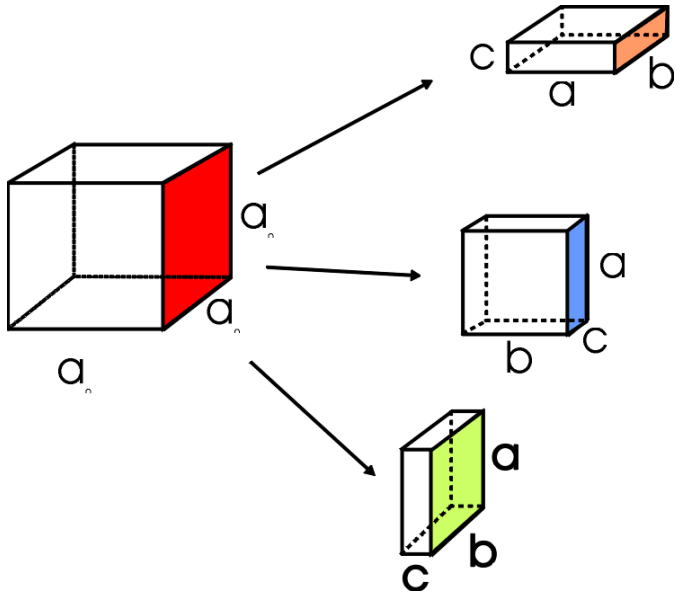

Fig. 4.2: Schematic view of the three variants of martensite in a cubic to tetragonal transformation.

The transformation matrices of these martensitic variants are listed in Table 4.2. Equation (1) and (2) also holds for the calculating the lattice correspondences between austenite and martensite directions or planes, only the transformation matrices *R* are different (Table 4.2).

Table 4.2: Transformation matrices R for tetragonal martensite variants

LCV	1	2	3
Transformation matrix **R** for planes A → M	$\begin{pmatrix} 1 & 0 & 0 \\ 0 & 1 & 0 \\ 0 & 0 & 1 \end{pmatrix}$	$\begin{pmatrix} 0 & 1 & 0 \\ 0 & 0 & 1 \\ 1 & 0 & 0 \end{pmatrix}$	$\begin{pmatrix} 0 & 0 & 1 \\ 1 & 0 & 0 \\ 0 & 1 & 0 \end{pmatrix}$

4.3 Magnetic properties of NiMnGa

The magnetic anisotropy and the magnetization of the material are important factors for the MSM effect. Ferromagnetic material is comprised of a domain structure consisting of regions (domains) in which magnetic moments are aligned and hence exhibit a spontaneous

magnetization (M) [51]. Magnetization is defined as a magnetic moment per unit volume [52]. The moment alignement within domains is due to a mean or molecular field $H_I = \alpha M$ which is proportional to the magnetization [51]. In the demagnetized state, the random ordering of domains yields zero net magnetization whereas the application of a field aligns domains to produce a bulk magnetization. Domains are separated by small regions called domain walls in which the magnetization changes direction. Fig. 4.3 schematically shows twinned 90° and 180° domain structure of NiMnGa.

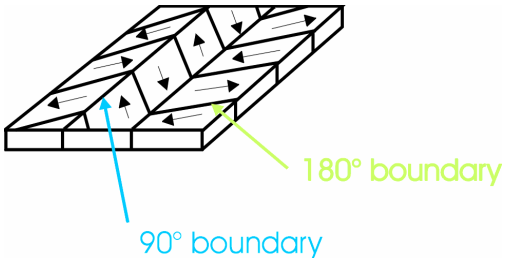

Fig. 4.3: Schematic sketch of the twinned 90° and 180° magnetic domains.

Ge et al [53, 54] investigated the magnetic domain structure in 5M NiMnGa martensite by scanning electron microscopy. They observed the 90° and 180° magnetic domains in a two-variant state (Fig. 4.4a). The 90° domains coincide with the twin boundaries. They also found that the sample contains strip magnetic domains pattern when is in nearly a single-variant state (Fig. 4.4b). The bands of the minor martensite variant are deformed and create a zigzag pattern following the magnetic domain structure of the major variant. Evolution of the magnetic microstructure in the magnetization of magnetic shape memory alloys (MSMAs) is theoretically described in detail in [55].

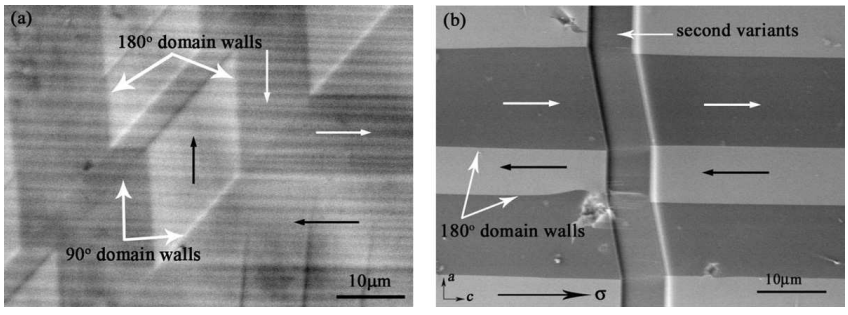

Fig. 4.4: Twinned 90° and 180° magnetic domains structure in 5M NiMnGa (a) and the 180° domains in a nearly single-variant of martensite together with the deformed minor variant (b).

The magnetization M in a domain tends to point in certain preferred (easy) crystallographic directions. The process of magnetizing a material involves domain wall motion or the rotation

of magnetization away from the preferred direction. The work required to rotate the magnetization away from one of the easy, or preferred axes with an applied field is described by the magnetocrystalline anisotropy energy *E*. For a cubic crystal a usual expression for *E* is [56]:

$$E = K_0 + K_1 (\alpha_1^2 \alpha_2^2 + \alpha_2^2 \alpha_3^2 + \alpha_3^2 \alpha_1^2) + K_2 (\alpha_1^2 \alpha_2^2 \alpha_3^2) + ... \quad (16)$$

where α_i are direction cosines of the magnetization *M* with respect to the cubic axis. K_1, K_2, etc. are anisotropy constants and indicates the strength of the anisotropy in particular crystal. First term K_0 is independent of angle and is usually ignored. Higher terms are generally not needed and sometimes K_2 is so small that the term involving it can be neglected [56].

Magnetocrystalline anisotropy has been studied in the Ni-Mn-Ga system experimentally both for cubic phase and for the different martensites [57, 58]. The magnetic anisotropy energy density is calculated as the area between easy and the hard magnetization directions. For the 5M martensite the easy axis of magnetization is its crystallographic short *c*-axis. For the uniaxial anisotropy constant K_u at ambient temperature values in the range of 1.2-5 x 10^5 J/m^3 have been reported, while the second anisotropy constant is negligible [58].

4.4 Temperature dependence of magnetic field induced strain

According a simply model [59] the MSME occurs at a given temperature *T*, when difference of magnetic energy *ΔE* of differently oriented martensitic variants exceeds the elastic energy needed to move twin boundary between these variants

$$\Delta E > \varepsilon_0(T) \, . \, \sigma_{TW}(T,\varepsilon) \quad (17)$$

where $\varepsilon_0(T) = (1\text{-}c/a)$ is the tetragonal distortion of the lattice. Twinning stress, $\sigma_{TW}(T,\varepsilon)$, is defined as an external stress necessary to reorientate structure or to move the twin boundaries to produce macroscopic strain $\varepsilon < \varepsilon_0$. This strain ε is defined as $\varepsilon = (l\text{-}l_0)/l_0$ where l is the length of the sample and l_0 is the initial length.

When a sample is magnetized to saturation perpendicularly to the easy magnetization axis of one variant and along the easy axis of the adjoining variant, the difference of the magnetic energy is equal to the difference of the magnetic anisotropy energy of these variants and we can rewrite the equation (16) as:

$$\frac{K_1(T)}{\varepsilon_0(T)} > \sigma_{TW}(T,\varepsilon) \quad (18)$$

where $K_1(T)$ is magnetic anisotropy constant.

The MSM effect is limited by the martensitic phase transformation and affected by the temperature dependence of the twinning stress, the tetragonality of lattice and the magnetic anisotropy [60]. In the 5M Ni-Mn-Ga martensite the lattice parameter *a* increases slightly, while the parameter *c* decreases with decreasing temperature [61] resulting in increasing of the lattice distortion (1 – *c/a*) and consequently in an increase of the MFIS. The saturation magnetization and magnetic anisotropy increase with decreasing temperature [36]. The temperature dependence of the twinning stress has an exponential-like character and strongly increases at low temperature [60].

From the abovementioned results it implies that the high temperature limit of the MSME in 5M martensite is the transformation to austenite at 315 K and the low temperature limit, determined as a temperature where rapid growth of the twinning stress exceeds $K_1(T)/\sigma_{TW}(T)$, is 165 K.

5. Single crystal neutron diffraction

One of the most fundamental properties of materials is their atomic structure and in the case of crystalline materials the structure, the arrangement of the atoms within the unit cell, is the key to many of their macroscopic properties [62]. Single crystal neutron diffraction is mostly used to measure elastic, coherent scattering *i.e.*, the Bragg reflection intensities from crystals of a material, the structure of which is the subject of investigation [63]. A single crystal is placed in a beam of neutrons produced at a nuclear reactor or at a proton accelerator-based spallation source. Single crystal diffraction measurements are commonly performed at thermal neutron beam energies, which correspond to neutron wavelengths from 1 to 4 Å. For high-resolution studies requiring shorter wavelengths (0.2 – 1 Å), a pulsed spallation source or a high-temperature moderator (a hot source) at a reactor may be used. When complex structures with large unit-cell repeats are under investigation, as is the case in structural biology, a cryogenic temperature moderator (a cold source) may be employed to obtain longer neutron wavelengths (4 – 10 Å).

5.1 Reciprocal lattice

The concept of reciprocal lattice gives a very elegant and useful method for representing the lattice planes (*hkl*) and hence the possible reflections from a crystal. Reciprocal lattice points lie on lines through the origin perpendicular to crystal planes and at distances from the origin that are reciprocals of the interplanar spacings of the corresponding crystal planes, *i.e.*,

$G_{hkl} = 1/d_{hkl}$ [64]. G_{hkl} is called reciprocal lattice vector and individual reciprocal lattice vectors can be expressed as [65]:

$$G_{hkl} = ha^* + kb^* + lc^* \qquad (19)$$

where a^*, b^*, c^* are elementary translations vectors of reciprocal lattice and *h, k, l* are Miller indices.

Vectors a^*, b^*, c^* are defined as:

$$a^* = \frac{b \times c}{a \,.\, b \times c} \qquad b^* = \frac{c \times a}{a \,.\, b \times c} \qquad c^* = \frac{a \times b}{a \,.\, b \times c} \qquad (20)$$

Where a, b, c are elementary translations of direct or real lattice.

A typical reciprocal lattice for an orthorhombic crystal is shown in Fig. 5.1. Every point in reciprocal lattice represents a possible reflection *hkl*. A diagram showing the reciprocal lattice with each point weighted to represent the intensity of the corresponding reflection is called an intensity-weighted reciprocal lattice and represents the complete "diffraction pattern" of the crystal [66]. It is useful when considering the collection of these reflections by various techniques. Those reciprocal planes, which lie parallel to two reciprocal axes, have one index constant. For example, the a^*, b^* - plane is called the hk0-plane or the 0-layer in the c^*-direction. Parallel to this is 1st layer or hk1-plane.

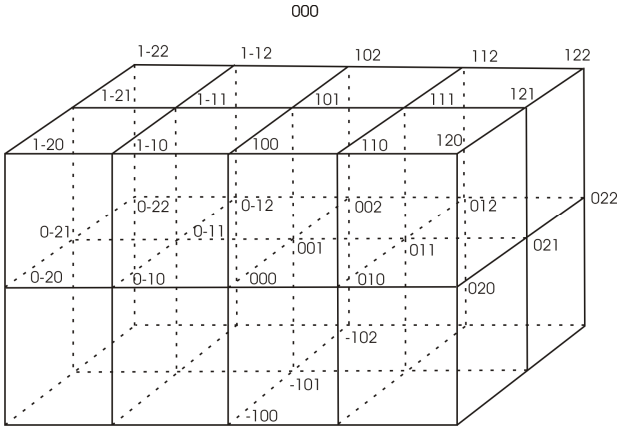

Fig. 5.1: Reciprocal lattice for orthorhombic lattice.

5.2 Integrated intensity of the reflection and the Bragg's equation

Most crystallographic experiments are considered either with a determination of the lengths and orientations of the reciprocal lattice vectors at which finite nuclear scattering occurs; or with the determination of the structure factors F_h [62]. The first type of measurement enables the reciprocal lattices to be constructed and hence the shape and size of the unit cell of the

crystal to be determined. Measurement of the structure factor on the other hand enables the positions of atoms within the unit cell to be determined.

The relationship between the crystal lattice and maxima in the diffraction pattern is expressed in the Bragg equation:

$$2d \sin\theta = n\lambda \qquad (21)$$

where λ is the neutron wavelength, d the spacing of the reflecting plane, θ the glancing angle of incident of the neutron beam on this plane and n is order of diffraction.

The geometrical conditions of the Bragg equation can be represented diagrammatically by the Ewald construction (Fig. 5.2). A sphere with center C and radius $1/\lambda$ is drawn so that the incident neutron beam travels along a diameter ICO which passes through the origin O of the reciprocal lattice. If P is a reciprocal lattice point such that $OP = G_{hkl}$, then the Bragg condition for reflection by the set of planes perpencidular to G_{hkl} is satisfied when P lies on the surface of the sphere [62]. From the Ewald construction it is seen that in order to obtain the diffraction in direction CP the reciprocal lattice vector $G_{hkl}=OP$ must be parallel to the *scattering vector* $Q_{hkl} = (k_0 - k_1)/\lambda$ and of length $2\sin\theta/\lambda$ [67].

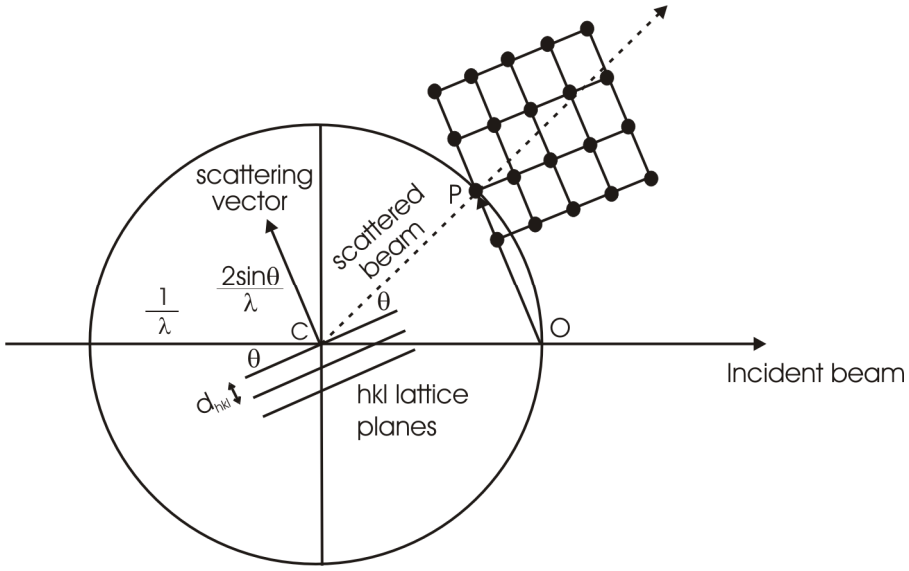

Fig. 5.2: Ewald sphere construction.

Due to the influence of the defects in the crystal, mosaicity of the crystal, collimation of the neutron beam and the range of wavelengths $\delta\lambda$ about the nominal value of λ the reciprocal lattice points are observed experimentally as small three-dimensional ellipsoids. Because of these reasons in the diffraction experiment we do not measure the maximal intensity of reflection but the *integrated intensity of the reflection*, it means that the crystal is rotated for a

fixed time and during this movement the intensity of the reflection is continuously measured [68]. The integrated intensity for the mosaic single crystal can be expressed as [69]:

$$I_{hkl} = I_0 \lambda^3 \frac{|F_{hkl}|^2}{V_0^2} \frac{1}{\sin 2\theta} V \qquad (22)$$

where I_0 is the intensity of the incident neutron beam with corresponding wavelength λ, V is the volume of the crystal (specimen), V_0 is the unit cell volume, expression $1/2\sin\theta$, called the Lorentz factor L, is related to the time the reciprocal lattice volume around a node takes to go through the Ewald sphere during the scan, hence it depends only on the geometry used. F_{hkl} is structure factor [70].

In almost all crystallographic studies in which structural information is sought, it is the integrated intensity, which is measured. The experimental values of I_{hkl} are measured on relative scale.

5.3 Principles of magnetic neutron scattering

The neutron`s interaction with magnetically ordered matter is twofold: with the nuclei first, and secondly with the electrons of incompletely filled *3d-*, *4d-*, *4f-*, *5f-* shells [71]. Second interaction is a consequence of the energy of the neutron magnetic moment μ_N in the magnetic field H arising from the electrons of incompletely filled shells [72]. The magnetic field H is due to the contribution of the magnetic dipole (spin part) and the momentum of the electrons that leads to a current (orbital part). Scattering from the nuclei is isotropic, and the scattering length b is independent of $\sin\theta/\lambda$, because the radius of the nucleus (~ 10^{-13} cm) is much smaller than the wavelength of thermal neutrons (10^{-8} cm) [71]. Magnetic scattering amplitude p, depends on $\sin\theta/\lambda$, because the extension of the magnetic shells is comparable to the wavelength of the neutrons. This fact is described by the magnetic form factor f, which falls off more rapidly with increasing angle than does the x-ray form factor as there is no contribution from the core electrons. The magnetic scattering amplitude p for the atoms with defined orientations of the magnetic moments can be expressed as [73]:

$$p = (e^2 \gamma / m c^2) S f \qquad (23)$$

where e and m are the electronic charge and mass respectively, γ is the magnetic moment of the neutron, S is the spin quantum number and f is the magnetic form factor.

In paramagnetic crystal the magnetic moments are all randomly oriented, the magnetic scattering will be entirely incoherent and will contribute to the background of the diffraction pattern [73]. In ordered magnetic crystals the magnetic moments are oriented in a regular

manner and coherent Bragg reflections occur. If the magnetic unit cell is the same size as the chemical unit cell, as is usual in ferromagnetic materials, then the coherent magnetic peaks will occur at the same positions as the coherent nuclear peaks. If unpolarized neutrons are employed there is, however, no coherence between the magnetic and nuclear amplitudes, it is merely their intensities that are additive. The total intensity of a combined magnetic and nuclear reflection is thus proportional to F^2_{total} which is given by the expression [73]:

$$F^2_{total} = F^2_{nuclear} + q^2 F^2_{magnetic} \quad (24)$$

where q is the magnetic interaction vector given by

$$q = \varepsilon (\varepsilon . K) - K = \sin \alpha \quad (25)$$

where K is a unit vector in the direction of the atomic magnetic spin and ε is a unit vector in the direction perpendicular to the effective reflective planes, *i.e*. the so called scattering vector, as indicated in Fig. 5.3.

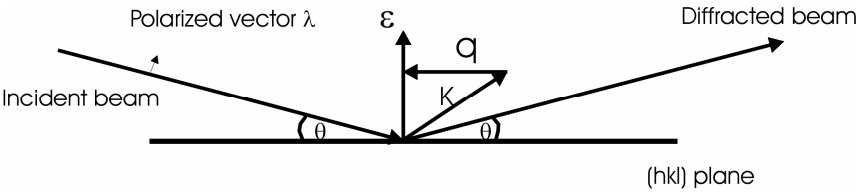

Fig. 5.3: Identification of the unit vectors ε, K and q used in the discussion of the magnetic scattering.

In antiferromagnetic materials the magnetic unit cell is usually twice the dimensions of the chemical unit cell, and consequently the magnetic and nuclear diffraction peaks are not normally superimposed and there is no difficulty in distinguishing between the two types of reflections [74, 75]. In ferromagnetics where the peaks are superimposed the nuclear and magnetic contributions may be separated in three ways. The best method is to vary q^2 by applying a magnetic field sufficiently large to saturate the sample alternately along and perpendicular to the scattering vector. In the first case the $q^2 = 0$ and the observed reflections are entirely nuclear, whereas in the second $q^2 = 1$. The magnetic contribution is thus readily obtained from the difference between the two patterns. Alternative method is to compare diffraction patterns taken above and below the Curie temperature, but the temperature corrections need to be made. The last method is to compare intensities of diffraction peaks of

the same form at low and at high scattering angles. At low angles the magnetic contribution may be large, but there is a rapid fall-off with angle due to the magnetic form factor.

5.4 Single crystal diffractometers

The most commonly used diffractometers are based on the normal beam geometry. In this kind of geometry the incident and diffracted beams lies in the equatorial plane and this plane is normal to the crystal rotation axis [76]. Instruments using this kind of geometry are known as three-circle or four-circle diffractometers. We shall use the term three-circle diffractometer to denote an instrument in which the detector shaft is geared to one of the crystal shafts and the term four-circle diffractometer for an instrument with four independently driven shafts. A schematic drawing of a four-circle diffractometer is given in Fig. 5.4.

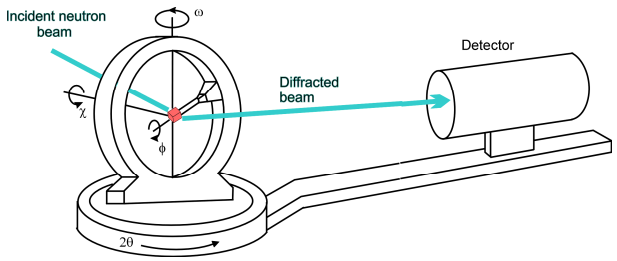

Fig. 5.4: Four-circle single crystal diffractometer

The four angles that are set before any measurement are conventionally named $2\theta, \omega, \chi, \phi$. The angle 2θ is the setting of the arm carrying the detector to the scattering angle, the other three movements allow the crystal to be oriented so that a selected direction lies along the scattering vector. The 2θ axis is always perpendicular to the plane of the incident and diffracted beams and hence to the scattering vector. Conventionally the ω axis is coincident with the 2θ axis and the χ axis perpendicular to it [62]. The ϕ circle is mounted on the χ circle and carries the goniometer head supporting the crystal [76]. Rotation of the goniometer head about its own axis is ϕ rotation.

It is possible to bring any direction in the crystal parallel to the scattering vector by setting ω and χ only but there may be some situations in which either the incident or diffracted beams are obstructed by parts of the diffractometer. The ϕ movements is introduced to enable these blind spots to be avoided. The flexibility introduced by the ϕ circle may also be used to measure variations in the scattering as the crystal is rotated around the scattering vector (azimuthal ψ scan) by means of an appropriate combination of angles ω, χ, ϕ.

The four-circle diffractometer have one important disadvantage; it is difficult to mount cryostats, pressure cells, or large magnets inside the χ circle [62]. Perhaps the simplest solution is to use *lifting counter diffractometer*, which allows a more elaborate sample environment around the crystal [77]. In this kind of diffractometer the crystal rotates about a single (usually vertical) axis ω, but the detector in addition to rotating about the axis 2θ, coincident with ω, may be tilted toward this axis by an angle ν.

There are basically two diffractometer scanning modes that are widely used [68]:

- ω scan – the detector is left stacionary while the crystal and thus, the chosen reciprocal lattice node, is made to cross the Ewald sphere by a rotation of $\Delta\omega$ about the main axis [68]. The path of the scan is tangential to the radial reciprocal lattice vector G_{hkl} (Fig. 5.5) [76].
- ω–2θ scan the crystal is moved in the same way but the detector follows the ω rotation at twice angular speed of the crystal [76]. The scanning path through the reciprocal space is along a line passing radially through the *O* (Fig. 5.5).

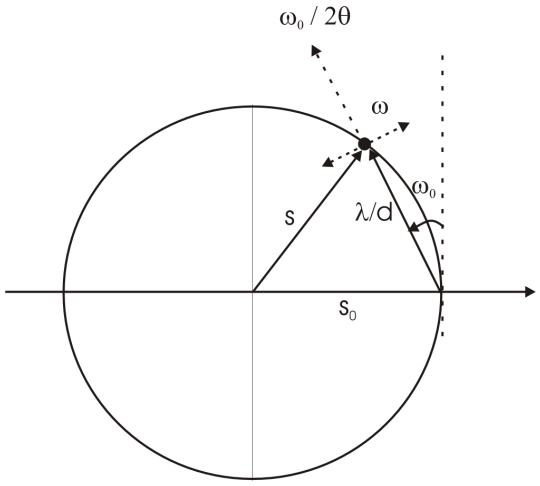

Fig. 5.5: Schematic diagram of scanning modes ω and ω/2θ.

5.5 Experimental aspects of single crystal diffraction

The simplest experimental entails the following steps [78]:

a) Find the orientation of the reciprocal lattice with respect to the instrument – the values of the Eulerian cradle angles 2θ, ω, χ, ϕ to allow observation of a particular reflection are calculated via a *3x3* matrix called the *orientation matrix* (UB matrix). On an

Eulerian cradle, if all setting angles are zero the scattering vector in the laboratory frame is

$$h_\phi = UBh \qquad (26)$$

where h is reciprocal lattice vector (h, k, l), B is the $3x3$ matrix that relates the generally triclinic reciprocal lattice to a set of cartesian axes fixed to the reciprocal axes, and U is the $3x3$ rotation matrix that relates these Cartesian axes to the laboratory frame. For non-zero values of the setting angles the scattering vector in the laboratory frame has an orientation described by

$$h_\theta = \Omega X \Phi U B h \qquad (27)$$

where Ω,X and Φ are the $3x3$ rotation matrices corresponding to the setting angles ω, χ and ϕ.

Eq. 27 applies to all Eulerian-cradle diffractometers. For each diffractometer though there will be a particular definition for the senses and origins of the settings angles and for the orientation of the axes of the laboratory frame. Busing and Levy [79] proposed a matrix method of setting angle calculations, which is widely used in modern four-circle diffractometers.

b) Characterize the crystal with regard to quality, absorption and extinction
c) Choose the measurement strategy including aperture size, scan ranges and counting times
d) Collect the data

The goal of the project

The goal of this thesis was to develop a single crystal neutron diffraction method for characterization of the quality of martensite single crystals and for *in situ* investigation of twinning processes in the martensite phase. The neutron diffraction was selected since neutrons penetrate deeply into solids and provide structural sensitive information from bulk volumes of the crystals (~1 cm^3) subjected to external stress, magnetic field or temperature changes driving the martensitic transformations and twinning processes in SMAs.

First part of the thesis describes the experimental issues related with the development of the method using CuAlNi single crystal as model material, in particular:

- ✧ Development of the single crystal neutron diffraction method for application to evaluation of the quality of martensitic SMA single crystals and twinning processes in martensites.
- ✧ Testing the method while performing *in situ* neutron diffraction studies of reorientation of 2H martensite in CuAlNi single crystals, characterization of twinning processes and evaluation of the presence of individual 2H martensite variants.

The second part of the thesis is devoted to the application of the method to describe the twinning processes in NiMnGa magnetic shape memory alloy single crystals, which are currently focused by many research groups worldwide due to its application as magnetic actuator. The tasks were defined as follows:

- ✧ Characterisation of stress induced reorientation in NiMnGa single crystalline sample by neutron diffraction in order to evaluate the completeness of the transformation processes.
- ✧ Evaluation of twinning processes taking place during magnetic field induced reorientation under stress by neutron diffraction technique to explore the physical and crystallographic basis of the magnetic actuation.

6. Deformation processes in CuAlNi single crystals of SMA

Shape memory alloys are used as functional materials. In order to understand the behavior and response of SMA in practical applications it is important to characterize the deformation processes in martensite that are responsible for the unique behavior of this class of materials. In this chapter the method of preparation of single crystals of martensite from austenite single crystal by compressive deformation is described and the deformation processes in such a single crystal of CuAlNi martensite are characterized. The dimensions of each individual martensitic variant is calculated and are compared with experimental data in order to characterize martensitic variants as well as the type of twinning is evaluated from optical observation of twinning plane traces.

6.1 Experimental material

A single crystal of Cu-14.3Al-4.2%Ni (wt %) alloy was prepared by the Bridgman method. The transformation temperatures were determined by differential scanning calorimetry (DSC) as M_s ~ 288K and A_f ~ 313K. Due to the thermal hysteresis and a shift of A_f due to deformation, such a crystal may exist at room temperature either in the bcc austenite or in the 2H martensite phases. Cuboid specimen (5.2 x 5.2 x 5.3 mm) was spark cut in the austenite phase. After grinding and polishing the crystal lattice orientations (Table 6.1) were determined in the austenitic state by back reflection Laue technique.

Table 6.1: Orientation of the sample F2 in the austenite state (direction cosines between hkl crystal and xyz space coordinates aligned with cube axes).

	100	**010**	**001**
Red	-0.03489	0.70710	0.70710
Blue	-0.58779	0.57358	-0.58779
Green	-0.80902	-0.42262	0.40674

For easy manipulation, three different faces (different crystallographic orientations) of the prism sample are denoted *R*, *G* and *B* according to the red, green and blue markings on the sample faces (Fig.6.1).

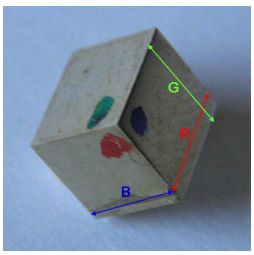

Figure 6.1: Image of the experimental cuboid sample and the three faces denoted as Red (R), Blue (B), and Green (G).

CuAlNi single crystals in austenite have cubic crystal lattice with space group Fm3m and martensite phase has 2H orthorhombic structure with space group Pnmm. Lattice parameters of austenite structure and 2H martensite structure are listed in Table 6.2.

Table 6.2: Lattice parameters of cubic austenite and 2H orthorhombic martensite of CuAlNi

Phase and crystal structure	**Lattice parameters**
Austenite (cubic)	a_0 = 5.836 Å
Martensite (orthorhombic)	a = 4.382 Å, b = 5.356 Å, c = 4.222 Å

6.2 Experimental procedures

During the preparation of single crystal of austenite and consequently the single crystal of martensite the following experimental procedures have been performed:

Single crystal growth by Bridgmann method

The Bridgman technique is a classical approach to the single crystal growth [80] (Fig. 6.2). A melt of appropriate composition is placed vertically in a furnace under a well defined temperature gradient. By slow movement of the melt relative to the gradient, such that the crucible leaves the hot zone with the lowermost part ahead, solidification of the melt takes place starting at the bottom of the crucible. Nucleation of as small as possible number of grains is required. This is attained by geometrically reducing the volume of spontaneous nucleation using a pointed-tip shaped crucible in combination with a cold finger. CuAlNi single crystal grown by this method is a rod shaped ingot with a diameter of the crucible. The velocity used to growth the CuAlNi single crystal was 5 mm/h.

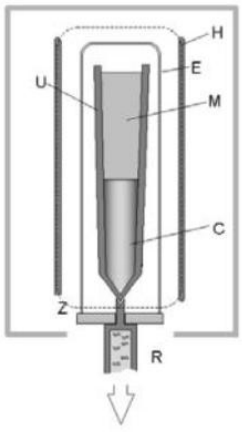

Fig. 6.2: The set-up used for single crystal growth according to the Bridgman. C: crystal grown, M: melt, U: crucible, E: protecting envelope, H: heater, Z: hot zone, R: pulling rod.

Differential scanning calorimetry

The characteristic temperatures of martensitic transformation were determined by differential scanning calorimetry (DSC). DSC is a technique in which the difference in heat flow into or out of a substance and a reference material is measured as a function of temperature [81]. DSC profiles of CuAlNi single crystals were measured by PerkinElmer 7 instrument. The samples for DSC measurements were spark cut and polished. The dimensions of the sample are 4 x 2 mm. The samples were placed in aluminum pans. The heating and cooling rate was 10 °C/min. DSC measurement was performed in temperature range from -50 °C to 60°C.

Mechanical testing

Compression tests were performed in an INSTRON 1362 electromechanical testing machine at room temperature. All tests were performed in a position control regime. Strain rates during the deformation were in the range from 4 x 10^{-5} to 4 x 10^{-3} s^{-1}. Stress and strain values are calculated form the measured position and load values. Since the shape change of the SMA single crystal during compression tests is large, it is crucial to try to avoid sample-grip constraint effects as much as possible. Therefore, contact faces of the compression grips were made exactly parallel, polished and slightly lubricated by silicon oil.

Optical microscopy

The three different faces of cuboid samples were polished for microscopic observation of surfaces. After the test and also during test interrupts a detailed evaluation of the shape of sample and orientation of the surface traces was made. The Zeiss Axio Imager Z1m optical microscope and the two surface trace analyses were used to evaluate the activated twinning planes. The notation of the measured angles with respect to sample edges for determination of twinning plane is shown in Fig. 6.3.

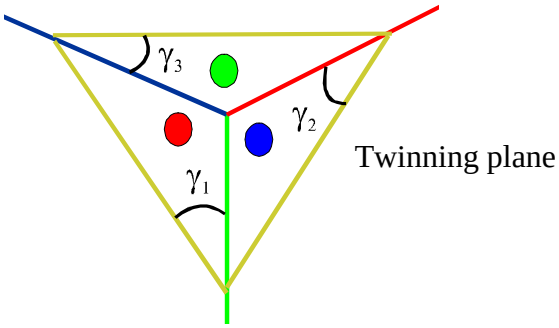

Fig. 6.3: Schematic view of the twinning plane and notations for angles.

6.3 Preparation of the single crystal of martensite from single crystal of austenite by compression deformation

CuAlNi single crystal of austenite can be prepared by one of the crystal growth techniques (*e.g.* Bridgman method). If such a single crystal of austenite is cooled below the characteristic temperature where martensitic transformation proceed, the multiple habit planes variants form in the sample *i.e.* as a result we do not obtain single crystal of martensite. One of the possible ways how the single crystal of martensite can be prepared is the successive compressive deformation on different faces of a cuboid sample [82].

When the martensite prism obtained as a result of stress induced transformation at room temperature (stress applied on R face of the sample F2 Figs. 6.4a) is turned 90 degrees to align a different sample face normal (G face) with the compression load axis, the prism can be deformed in martensite at relatively low stress (Figs. 6.4b) again. This time, although the temperature has not changed, the sample deforms via twinning deformation in the 2H martensite phase (Fig. 6.4b, c) *martensite reorientation*).

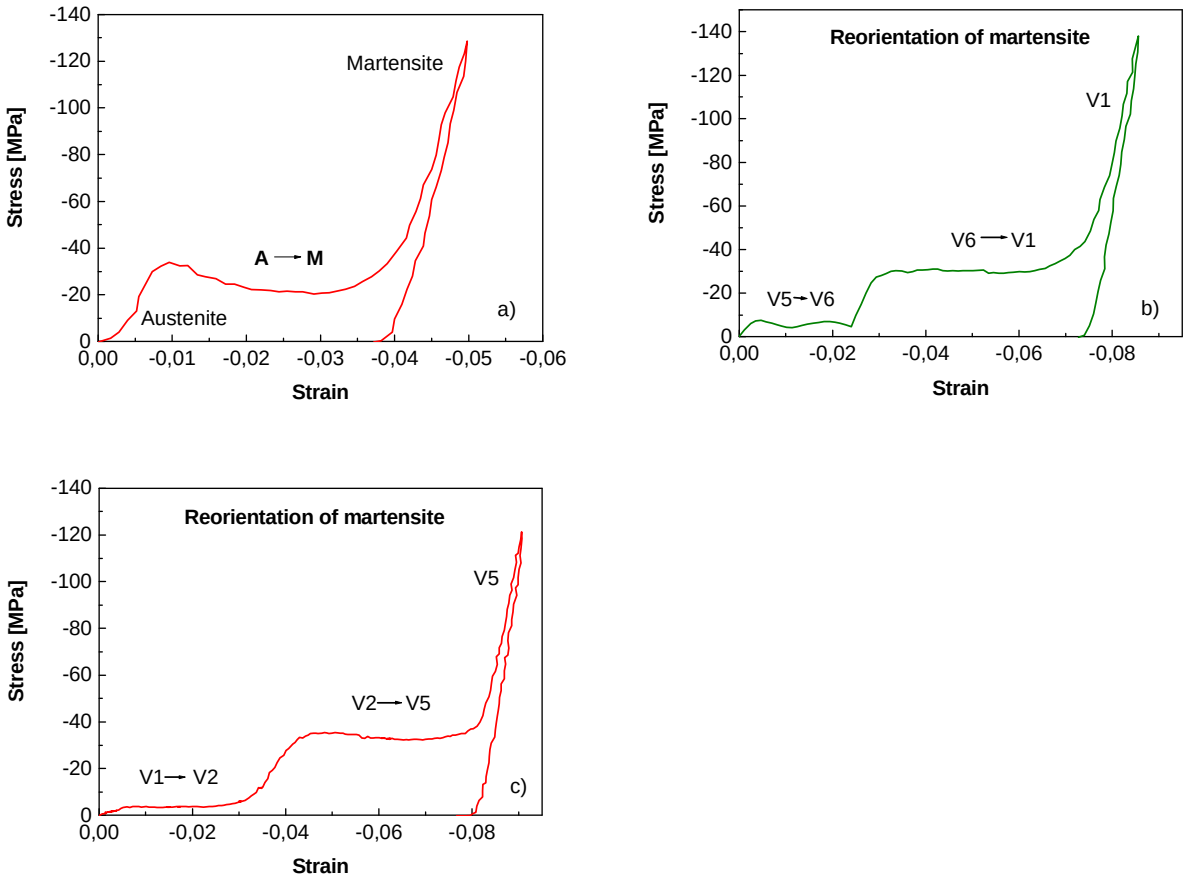

Fig. 6.4: Stress induced martensitic transformation F2 (a) and reorientation of martensite during the deformation on green face (two-stage stress-strain curve) (b) and then reorientation on red face in martensite (c).

By performing compression sequences in closed cycles (RGRG…etc.) repetitively, we achieve a situation, where the martensite sample passes through multiple well defined states (martensite variant single crystals) existing always when the crystal is deformed beyond each of the stress plateaus in Figs. 6.4. Martensite twinning processes (Fig. 6.4 b, c) take place at the strains within the stress plateaus.

Table 6.3: Calculated (theoretical) dimensions and edge angles of all 6 variants for sample F2.

LCV	Dimension [mm]			Angles [degrees]		
	a	b	c			
1	5.465	4.922	4.882	95.89	90.32	90.23
2	5.265	5.054	4.956	97.90	90.24	90.16
3	5.051	5.066	5.153	86.17	87.08	96.53
4	5.061	4.929	5.286	87.25	84.49	94.80
5	5.051	4.922	5.296	87.27	95.17	85.04
6	5.061	5.054	5.158	86.34	92.67	83.19

Each martensitic variant, which exists beyond this plateau, has characteristic shape (Figure 6.5) and crystallographic orientation of its faces. These geometrical parameters (dimensions, edge angles) can be experimentally measured after unloading the sample and compared with calculated one (Table 6.3). This can help us to identify martensitic variants. The dimensions of the martensite prism specimens for each variant of martensite are calculated using the equation (12). Using this equation we firstly calculate what are the deformations in each direction (R, B, G) of the specimen, and than the final dimensions of the specimen for all 6 martensite variants are calculated.

a) 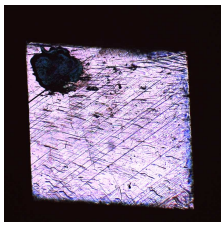 b) 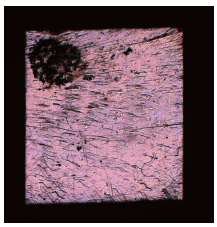

Fig. 6.5: Shape changes of martensitic samples during the reorientation of martensite induced by application of compressive deformation on green face. The shape of the sample in variant 6 (a) and macroscopic shape of the sample in variant 1 (b). Images of green face.

6.4 Determination of martensite variant from shape changes

Large number of deformation experiments on the samples with different orientations was carried out. The results presented here will be for one particular sample (table 6.1) deformed in cycles R, G, R.

By deforming the studied sample on green face and then on red face in martensite phase for all cases the two stage stress-strain curves were observed (Fig. 6.4b, c). It means *e.g*. that during the deformation on green face (Fig. 6.4b) the martensite sample transform from martensitic variant 5 to the variant 6 firstly by activating one twinning system at the first stress plateau (~10 MPa) producing the strain in order of ~2 % then followed by elastic deformation where martensitic variant 6 exist and then at higher stress level (~30 MPa) the other twinning system is activated which maintain the transformation from variant 6 to variant 1 and produces ~5% transformation strain. Finally after the end of the second stress plateau in the elastic region the sample is in the martensitic variant 1.

The individual martensitic variants were characterized based on above mentioned principles. The geometrical parameters of the prism shaped sample measured after the deformation are listed in (Table 6.3). As it can be seen the calculated parameters of individual martensitic variants from Table 6.4 do not match precisely with the experimental one. This can indicate that the prism shaped sample is not in one martensitic variant (twinning interfaces can exist in the martensitic sample). Also the calculated dimensions of the samples in some cases are very similar (*e.g.* variant 3, 4, 5) and when the sample contains the mixture of the variants it is not easy to characterize the individual martensite variants based on this observations.

Table 6.4: Experimental and calculated dimensions and edge angles of the sample F2 for martensite variants 1, 2, 5, 6.

	Dimension [mm]			Angles [degrees]		
	a	b	c			
Austenite	5.147	4.978	5.110	R	B	G
LCV 6						
Experimental	5.012	4.993	5.147	85.26	94.23	83.91
Calculated	5.061	5.054	5.158	86.34	92.67	83.19
LCV 5						
Experimental	5.004	4.964	5.246	86.53	94.87	85.23
Calculated	5.051	4.922	5.296	87.27	95.17	85.04
LCV 1						
Experimental	5.440	4.911	4.873	94.91	91.72	92.05
Calculated	5.465	4.922	4.882	95.89	90.32	90.23
LCV 2						
Experimental	5.253	4.995	4.922	96.98	89,87	89.91
Calculated	5.265	5.054	4.956	97.90	90.24	90.16

6.5 Optical observation of CuAlNi single crystal surfaces during the compression deformation

Fig. 6.4b, c shows the stress-strain curves obtained during the reorientation of 2H orthorhombic martensite. At the stress plateaus on the σ - ε curves, various twinning processes

take place at different stress levels. In order to characterize the twinning plane and in this way together with the known martensitic variants the type of the twinning at each stress plateau on the stress-strain curve (Fig. 6.4b), the sample was unloaded at each of the stress plateau and the optical photographs were taken from the different faces of the prism shaped sample (Fig. 6.6).

a) b)

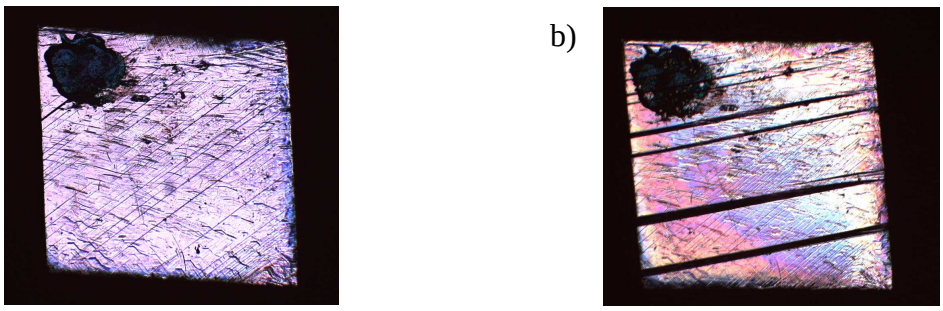

Fig. 6.6: Traces of twinning plane at the first stress plateau (a) and the twinning plane traces at the second stress plateau (b) of stress-strain curve on Fig. 6.4b.

The higher magnification of green face at the second stress plateau is shown in Fig. 6.7, where the martensitic variant 6 and variant 1 are seen from macroscopic point of view as a bands with different optical contrast. Different optical contrast is due to the different deformation concentrated inside the bands. Bands with the same optical contrast have equal deformations. Martensitic variant appear on the stress plateau of the stress-strain curve as thin bands and as the strain increases during the stress plateau, the width of the existing bands increases and new ones appear so long the sample becomes the single crystal of 2H martensite.

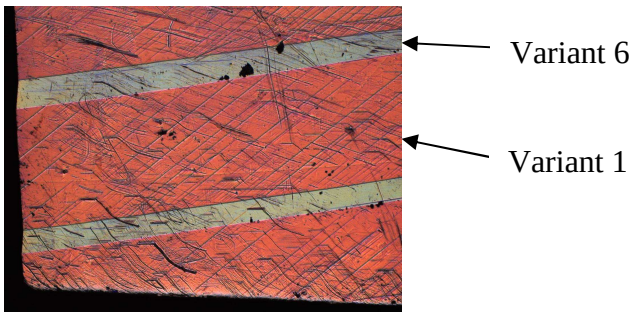

Fig. 6.7; Optical photograph of twins at the second stress plateau on the stress-strain curve from Fig. 6.4b.

The inclination of the twin bands to the sample edges is different at each of the stress plateaus. Twinning plane can be exactly determined from the two traces obtained from different faces of the sample. This method is called two-trace analysis. The denotation of the angles is shown in Fig 6.3 and the measured angles for stress-strain curve from Fig. 6.4b are listed in Table 6.5.

Table 6.5: Measured angles of twin traces to the three different edges at both stress plateaus of stress-strain curve

Angle	First plateau	Second plateau
γ_1	81,64°	83,62°
γ_2	96,82°	43,03°
γ_3	39,85°	10,51°

Results of the trace analysis and theoretical calculations confirm that the twinning process, which occurred on the first stress plateau in Fig. 6.4b, is compound type twinning and the second plateau corresponds to the type II twinning. The observed twinning planes from both stress plateaus are listed in Table 6.6.

Table 6.6: Twinning planes characterized from stress-strain curve in Fig. 6.4

Stress plateau	**Twinning plane**
First plateau	(01-1)
Second plateau	(-0.744; 1.801; -1)

From the evaluated types of the twinning and from optical photographs the morphological characteristics of the compound type twining and type II twins are made. Compound type twins, which appear at the first plateau on the stress-strain curve (Fig. 6.4b) are very narrow and gives a relatively small optical contrast, which corresponds to the smaller deformation concentrated in the twin band. While the type II twins at the second plateau of the stress-strain curve are much wider with much larger deformation in the twin band (see Fig. 6.6).

6.6 Summary:

Compressive deformation method for the preparation of single crystals of martensite was introduced, where by running various sequences (e.g. RGRG…) on a single crystal Cu–Al–Ni sample, one can measure multiple compression stress–strain curves with well defined starting microstructure (martensite variant single crystals denoted V1–V6) for various load axis orientations with respect to the orthorhombic lattice. In such a way single crystal of martensite can be prepared [82-84]. Successive compressive deformation on different faces of studied sample is useful method for the systematic studies of the twinning processes in SMA single crystal.

During the compressive deformation on green face (Fig. 6.4b) the transformations in following sequences occurred: V5, V5→V6, V6→V1, Vl. Applying the compressive deformation on red face (Fig. 6.4c) leads to the different twinning processes (reorientations of martensite): V1, V1→V2, V2→V5, V5. Individual variants of martensite were characterized by comparing calculated and experimentally measured dimensions of the sample beyond each stress plateau.

Type of twinning was evaluated for both stress plateaus on Fig. 6.4b. It was confirmed that the first plateau corresponds to the compound type twinning and the second plateau for the type II twinning. From the measured stress-strain curves for the deformation cycles G, R, it is concluded that the stress for the movement of compound type twins is low (10MPa) and that this type of interface is easily mobile. On the other hand the mobility of type II twins is considerably lower and the higher stress is needed for the movement of type II twin interfaces. The stress needed for the twin boundary movement is orientation dependent [82].

7. Neutron diffraction studies of CuAlNi SMA single crystals

The above explained technique of the evaluation of martensite variant is an indirect technique. The obtained information is from surfaces of the studied sample and when any differences between the theoretical and measured data are obtained the different method is needed to get representative information. Because of this, the single crystal neutron diffraction method, which allows to identify the individual martensitic variants and to follow the twinning processes in SMA, was developed. This method was developed on 2H orthorhombic CuAlNi martensite crystals. In this chapter the principle of this method will be explained and the application of this method to the studies of reorientation of martensite in 2H orthorhombic martensite is explained (7.3). The single crystal neutron diffraction technique was also used for the in-situ studies of stress-induced martensite transformation in CuAlNi crystal (7.4). The process of stress-induced martensite transformation was studied and the individual phases and their martensitic variants were characterized.

7.1 Neutron diffraction single crystal method for the detection of lattice correspondence variants

The presented neutron diffraction single crystal method of detection and evaluation of individual lattice correspondence variants in CuAlNi single crystal is based on the principles of crystallography of the martensitic transformation as well as on the diffraction principles. Due to the difference in crystal symmetry between the parent phase (cubic austenite) and

product phase (2H orthorhombic martensite), there are six lattice correspondence variants /LCV/ of the martensite phase (same 2H orthorhombic structure but different orientation with respect to the parent austenite phase).

Table 7.1: Transformation matrices for austenite to martensite planes.

LCV	**1**	**2**	**3**	**4**	**5**	**6**
Transformation matrix **R** for planes **A→M**	$\begin{pmatrix} 0 & 1/2 & 1/2 \\ -1 & 0 & 0 \\ 0 & -1/2 & 1/2 \end{pmatrix}$	$\begin{pmatrix} 0 & -1/2 & 1/2 \\ -1 & 0 & 0 \\ 0 & -1/2 & -1/2 \end{pmatrix}$	$\begin{pmatrix} 1/2 & 0 & 1/2 \\ 0 & -1 & 0 \\ 1/2 & 0 & -1/2 \end{pmatrix}$	$\begin{pmatrix} 1/2 & 0 & -1/2 \\ 0 & -1 & 0 \\ -1/2 & 0 & -1/2 \end{pmatrix}$	$\begin{pmatrix} 1/2 & 1/2 & 0 \\ 0 & 0 & -1 \\ -1/2 & 1/2 & 0 \end{pmatrix}$	$\begin{pmatrix} -1/2 & 1/2 & 0 \\ 0 & 0 & -1 \\ -1/2 & -1/2 & 0 \end{pmatrix}$

Due to the lattice correspondence between austenite and martensite (*e.g.* for first LCV $\frac{1}{2}[011]_A \parallel [100]_M$, $[\bar{1}00]_A \parallel [010]_M$, $\frac{1}{2}[0\bar{1}1]_A \parallel [001]_M$), $(hkl)_M$ indices of martensitic plane correspondent to the $(HKL)_A$ austenitic plane can be calculated using transformation matrix **R** (see Tab. 7.1) by the following equation:

$$(hkl)_M^T = \boldsymbol{R} * (HKL)_A^T \qquad (7.1)$$

$(hkl)_M^T$ are indices of martensitic plane and $(HKL)_A^T$ are indices of austenitic plane. *T* means transpose of row vector.

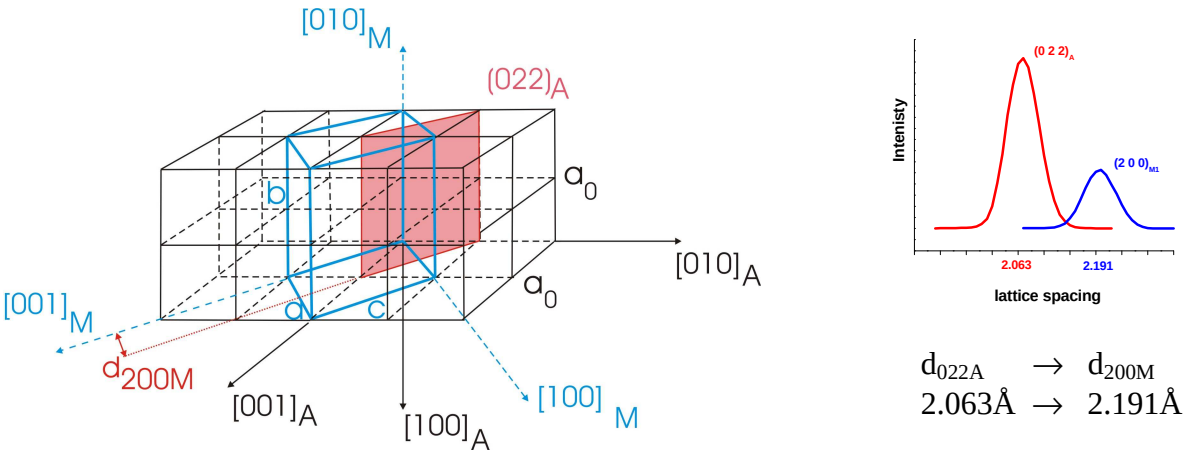

Fig. 7.1: Lattice correspondence between variant 1 (blue) in two unit cells of austenite (black). Austenitic plane $(022)_A$ give rise to the martensitic plane $(200)_M$ in variant 1. The martensitic plane $(200)_M$ is slightly rotated (approximately 2 degrees) with respect to the austenitic $(022)_A$ plane.

Transformation matrices of the six lattice correspondence variants of the 2H martensite are listed in Table 7.1 and the lattice correspondence of the first martensitic variant is suggested in Figure 7.1. The martensite crystal lattice is drawn in blue colour and denoted by M while austenite is in black colour and denoted by A.

Since particular austenitic lattice planes transform to various martensitic planes in distinct martensitic variants, different martensitic variants existing in the prism shaped martensitic sample can be mutually distinguished in the neutron diffraction method providing bulk information. There are, however unique technical problems related with the fact that diffraction geometry of both parent austenite and product martensite must be dealt with when developing the method. This is outlined below.

For example, martensitic planes in six martensitic variants corresponding to austenitic plane $(220)_A$ can be calculated using the equation (7.1) (Table 7.2). The martensitic planes are not exactly parallel to the austenite planes and have lattice spacings different from the original austenitic plane $(220)_A$ due to the Bain distortion characteristic for the cubic to orthorhombic transformation in CuAlNi. It can be seen from Table 7.2 that, the six martensitic variants have three different lattice spacings. Equivalent martensitic planes $\{121\}_M$ in four LCV (1 to 4) have common lattice spacing 2.0096 Å. Martensitic plane $(200)_M$ in LCV 5 have lattice spacing 2.191 Å and plane $(00\bar{2})_M$ in LCV 6 have lattice spacing 2.111 Å. From the diffraction point of view, the martensitic planes will yield 3 different diffraction peaks at different diffraction angles 2θ, if all six martensitic variants exist in the sample. If martensitic peaks $(2\ 0\ 0)_M$ or $(00\bar{2})_M$ are detected, we can conclude that the sample contains variant 5 or variant 6, respectively. From the observation of $(1\ 2\ 1)_M$ peaks, however, we are not able to distinguish which of the martensitic variants 1 to 4 contribute to the intensity of this peak and thus exist in the sample. For this reason, we have to look for other diffraction peaks correspondent (originating from) to other austenitic planes – *e.g.* $(202)_A$ and $(022)_A$. Four martensitic planes correspondent to austenitic plane $(202)_A$ in variants 1, 2, 5, 6 have same lattice spacing 2.0096 Å, $(200)_M$ martensitic plane in variant 3 has lattice spacing 2.191 Å and $(00\bar{2})_M$ martensitic plane in variant 4 has lattice spacing 2.111 Å. This allows us to distinguish between variant 3 and variant 4 (Table 7.2). In the same way, martensitic variants 1 and variant 2 can be distinguished by looking at martensitic peaks originating from austenitic plane $(022)_A$.

Table 7.2: Lattice correspondence martensite planes (LCMP) and their lattice spacings for $(220)_A$, $(202)_A$ and $(022)_A$ austenitic planes.

LCV	LCMP to $(220)_A$ austenitic plane	d_{hkl} martensite [Å]	LCMP to $(202)_A$ austenitic plane	d_{hkl} martensite [Å]	LCMP to $(022)_A$ austenitic plane	d_{hkl} martensite [Å]
1	$(1\bar{2}\bar{1})$	2.00961	$(1\bar{2}1)$	2.00961	(200)	2.191
2	$(\bar{1}\bar{2}1)$	2.00961	$(1\bar{2}\bar{1})$	2.00961	$(00\bar{2})$	2.111
3	$(1\bar{2}1)$	2.00961	(200)	2.191	$(1\bar{2}\bar{1})$	2.00961
4	$(1\bar{2}\bar{1})$	2.00961	$(00\bar{2})$	2.111	$(\bar{1}\bar{2}\bar{1})$	2.00961
5	(200)	2.191	$(1\bar{2}\bar{1})$	2.00961	$(1\bar{2}1)$	2.00961
6	$(00\bar{2})$	2.111	$(\bar{1}\bar{2}1)$	2.00961	$(1\bar{2}\bar{1})$	2.00961

In conclusion, in order to detect and distinguish all six martensitic variants in CuAlNi 2H martensite single crystal sample, we need to search for the $(200)_M$ and $(002)_M$ martensitic peaks correspondent to three different austenitic planes $(220)_A$, $(202)_A$, $(022)_A$. In this way, the variant reorientation processes (twinning) occurring in orthorhombic martensite subjected to mechanical loads can be studied. Martensite variants can be evaluated also from the other austenitic reflections originating from the less symmetric austenitic planes, but the intensity of the martensite reflections is significantly lower comparing to the martensitic reflections obtained from the more symmetrical martensitic planes.

Characterization of all six martensitic variants is only possibly with single crystal diffraction. In powder diffraction you can not probe to different austenitic plane $(220)_A$, $(202)_A$, $(022)_A$, and one observes only three martensitic reflections around one of the $\{220\}_A$ austenitic reflection if all six martensitic variants are presented in the sample (Table 7.2).

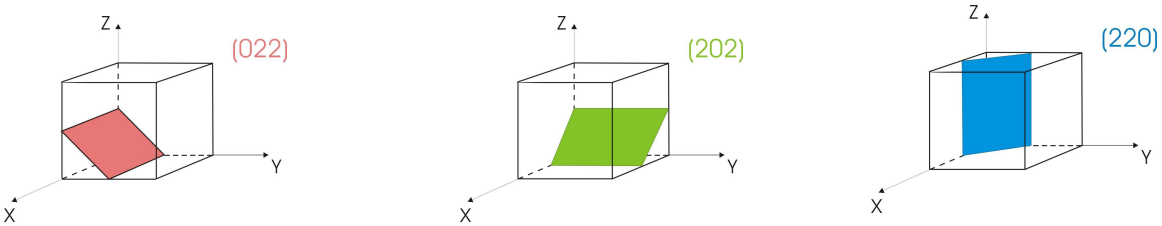

Fig. 7.2: Schematic view of three $\{220\}_A$ austenitic planes in single crystal of cubic austenite.

In single crystal diffraction one can rotate the sample to bring the desired plane to the diffraction, and in such a way by rotating the sample to the position for one of the three austenitic planes $(220)_A$, $(202)_A$, $(022)_A$ the individual martensitic variants can be observed (Fig. 7.2).

7.2 Neutron diffraction studies of reorientation of martensite in CuAlNi single crystal

7.2.1 Experimental material

A single crystal of Cu-13.8Al-4.1Ni (wt %) alloy was used for the in-situ neutron diffractions studies of reorientation of martensite induced by compressive deformation. The transformation temperatures are as follows: M_s = 247K and A_f = 295K. Due to the thermal hysteresis and a shift of A_f due to deformation, such a crystal may exist at room temperature either in the bcc austenite or in the 2H martensite phases. Cuboid specimen (5.7 x 5.5 x 5.2 mm) was spark cut in the austenite phase. The crystal lattice orientations are shown in (Table 7.3)

Table 7.3: Orientation of the sample BA4 in austenite state (direction cosines between hkl crystal and xyz space coordinates aligned with cube axes).

	100	**010**	**001**
Red	0.0057	0.0219	0.9997
Green	0.5586	0.8294	0.0083
Blue	0.8295	-0.5583	-0.0169

7.2.2 Neutron diffraction experiment

The neutron diffraction experiments were carried out at LVR-15 research reactor in Řež using three-circle single crystal diffractometer (Fig. 7.3a).

a)

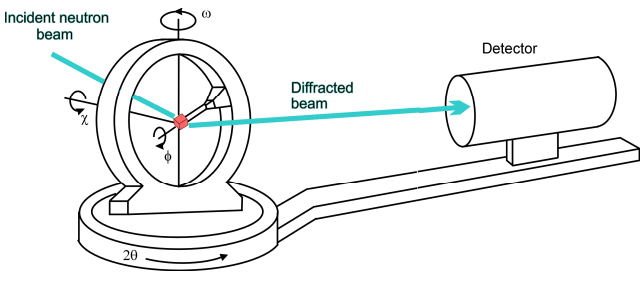

b)

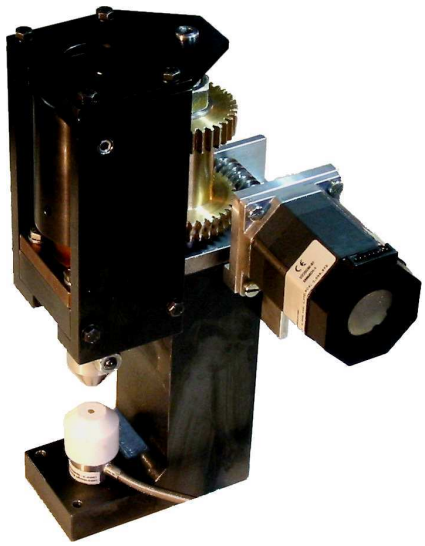

Fig. 7.3 Schematic view of the diffractometer HK-6 (a) and the small deformation rig (b).

Diffractometer was installed at channel HC-6 of the reactor and operates with the neutron wavelength of λ = 1.44 Å provided by Zn (002) mosaic monochromator, which delivers neutron flux of 10^5 n s^{-1} cm^{-2} on the sample position. A ^{3}He counter with Soller collimator is mounted on the mobile detector arm of the diffractometer. A rather high neutron flux and the larger aperture in front of the detector contribute to higher counting intensity. However, it is paid by relatively low resolution of the diffractometer ($\Delta d/d \leq 2.8 \times 10^{-2}$). The diffraction data can be measured in the range from 0° to 81° of the 2θ scattering angle. The diffractometer is equipped with special deformation rig for tension/compression loading up to the force of 10 kN (Fig. 7.3b). The applied force is directly measured by loading cell and macroscopic strain is recorded simultaneously by a digital micrometer. A small deformation rig was specially designed to fit to the Eulerian cradle of the diffractometer. This small deformation rig can be used in strain controlled regime or in a stress controlled regime during the measurement. The diffractometer and the deformation rig are fully PC controlled by the SCP program.

7.2.3 Neutron diffraction and martensitic variants in CuAlNi SMA

Single crystals of CuAlNi martensite were firstly studied in order to check the quality of prepared single crystal. A single crystal sample with orientation given in Table 7.3 was brought from austenite to the martensite by application of compressive deformation on Red face and then turned about 90° to bring the normal of the Blue face parallel with the stress loading direction. Then the compression load was applied on this face and the reorientation of martensite was observed. The stress-strain curve obtained in INSTRON deformation machine from this reorientation process (compressive deformation on B face) is shown in Fig. 7.4.

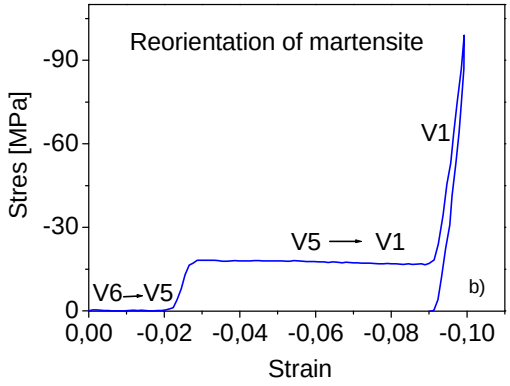

Fig. 7.4: Stress-strain curve measured during the deformation on B face.

The measured dimensions of the prism shape of martensitic sample after deformation indicates, that the sample is not true single crystal of martensite (one martensitic variant). In order to confirm or to rebut this fact the martensitic prism sample after the deformation in INSTRON machine was placed to the three-circle single crystal neutron diffractometer and with the above-mentioned neutron diffraction method studied for the presence of individual martensitic variants. The obtained results are shown in Fig. 7.5.

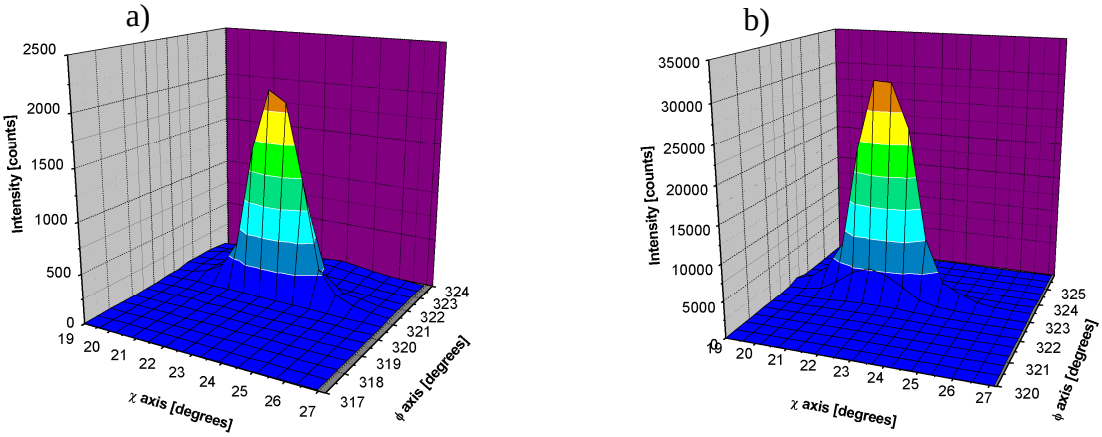

Fig. 7.5: Intensity measurement of $(002)_M$ martensitic reflection as a function of crystal rotation angles ϕ and χ (a) and martensitic reflection $(200)_M$ (b).

The $(200)_M$ and $(002)_M$ martensitic reflections were observed at the position of $(220)_A$ austenitic plane. From the Table 7.2 it is seen that these reflections are related to the variant 5 and variant 6. The $(200)_M$ martensitic reflection corresponds to the variant 5 and $(002)_M$ reflection to the variant 6. Sample is mainly in variant 5 but also the small fraction (~ 10%) of variant 6 is present in the prism sample. These martensitic variants are joined together through the compound type twinning because only this type of twinnng can be formed between these two variants [20]. The neutron diffraction confirmed that martensitic prism sample after the reorientation consists of two martensitic variants. It means that it is not perfect single crystal of martensite. In order to obtain detail information about the twinning processes the in-situ neutron diffraction experiment was performed on CuAlNi sample. The obtained results are presented in the next chapter.

7.3 *In situ* neutron diffraction studies of reorientation processes in CuAlNi single crystals induced by compressive deformation

Stress induced cubic to orthorhombic martensitic transformation upon mechanical loading of the cuboid specimen in austenite phase at room temperature (compression on the red face) was activated at relatively large stress 100MPa, progress of the transformation is accompanied by unloading in position controlled experiment (Fig. 7.6a).

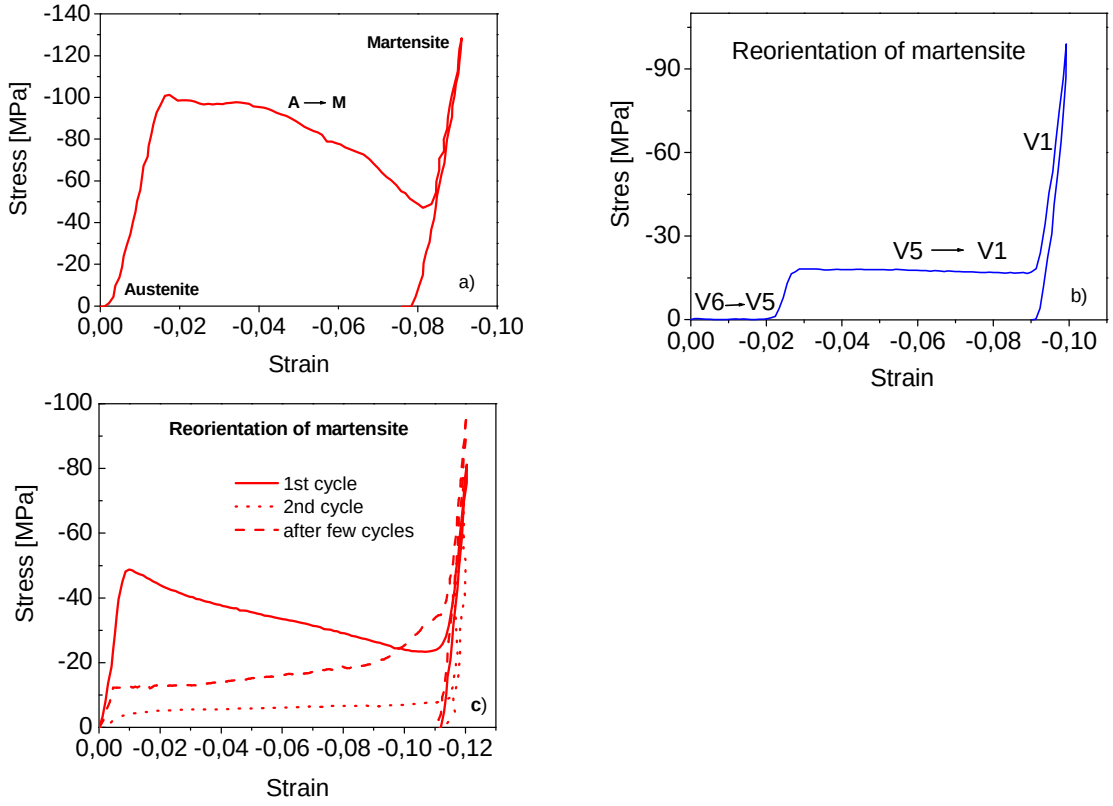

Fig. 7.6: Stress induced martensitic transformation BA4 (a) and reorientation of martensite during the deformation on blue face (two-stage stress-strain curve) (b) and then reorientation on red face in martensite (c).

Then the sample was turned 90 degrees and compressed in the other direction (on the blue face), turned again and compressed on the red face. Sample responses upon subsequent repetitive compression loadings at room temperature on the red and blue faces in the martensite state are due to the reorientation of the orthorhombic 2H martensite. Stress-strain curve measured during compression on the blue face (Fig. 7.6b) evidences that, in this case, there are two subsequent distinct twinning processes taking place. Sample for in-situ neutron diffraction studies during martensite reorientation was prepared by such sequence of compression deformations on different faces of the prism shape sample. The sample was then placed into the small deformation rig installed on 3-axis neutron diffractometer. Compression loading test on the blue face was run (Fig. 7.8b) and neutron diffraction data (Fig. 7.7) were

collected in stopovers (points 1 to 6 in Fig. 7.8b). Only part of the first plateau on the stress-strain curve (well seen in Fig. 7.6b) was observed, since the reorientation stress was too small (smaller than 1 MPa) and the reorientation processes were activated already during the manipulation with the sample prior the experiment.

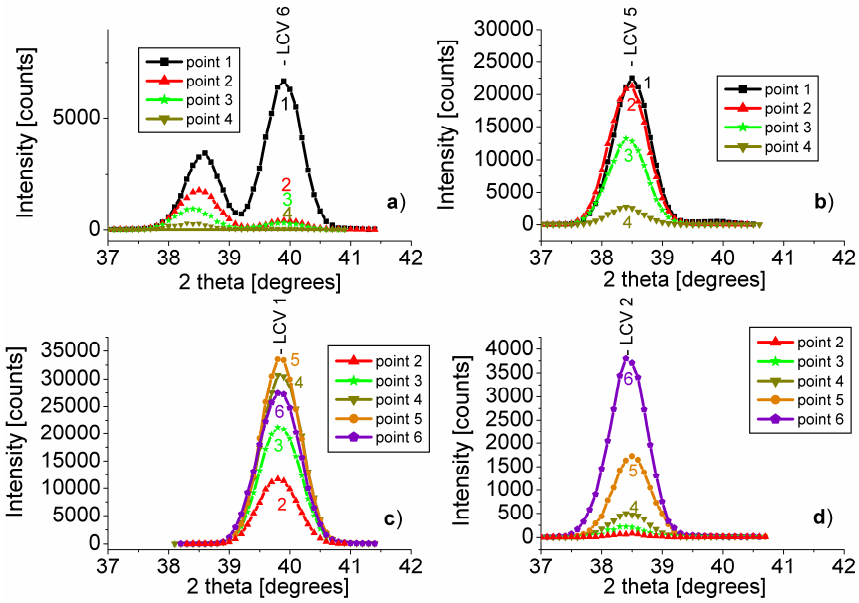

Fig. 7.7: Neutron diffraction profiles measured during compression test on martensite sample (points in Fig. 4b). Variant 6 (LCV 6) - peak $(002)_M$ at $2\theta = 39.9°$ (a), variant 5 (LCV5) - peak $(\bar{2}00)_M$ at $2\theta = 38.4°$ (b), variant 1 (LCV 1) - peak $(00\bar{2})_M$ at $2\theta = 39.9°$ (c), variant 2 (LCV 2) - peak $(\bar{2}00)_M$ at $2\theta = 38.4°$ (d).

The evidence for the existence of martensitic variants and twinning processes during the compression test was drawn from the neutron diffraction data (Fig. 7.7) using the principles outlined in section 7.1. Particularly, changes of the integral intensities of the diffraction peaks from the martensitic planes (Fig. 7.8a) corresponding to the $(\bar{2}\bar{2}0)_A$ and $(02\bar{2})_A$ austenitic planes are taken as measures for the changes of the sample volumes in particular martensite variants.

Variant 6 and variant 5 (Fig.7.7a, b) were detected from martensitic reflections $(\bar{2}00)_M$ and $(002)_M$ (both originating from $(\bar{2}\bar{2}0)_A$ austenitic plane), respectively. Different diffraction profiles were measured in different geometry with respect to the incoming neutron beam (different omega angles). For example, in Fig. 7.7a we are concerned only about the right side martensitic peak $(002)_M$ of variant 6 at the $2\theta = 39.9°$. The diffraction peak $(\bar{2}00)_M$ on the left side corresponds to the variant 5. It appears because the variant 5 exist in the sample as well, but the diffraction geometry has been chosen in such a way that the integral intensity of

the V6 is at its maximum. The alignment for maximum intensity of the variant 5 has been used to obtain Fig. 7.7b. Martensitic variants 1 and variant 2 (Fig. 7.7c, d) were detected from martensitic reflections $(00\bar{2})_M$ and $(\bar{2}00)_M$ (both originating from $(02\bar{2})_A$ austenitic plane), respectively.

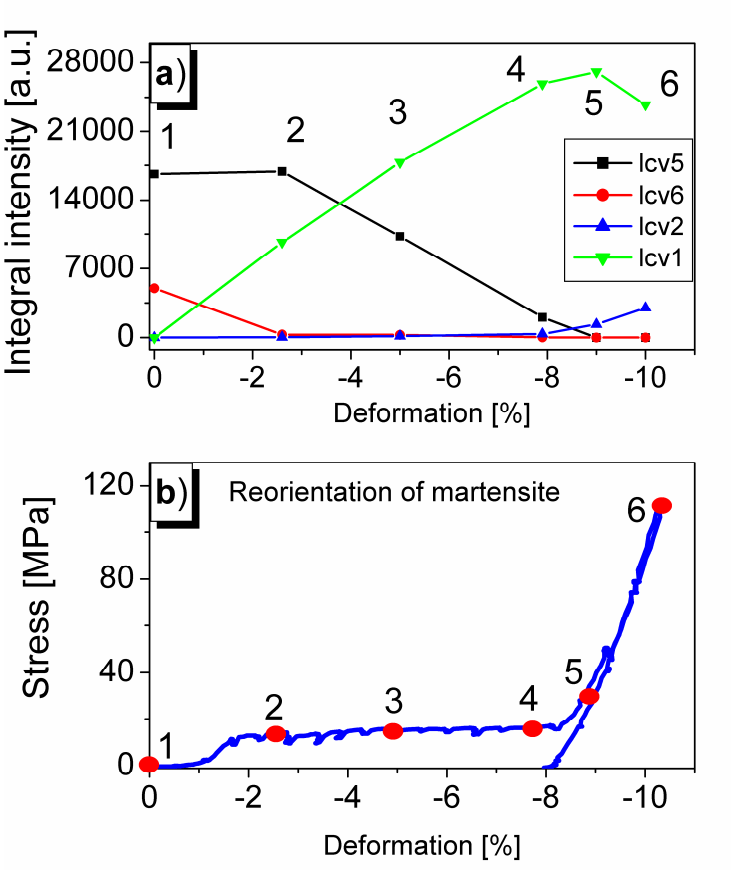

Fig. 7.8: a) Variation of integral intensities of 4 martensite diffraction peaks (a) measured during compression test (points 1 to 6 on the stress-strain curve (b) on martensite prism specimen (compression on the blue face).

7.3.1 Summary:

The evolution of the integral intensities during the compression test is plotted in Fig. 7.8a. One can clearly see that the sample was initially mainly in the variant 5 and partially also the variant 6 was present. Variants 5 and 6 are compound twins, as confirmed by theoretical calculation [20] and by the analysis of the twinning plane traces observed on the prism surface by optical microscopy. In the early stage of the test (between points 1 and 2 on the stress-strain curve), the variant 6 practically disappeared (most likely transformed into the variant 5). In point 2 the variant 5 already started to transform into the variant 1 and this process dominated the second plateau at larger stress 20MPa (points 2 to 4). Variant 5 and variant 1

are type II twins. Just beyond the end of the second plateau (point 5), the sample contains mainly the variant 1 and a small fraction of variant 2 that appeared near the end of the plateau. The subsequent deformation in the elastic region (from point 5 to 6) leads surprisingly to the decrease of the volume fraction of the major variant 1 and increase of volume fraction of variant 2. These two variants (variant 1 and variant 2) are compound twins. The variant 2 remains significantly present in the sample even after final unloading.

Several conclusions can be drawn from the presented results. First, the sample was not martensite variant single crystal prior the test. Since the reorientation stress for compound twinning can be very low, it is not trivial to bring the prism into a single variant state and keep it in it. Overloading in compression does not help, since it favours the second unwanted variant (variant 2). Best approach to obtain the martensite variant single crystal is to compress the sample to the end of the first or second plateau (here, only 1 variant exist in the sample) and unload. Second, in the reorientation plateau (between the point 2 and 5), the integral intensities of variants 5 and 1 changes linearly with the external strain (Fig. 7.8a). This is interpreted as a linear switching of the volume fractions of variants 5 and 1 due to type II twinning in the second stage of the stress-strain curve. Third conclusion concerns the last part of the stress-strain curve (between points 5 and 6), where only the elastic deformation would be expected. Diffraction experiment shows that this is clearly not the case. The integral intensity of the observed peaks changes suggesting significant activity of the twinning processes (compound twinning between variants 1 and 2) proceeding this time at relatively large compression stresses. It is believed that this is due to the fact that the prism samples undergo huge shape change visible by naked eye [82] and the deformation state in the sample does not correspond to the uniaxial compression anymore during the final “elastic” loading.

Reorientation processes during compression deformation of CuAlNi martensite variant single crystal were investigated by neutron diffraction single crystal method. This method allows to detect and distinguish the presence of individual lattice correspondence variants of martensite phase as well as to follow the activity of twinning processes during the deformation test on the martensite variant single crystal. It was found that, due to the easiness by which compound twinning is activated, it is not trivial to bring and mainly to keep the martensite sample in the single variant state simply by the application of compression stress.

7.4 Stress-induced martensitic transformation in CuAlNi single crystals

The aim of this experiment was to determine the mechanism of stress-induced martensitic transformation in CuAlNi single crystal. During the martensitic transformation two types of

martensite appear. Firstly the monoclinic $\beta`_1$ martensite, which is stable only under the stress and vanishes in stress free sample. The second martensite is the 2H orthorhombic martensite which is stable after the unloading. From optical photographs it is not possible to identify the individual martensitic variants, which appear during the transformation. There is not clear evidence whether the habit plane variant of 2H orthorhombic martensite is created or the sample transforms directly to one martensitic variant. In my work I tried to use the single crystal neutron diffraction method in order to identify the martensites created during the stress martensitic transformation. The diffraction technique is capable to see individual martensitic variants of different phases and neutrons can penetrate deeply into the material, so these characteristics can help us to obtain reliable information about the processes occurring during the stress induced martensitic transformation in CuAlNi single crystal.

7.4.1 Experimental material

A single crystal of Cu-13.8Al-4.1Ni (wt %) alloy was used for the in-situ neutron diffraction studies of stress - induced martensitic transformation. It is the same alloy as was used in section 7.2 for in-situ neutron diffraction studies of reorientation of martensite. Crystal structures and lattice parameters of austenite, 2H orthorhombic martensite and $\beta`_1$ monoclinic martensite are listed in Table 7.4. Deformation tests were performed in position controlled regime.

Table 7.4: Lattice parameters of austenite and 2H orthorhombic and $\beta`_1$ monoclinic martensite in CuAlNi single crystal

Phase	**Lattice parameters**	**Space group**
Austenite	a_0 = 5.836 Å	Fm3m
2H martensite	a = 4.382 Å, b = 5.356 Å, c = 4.222 Å	Pnmm
$\beta`_1$ martensite	a = 4.382 Å, b = 5.356 Å, c = 38 Å, β = 88.4°	I2/m

7.4.2 Experimental technique for studying the stress-induced martensitic transformation by neutron diffraction

During the stress-induced martensitic transformation two different kinds of martensite appear monoclinic $\beta`_1$ martensite and orthorhombic 2H martensite. The principles of the determination of individual martensitic variants of 2H orthorhombic martensite by neutron diffraction technique are explained in section 7.1. The way, how to identify the monoclinic martensite will be described in this chapter.

From the symmetry reason between the cubic structure and monoclinic structure there are twelve lattice correspondence martensitic variants of β'_1 martensite (table 7.5). Due to the lattice correspondence between austenite and martensite (table 7.5) it is possible to calculate the corresponding martensitic plane to individual austenitic plane for all 12 martensitic variants using the equation 7.1. It means to obtain twelve martensitic planes to each austenitic plane.

Table 7.5: Lattice correspondence variants of monoclinic 18R martensite.

LCV	**$[100]_M$**	**$[010]_M$**	**$[001]_M$**
1	$\frac{1}{2}[011]$	$[\bar{1}00]$	$[0\bar{4}5]$
2	$\frac{1}{2}[0\bar{1}\bar{1}]$	$[\bar{1}00]$	$[0\bar{5}4]$
3	$\frac{1}{2}[0\bar{1}1]$	$[\bar{1}00]$	$[0\bar{5}\bar{4}]$
4	$\frac{1}{2}[0\bar{1}1]$	$[\bar{1}00]$	$[045]$
5	$\frac{1}{2}[101]$	$[0\bar{1}0]$	$[50\bar{4}]$
6	$\frac{1}{2}[\bar{1}0\bar{1}]$	$[0\bar{1}0]$	$[40\bar{5}]$
7	$\frac{1}{2}[10\bar{1}]$	$[0\bar{1}0]$	$[\bar{4}0\bar{5}]$
8	$\frac{1}{2}[10\bar{1}]$	$[0\bar{1}0]$	$[504]$
9	$\frac{1}{2}[110]$	$[00\bar{1}]$	$[\bar{4}50]$
10	$\frac{1}{2}[\bar{1}\bar{1}0]$	$[00\bar{1}]$	$[\bar{5}40]$
11	$\frac{1}{2}[\bar{1}10]$	$[00\bar{1}]$	$[\bar{5}\bar{4}0]$
12	$\frac{1}{2}[\bar{1}10]$	$[00\bar{1}]$	$[450]$

Martensitic planes in all twelve martensitic variants corresponding to $(022)_A$ austenitic plane (table 7.6) can be calculated using equation 7.1. The martensitic planes are not exactly parallel to the austenite planes and have lattice spacings different from the original austenitic plane $(022)_A$. Among these twelve martensitic variants there are four different groups of lattice spacings (Table 7.6) *i.e.* 2.1827 Å, 2.1103 Å, 2.0472 Å, 1.9706 Å. From the diffraction point of view the martensitic planes will yield four diffraction peaks at different diffraction angles 2θ, if all twelve martensitic variants exists in the sample. From this diffraction peaks we can not conclude which martensitic variants exist in the sample, because always at least two martensitic planes have the same lattice spacing. In order to check how many variants are in

the sample the so called omega scan has to be performed. It means that the detector is fixed at appropriate 2θ angle and the sample is rotated.

Table 7.6: Lattice correspondence martensitic planes (LCMP) to $(022)_A$ austenitic planes together with the lattice spacing and diffraction angle 2 θ calculated for λ = 1.66 Å.

LCV	LCMP to $(022)_A$ austenitic plane	Lattice spacing [Å]	Diffraction angle 2 θ [degrees]
1	$(2\,0\,2)_M$	2.1827	44,69
2	$(0\,0\,\overline{18})_M$	2.1103	46,32
3	$(\bar{2}\,0\,\bar{2})_M$	2.1827	44,69
4	$(0\,0\,18)_M$	2.1103	46,32
5	$(1\,\bar{2}\,\bar{8})_M$	2.0472	47,83
6	$(\bar{1}\,\bar{2}\,\overline{10})_M$	1.9706	49,82
7	$(\bar{1}\,2\,\overline{10})_M$	1.9706	49,82
8	$(\bar{1}\,2\,8)_M$	2.0472	47,84
9	$(1\,\bar{2}\,10)_M$	1.9706	49,82
10	$(1\,\bar{2}\,\bar{8})_M$	2.0472	47,84
11	$(\bar{1}\,2\,8)_M$	2.0472	47,84
12	$(1\,2\,10)_M$	1.9706	49,82

This omega scan can visualize the other martensitic reflection even if they have the same lattice spacing because these martensitic planes are slightly rotated to each other and in this way the individual martensitic variants can be characterized.

During the stress-induced martensitic transformation also the 2H orthorhombic martensite appears and as mentioned in section 7.1 we determine these orthorhombic martensite variants from martensite reflections of corresponding martensitic planes to three austenitic planes $(220)_A$, $(202)_A$ and $(022)_A$. For these three austenitic planes corresponding martensitic planes in orthorhombic martensite have lattice spacings very close to the lattice spacings of monoclinic β'_1 martensite. These can be seen by comparing Table 7.2 (2H martensite) and Table 7.6 (β'_1 monoclinic) where corresponding martensitic planes for both types of martensites to $(022)_A$ austenitic plane are shown. The neutron diffraction data were collected

using counter detector. During the experiment martensitic reflections moves in the ω – space because the corresponding planes rotates during the transformation. In order to study this transformation efficiently the 2D detector has to be used.

7.4.3 Optical studies of stress-induced martensitic transformation induced by compression deformation

Stress – induced martensitic transformation of CuAlNi single crystal sample from cubic structure was observed upon compression deformation at room temperature Fig. 7.9. Martensitic transformation was activated at relatively large stress 100 MPa. The deformation induced by martensitic trasnformation is ~ 8%. After unloading the sample is in γ'_1 orthorhombic martensite.

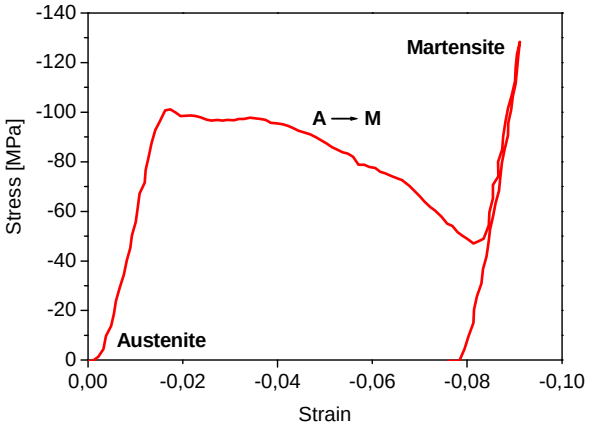

Fig. 7.9: Stress induced martensitic transformation of CuAlNi single crystal of martensite.

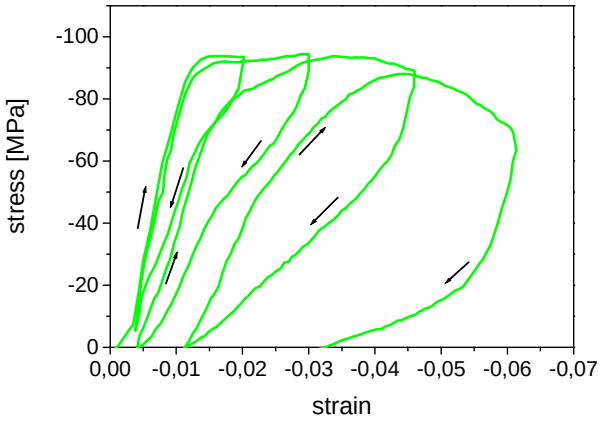

Fig. 7.10: Loading and unloading cycles during the stress-induced martensite transformation.

In order to study the morphology of the stress induced transformation optical photographs were taken during the stress induced martensitic transformation Fig. 7.11. Firstly it is clearly seen that the sharp thin needles appear in the volume of the sample (Fig. 7.11b). These needles have typical morphology of the monoclinic β'_1 martensite as observed by [85]. After further loading the interface of γ'_1 martensite appear and growth from the mixture of austenite and β'_1 martensite (Fig. 7.11c) until the whole sample is finally in the 2H orthorhombic martensite (Fig. 7.11d). Monoclinic β'_1 martensite should not appear in this temperature range [86]. The reason for the appearing of β'_1 martensite is that it is very easily nucleated. Transformation strain for (001) direction in compression for the most favored β'_1 martensite variant is 7.8% and for the γ'_1 martensite is 8.4%. That is the reason why the γ'_1 martensite will be preferred and stable after the unloading. β'_1 martensite is stable only under the applied stress. Without applied stress the β'_1 martensite disappear (reverse transformation to austenite occurs). This is supported indirectly through the stress-strain curves measurements (Fig.

7.10), where the sample was loaded to the stress plateau region and than unloaded in few cycles. As it can be seen the induced deformation is recovered back. In order to obtain detail information about the mechanism and microstructure during the stress induced martensitic transformation, *in situ* neutron diffraction experiment was performed and is presented in the next chapter.

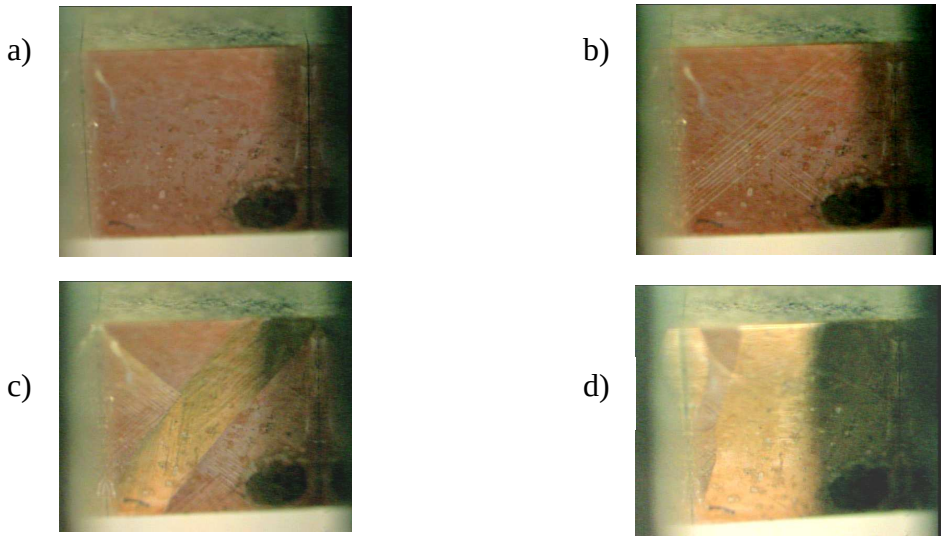

Fig. 7.11: Optical photographs of stress-induced martensite transformation. CuAlNi sample in austenite (a), needles of $\beta`_1$ martensite (b), band of 2H martensite (c) and finally sample in 2H martensite (d).

7.4.4 In-situ neutron diffraction studies of stress-induced martensitic transformation in CuAlNi single crystal

Neutron diffraction experiments were performed on single crystal diffractometer HK8 in NPI Řež. Diffractometer is equipped with the small deformation rig and the single ^{3}He counter. The monochromatic wavelength used in this measurement was λ = 1.66 Å. Single crystal cuboid specimen was mounted with $[001]_A$ cubic (austenite) axis parallel to the stress direction. The neutron diffraction data were measured in stopovers (points 1 to 7) at the stress-strain curve (Fig. 7.12).

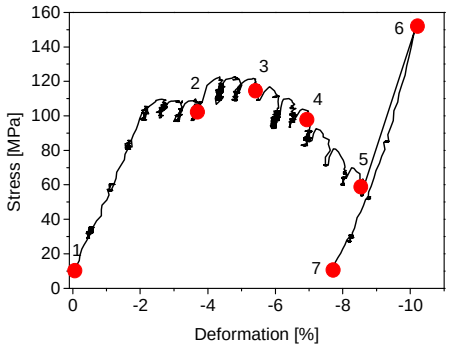

Fig. 7.12: Stress-induced martensitic transformation in CuAlNi single crystal and the points at which the neutron diffraction data were measured.

Stress induced martensitic transformation was studied by following two austenitic reflections $(220)_A$ and $(202)_A$ and corresponding martensitic reflections from these two austenitic planes. Principles of evaluation of 2H orthorhombic martensite variants are explained in section 7.1 and for the $\beta`_1$ monoclinic martensite variants in section 7.4.2. As was pointed out in the introduction the main reason to study this martensitic transformation was to evaluate whether during the martensitic transformation the habit plane martensitic variants of 2H martensite appears or the transformation proceeds directly to the detwinned one martensitic variant of 2H martensite. As it is seen from the section 7.1 to evaluate all six orthorhombic martensitic variants we need to look for the martensitic reflections from the three different austenitic reflections $(220)_A$, $(202)_A$ and $(022)_A$. In our study of stress induced martensitic transformation due to the constraints of deformations rig we were able to follow only the two austenitic planes $(220)_A$ and $(202)_A$ and the corresponding martensitic planes from them in the same time. In such a way we are able to observe four 2H orthorhombic martensitic variants from total amount of six variants. In order to find out whether the other two martensitic variants appear during the martensitic transformation we performed the same experiment with the configuration that allows us to see the $(022)_A$ austenitic reflection and corresponding martensitic reflection which appears during the transformation. We could do this because the stress-induced martensitic transformation is reproducible at the same conditions (temperature, pressure). Any of the $(200)_{2H}$ or $(002)_{2H}$ reflection of the 2H orthorhombic martensite has been observed from $(022)_A$ austenitic plane. This means that sample does not contain martensitic variant 3 and 4.

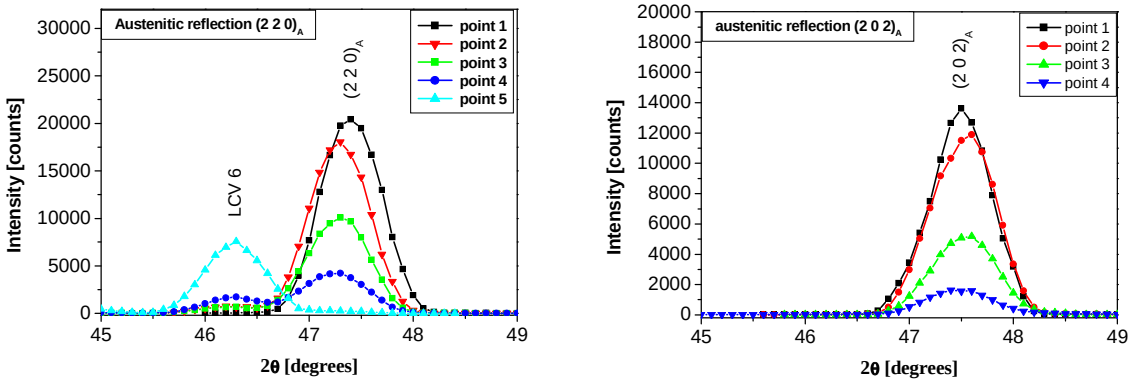

Fig. 7.13: Austenitic reflections $(220)_A$ (a) and $(202)_A$ (b) measured at different points of the stress-strain curve.

Fig. 7.13 shows the measured intensities of the austenitic reflections $(220)_A$ and $(202)_A$ during the martensitic transformation. Intensities of both austenitic reflections decrease during the

loading, which is clear evidence for the occurring of martensitic transformation. The left peak in Fig. 7.13a corresponds to the martensite phase, which nucleates and grows during the transformation. During the transformation, two different martensites appear - orthorhombic and monoclinic, and, as was mentioned above, the corresponding planes of both martensites have similar lattice spacings see (table 7.2 and 7.6). The $(\bar{1}\,2\,\overline{10})_{\beta`1}$ monoclinic plane with lattice spacing 1.9706 Å is one of the planes that is not overlapped with other orthorhombic martensitic reflections. From this one can clearly conclude that the sample contains monoclinic martensite variants (Fig. 7.14).

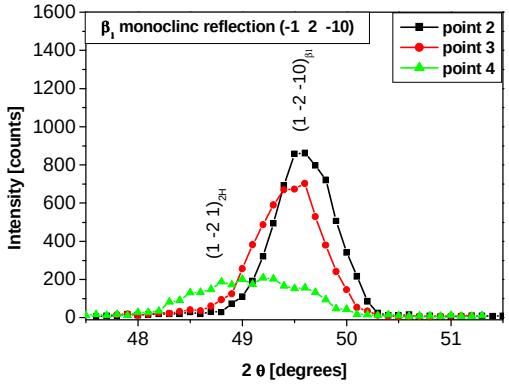

Fig. 7.14: Monoclinic martensite reflection $(\bar{1}\,2\,\overline{10})_{\beta`1}$ and $(1\bar{2}1)_{2H}$ orthorhombic reflection.

The evidence for the existence of 2H martensitic variants is made from the presence of the $(200)_{2H}$ and $(002)_{2H}$ orthorhombic martensitic reflections which are corresponding to the $\{220\}_A$ austenitic planes. The obtained results are shown in Fig. 7.15. Martensitic variant 6 is shown in Fig. 7.15a together with the $(220)_A$ austenitic reflection. Variant 5 is shown in Fig. 7.15b and also the variant 6 and $(220)_A$ austenitic reflection appear because they are also present in the sample.

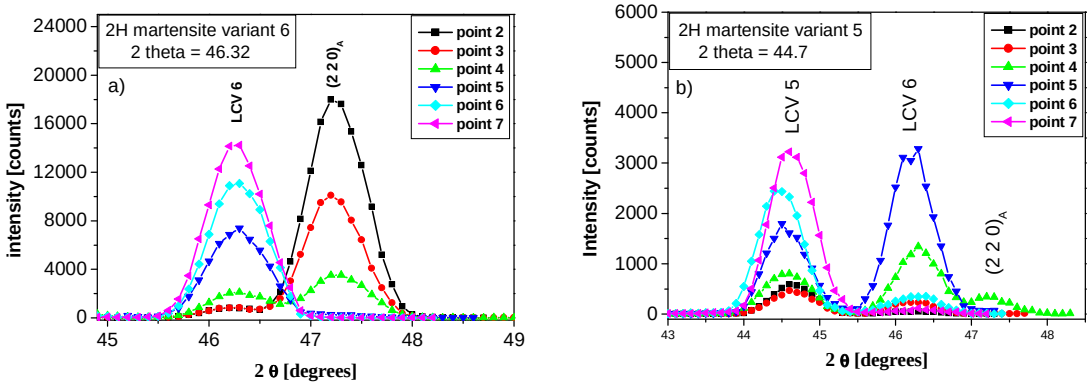

Fig. 7.15: Neutron diffraction data measured from $(220)_A$ austenitic plane. 2H martensite variant 6 (a) and martensite variant 5 (b) were observed in the sample.

During the stress induced martensitic transformation some $\beta`_1$ martensite reflections also appear close to the $(200)_{2H}$, $(002)_{2H}$ reflections this fact is confirmed by the omega scan at the $2\theta = 44.7°$ for the $(200)_{2H}$ reflection see Fig. 7.16. For the detailed study, the 2D detector is needed.

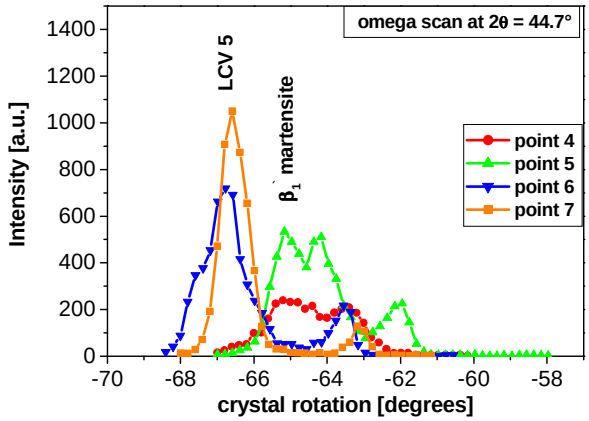

Fig. 7.16 Intensity measurement as a function of crystal rotation for 2H martensite $(200)_{2H}$ reflection.

The evolution of integral intensities of austenite $(220)_A$ reflection, $(200)_{2H}$, $(002)_{2H}$ 2H orthorhombic martensite reflections and $(\bar{1}\,2\,\overline{10})_{\beta`1}$ reflection of monoclinic martensite as a function of transformation strain induced during the compressive deformation is shown in Fig. 7.17.

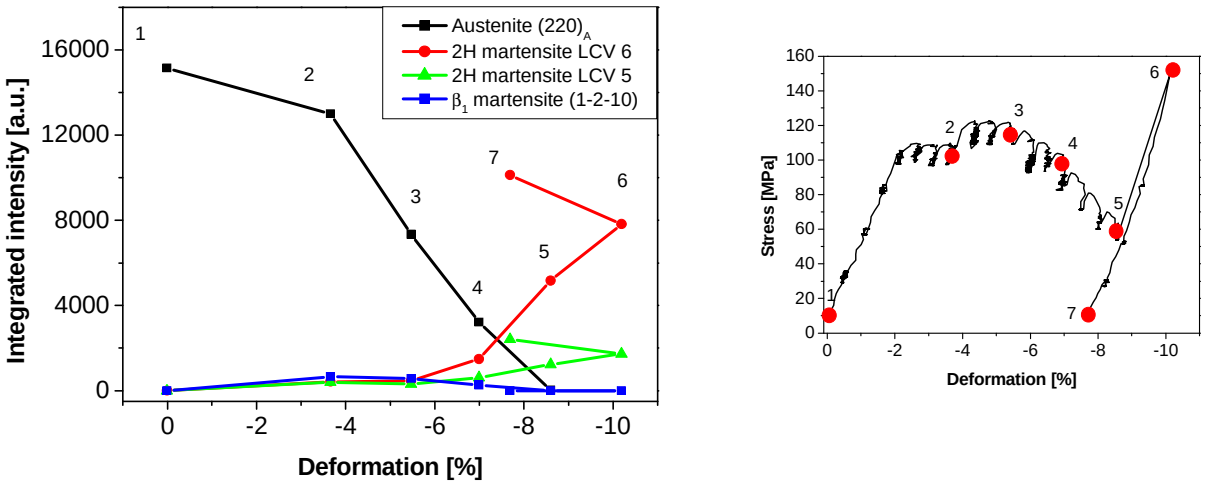

Fig. 7.17: Intensity changes of austenitic $(220)_A$ reflection, $(200)_{2H}$ martensite (LCV 5), $(002)_{2H}$ martensite (LCV 6) and monoclinic $(\bar{1}\,2\,\overline{10})_{\beta`1}$ during the stress-induced martensitic transformation (a) measured at points depicted on stress-strain curve (b)

Intensity of $(220)_A$ austenitic reflection slightly decreases to point 2. At this point the $(\bar{1}\,2\,\overline{10})_{\beta`1}$ monoclinic reflection appears as well as $(200)_{2H}$ and $(002)_{2H}$ martensite reflections

appear. These 2H reflections correspond to the orthorhombic martensite variant 5 and variant 6, respectively. Further loading to point 3 causes that the intensity of austenitic $(220)_A$ reflection decreases and the $(\bar{1}\,2\,\overline{10})_{\beta`1}$ monoclinic reflection slightly decreases. The intensities of $(200)_{2H}$ and $(002)_{2H}$ martensite reflections have not changed significantly. From point 3 there is significant increase in the intensity of $(200)_{2H}$ martensite reflection and also the $(002)_{2H}$ 2H martensite reflection increases. Intensity of monoclinic reflection $(\bar{1}\,2\,\overline{10})_{\beta`1}$ deceases and it totally disappear in point 5 of the stress-strain curve. Both martensite reflections $(200)_{2H}$ and $(002)_{2H}$ increase their intensity during the loading in elastic region and also during the unloading. The increase in the intensity of both martensite reflections during unloading is observed also in the neutron diffraction experiments performed on polycrystalline NiTi shape memory alloys samples [87].

From the measured data during the stress induced martensitic transformation it can be concluded that firstly the monoclinic $\beta`_1$ martensite appears in the sample (reflection $(\bar{1}\,2\,\overline{10})_{\beta`1}$). This conclusion is also supported by optical photographs taken during the stress induced martensitic transformation (see section 7.4.3). The monoclinic martensite is present in the sample for whole transformation process and disappears at the end of the stress plateau. Two 2H orthorhombic martensite variants (variants 5 and variant 6) were observed during the martensitic transformation. These variants are joined together through the compound type twinning. Volume fraction of orthorhombic martensite variant 6 is significantly larger than the volume fraction of orthorhombic variant 5. No other orthorhombic variant was observed during the stress induced martensitic transformation. From this observation it can be concluded that the transformation proceeds to the mainly orthorhombic martensitic variant 6 and small volume fraction of variant 5. These two variants are compound twins. Theoretical predictions [21] say that it is not possible for CuAlNi shape memory alloy to form the interface between cubic austenite and orthorhombic martensite, which contains the compound type twinning. In our experiment we observed compound type twinning during the stress induced martensitic transformation. Appearance of compound type twining can be explained through the fact that firstly the monoclinic martensite $\beta`_1$ appears and then the orthorhombic martensite. So the initial structure is not pure austenite (cubic) but it is the mixture of the cubic austenite and monoclinic martensite.

It was also observed that in the elastic region of the stress-strain curve the volume fraction of both orthorhombic martensite variants increase due to the transformation of $\beta`_1$ martensite variants to the 2H martensite variants (Fig. 7.16).

7.4.5 Summary:

Stress induced martensitic transformation in CuAlNi single crystal was studied *in situ* by neutron diffraction technique. It was observed that the $\beta`_1$ martensite is present in the sample during the whole transformation process and that the compound type twin 2H martensite variants appear. Finally, after the unloading, the sample consist of mixture of 2H martensite variant 5 and variant 6 which are compound type twins. Thanks to the neutrons properties the compound type twinning during stress induced martensitic transformation in CuAlNi single crystal was observed for the first time.

8. Magnetic shape memory effect in NiMnGa single crystal

8.1 Stress induced martensite variant reorientation in magnetic shape memory NiMnGa single crystal studied by neutron diffraction

NiMnGa is typical example of ferromagnetic shape memory alloy, which exhibits large deformations (up to 6 %) induced by magnetic field or by application of stress in martensitic state. These large deformations are caused by reorientation of martensite through the twin boundary motion [27]. The largest induced strains are observed if the sample is in single variant state and maximal strain is limited by crystallography of twinning in NiMnGa with tetragonal structure: $\varepsilon_0 = 1 - c/a$, where a and c are the lattice parameters of the martensite. In most cases, the transformation strain obtained from the experimentally measured stress-strain curve is lower than the maximal transformation strain ε_0. This can imply that the reorientation process in NiMnGa single crystal is not completed.

Martensitic transformation and reorientation in Ni-Mn-Ga single crystal under compression was also studied by ultrasonic method [88]. Large acoustic emission was observed during reorientation at low stress, about 2 MPa. The activity decreased in higher stress but it did not disappear up to 60 MPa. During the unloading the acoustic signal was also measured. The observed acoustic activity was ascribed to additional movements of twin interfaces occurred during further loading and unloading.

In this chapter, the first *in situ* measurement of stress-induced reorientation process in magnetic shape memory (MSM) Ni-Mn-Ga single crystal by neutron diffraction technique is presented. Due to the high penetration depth of the neutrons, the obtained data are from the whole volume of the sample and in such way reliable information can be obtained about the twinning processes and completeness of the reorientation of martensite in MSM NiMnGa single crystal.

8.1.1 Experimental material

A single crystal of $Ni_{49.7}Mn_{29.3}Ga_{21}$ magnetic shape memory alloy was cut from ingot produced by AdaptaMat Oy. The transformation temperatures were determined by DSC as Ms = 305 K and M_f = 301 K and Curie temperature T_C = 375 K. Rectangular specimen with dimensions 5x5x10 mm was cut along {100} faces of the austenite structure (Fig. 8.1). For easy manipulation the three different faces are denoted as R, B, G (Fig. 8.1).

Fig. 8.1: Denotation of three different faces of cuboid sample.

The parent phase of NiMnGa single crystal is cubic $L2_1$ structure with lattice parameter a = 0.584 nm. The structure of the martensite is tetragonal with five-layered modulation (5M) [42]. The lattice parameters of 5M martensite were measured by x-ray as $a_M = b_M$ = 0.595 nm, c_M = 0.561 nm with easy axis magnetization along the short c - axis of martensite. A contactless laser dilatometer was used for the measurement of strain induced by magnetic field in NiMnGa single crystal. The experimental arrangement is described in detail in [89].

The single crystal neutron diffraction experiment was carried out in NPI Řež on a three circle neutron diffractometer with monochromatic wavelength λ = 0.17 nm equipped with a miniature screw driven deformation rig mounted on a two axis cradle and a single ^{3}He counter.

8.1.2 Neutron diffraction method and tetragonal martensite of SMA

In the previous chapters, the neutron diffraction technique for the studies of martensite in single crystal shape memory alloys (SMA) was presented for orthorhombic and monoclinic martensite in CuAlNi single crystal SMA. In this section, the method was adjusted for the studies of tetragonal martensite. In the next paragraph the principles of this method are explained.

Due to the difference in crystal symmetry between the cubic structure of austenite and tetragonal martensite, there are three lattice correspondence variants of martensite. These

martensitic variants have the same tetragonal structure but different orientation with respect to the parent austenitic phase. The lattice correspondence between cubic austenite and tetragonal martensite can be chosen in two different ways. In our case, we use lattice correspondence where the crystallographic axes of cubic lattice are parallel to the crystallographic axis of tetragonal martensite.

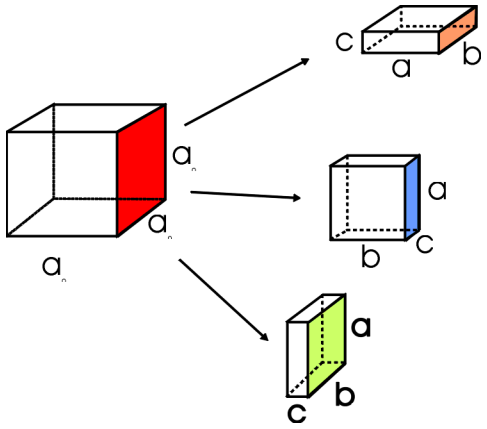

Fig. 8.2: Schematic view of the three tetragonal martensitic variants of NiMnGa single crystal

The schemes of the three lattice correspondence variants of the tetragonal martensite are depicted in Fig. 8.2. Each martensitic variant is described by transformation matrix ***R*** (see Table 8.1).

Table 8.1: Transformation matrices for planes A → M.

LCV	1	2	3
Transformation matrix **R** for planes A → M	$\begin{pmatrix} 1 & 0 & 0 \\ 0 & 1 & 0 \\ 0 & 0 & 1 \end{pmatrix}$	$\begin{pmatrix} 0 & 0 & 1 \\ 1 & 0 & 0 \\ 0 & 1 & 0 \end{pmatrix}$	$\begin{pmatrix} 0 & 1 & 0 \\ 0 & 0 & 1 \\ 1 & 0 & 0 \end{pmatrix}$

Using this transformation matrix ***R*** it is possible to calculate corresponding martensitic plane to each austenitic plane:

$$(hkl)_M{}^T = \boldsymbol{R} * (HKL)_A{}^T \qquad (8.1)$$

Where $(hkl)_M$ are indices of the plane in martensite and $(HKL)_A$ are the indices of the corresponding austenitic plane. *T* means transpose of row vector.

Using equation (8.1) for austenitic plane $(200)_A$ the martensitic corresponding planes for all three martensitic variants can be calculated (see Tab. 8.2).

Table 8.2: Corresponding martensitic planes (CMP) to $(200)_A$ austenitic plane for all three martensitic variants.

LCV	**CMP to $(200)_A$ austenitic plane**	**d_{hkl} martensite [nm]**
1	$(200)_M$	0.2975
2	$(020)_M$	0.2975
3	$(002)_M$	0.2805

The martensitic planes are not exactly parallel to the austenitic plane and have lattice spacings different from the original austenitic plane $(200)_A$ due to the Bain distortion, which is characteristic for the cubic to tetragonal transformation in NiMnGa. It can be seen from Table 2, that the three martensitic variants have two different lattice spacings. Martensitic plane $(002)_M$ in variant 3 have lattice spacing 0.2805 nm. Martensitic plane $(200)_M$ in variant 1 and martensitic plane $(020)_M$ in variant 2 have the same lattice spacing 0.2975 nm. From the diffraction point of view martensitic planes will yield two different diffraction peaks at different diffraction angles 2θ. The first diffraction peak from $(002)_M$ martensitic plane will characterize variant 3. The second diffraction peak at different 2θ originates from the martensitic planes $(200)_M$ and $(020)_M$ in variant 1 and variant 2, respectively. In order to distinguish between the variant 1 and variant 2 we need to perform the omega scan (the detector is left stationary while the crystal is rotated). In such a way it is possible to detect both martensitic planes $(200)_M$ and $(020)_M$, which have the same lattice spacing.

8.1.3 In-situ studies of the stress-induced martensite reorientation in NiMnGa single crystal

Ni-Mn-Ga single crystal with magnetic shape memory (MSM) effect was used for in-situ neutron diffraction experiment. In order to obtain defined initial state and to observe MSM effect the successive and cyclic compressive deformations (training process) were applied on two different perpendicular faces of prismatic sample. The aim of repeated compression was to eliminate the variant with c-axis perpendicular to the compression axes, i.e. to third variant, from the sample. The successive compressions thus secured that the sample was close to single variant state with the short crystallographic c-axis or [001] in the direction of compressive stress.

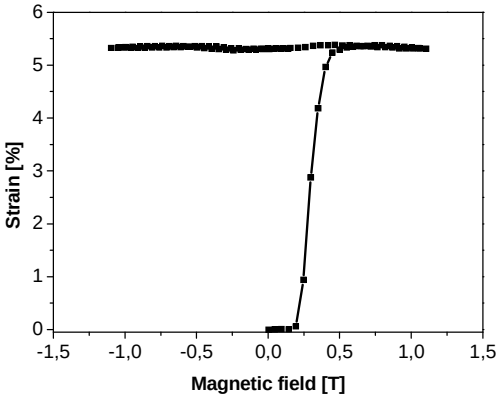

Fig. 8.3: Magnetic field induced strain in 5M tetragonal martensite of NiMnGa single crystal

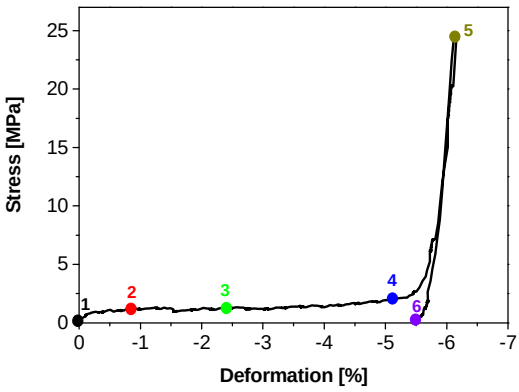

Fig. 8. 4: Stress –strain curve measured in-situ during the reorientation of martensite and the points in which the intensity of reflections were measured

After such a training process the magnetic field was applied in direction perpendicular to the last compression direction i.e. along [010]. As the field was applied in hard direction, variant reorientation or MSM effect occurred. This is shown in Fig. 8.3. The reorientation process started at magnetic field about $\mu_0 H = 0.20$ T and maximum strain is reached at about 0.50 T. The total deformation induced by magnetic field is $\varepsilon = 5.3$ %. This value suggests that the reorientation is nearly complete as it is close to the maximum deformation allowed by lattice $\varepsilon_0 = 1 - c/a = 5.7\%$ determined from the lattice constants of martensite. However some minor variants with different orientation remain after reorientation or were presented before the reorientation process.

The stress-strain curve measured after training is shown in Fig. 8.4. The compression is applied to the direction perpendicular to the last compression direction during training. The plateau in the stress-strain curve indicates the stress-induced reorientation of martensite. The stress plateau or mean stress for reorientation is at the stress value $\sigma = 1.25$ MPa. This confirms the fact that the twin interfaces in 5M Ni-Mn-Ga tetragonal martensite are easily mobile at very low stresses, which is consistent with the existence of the MSM effect in this sample.

Trained sample prepared by above described training process was used for neutron diffraction studies of martensite reorientation or variant redistribution by compression stress *in situ*. The sample was placed into the miniature deformation rig with martensitic crystallographic direction $[001]_M$ perpendicular to the applied stress, i.e. perpendicular to the last compression direction. The neutron diffraction data were measured during the compressive loading at

several points. These points from 1 to 6 are depicted on the stress-strain curve (Fig. 8.4). During measurement the strain was kept constant.

The fraction of differently oriented martensitic variants and twinning processes during the compression test was determined from the neutron diffraction data using the principles described in Experimental part. Martensitic variant 1 was detected from martensitic reflection $(2\ 0\ 0)_M$ and variant 3 was detected from martensitic reflection $(0\ 0\ 2)_M$. These planes corresponds to the $(2\ 0\ 0)_A$ austenitic plane. In order to be sure that the sample does not contain the variant 2, the omega scan was performed to search for $(0\ 2\ 0)_M$ martensitic reflection. Martensitic variant 2 was not found in the sample during the measurement.

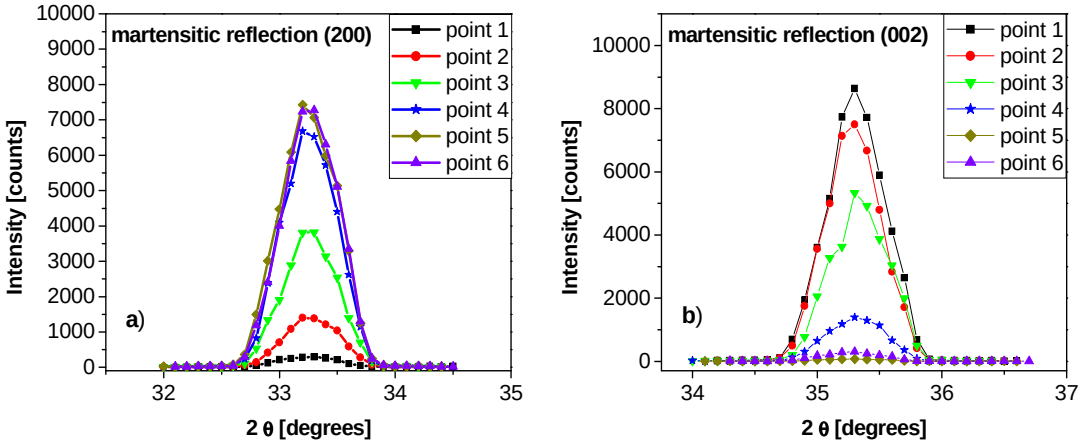

Fig. 8.5: Neutron diffraction reflections measured during the stress-induced reorientation. Martensitic variant 1 was characterized from $(200)_M$ martensitic peak at diffraction angle $2\theta = 33.2^\circ$ (a). martensitic variant 3 was evaluated from $(002)_M$ martensitic reflection at $2\theta = 35.3^\circ$ (b).

The evolution of the neutron diffraction reflections of respective martensite variants is plotted in Fig. 8.5. The integral intensity of the reflection is directly proportional to the volume fraction of material. The changes of the intensities are caused by the changes of volume fraction of differently oriented martensite variants due to compressive stress. The integral intensities of the reflections as a function of the measured strain are shown in Fig. 8.6.

Initially, point one at the stress-strain curve (Fig. 8.4), almost the whole volume of the sample diffracted into the $(0\ 0\ 2)_M$ martensitic reflection. Additionally low intensity of $(2\ 0\ 0)_M$ martensitic reflection was also measured. This indicates that initially the sample does not contain only one martensitic variant, variant 3, (true single crystal of martensite) but that the small fraction of martensitic variant 1 is also present in the sample.

During the compression (points 2 to 5) the intensity of $(0\ 0\ 2)_M$ martensitic reflection decreases and the intensity of $(2\ 0\ 0)_M$ martensitic reflection increases (Fig. 8.6). This is clear evidence for the stress-induced reorientation of martensite or variant redistribution, where the martensitic variant 3 transforms to the variant 1. It can be also concluded that only one twinning system is active during the reorientation of this trained sample because only the variant 1 and variant 3 were present in the sample. This is also supported from the optical photographs of different sample faces. A complete list of twinning planes can be found in [47].

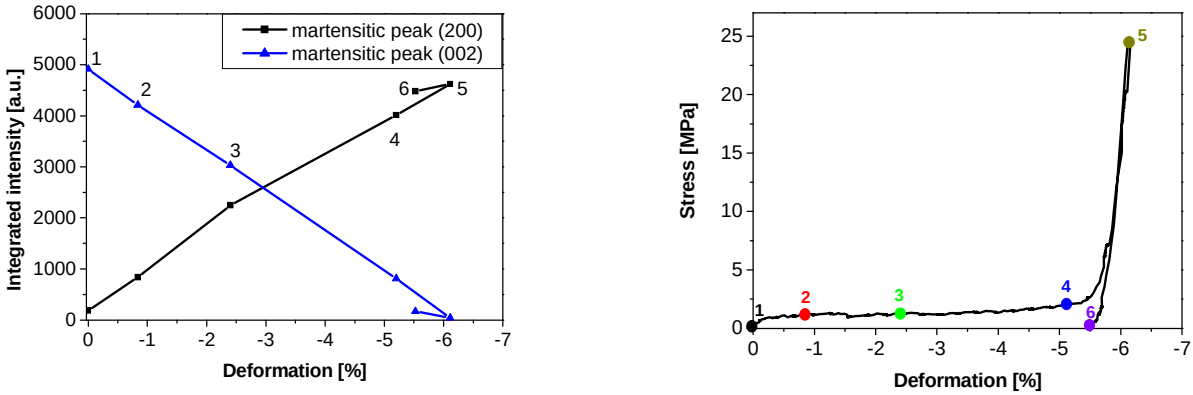

Fig. 8.6: Integrated intensity changes (a) measured during the reorientation of martensite (b) from martensitic variant 3 (diffraction peak $(002)_M$) to the martensitic variant 1 (diffraction peak $(200)_M$).

The integral intensities of the reflections are proportional to the measured external strain, which confirms that the macroscopic strain is due to reorientation of the variants and no other microstructural changes takes place. However, whereas the decrease of the intensity of $(200)_M$ reflection is linear, the $(002)_M$ intensity slightly deviates from the linearity. Also the profiles of the diffraction peaks change and there are slightly non-symetrical. This deviation and nonsymmetrical reflections needs further studies. The reorientation of the martensite is not totally finished even at the stress value of 25 MPa, *i.e.* point five at stress-strain curve (Fig. 8.4). There is still some very small intensity of $(0\ 0\ 2)_M$ martensitic reflection, which implies the presence of the martensitic variant 3. If we compare mean stress for the reorientation at plateau σ = 1.25 MPa and the stress σ = 25 MPa, it is clearly seen that the point five is highly in elastic region. Similar conclusion was made from the acoustic emission measurement where some acoustic activity ascribed to variant reorientation was detected up to 60 MPa [88]. For Ni_2MnGa it was found that some residual variant persist after application of 30 MPa compressive stress at 172 K [90].

During the unloading the intensities of both martensitic reflections change very slightly. Intensity of $(2\ 0\ 0)_M$ martensitic reflection decreases, but the decrease is in the range of experimental error. The intensity of $(0\ 0\ 2)_M$ martensitic reflection increases during unloading. In this case the increase in the intensity is slightly larger than the experimental error. The changes imply that during unloading the variant with different orientation re-emerged. This is also supported by deviation from the linearity of the unloading part of stress-strain curve. Further evidence of the re-emergence of the residual variant can be inferred from acoustic emission experiment [88]. The reversible deformation due to re-emergence of the residual variants upon unloading was also observed in magnetic shape memory effect. The deformation was ascribed to the residual stress [91, 92]. However, based solely on this neutron diffraction experiment we can not conclude with certainty that the additional movement of twin interfaces occurred during unloading.

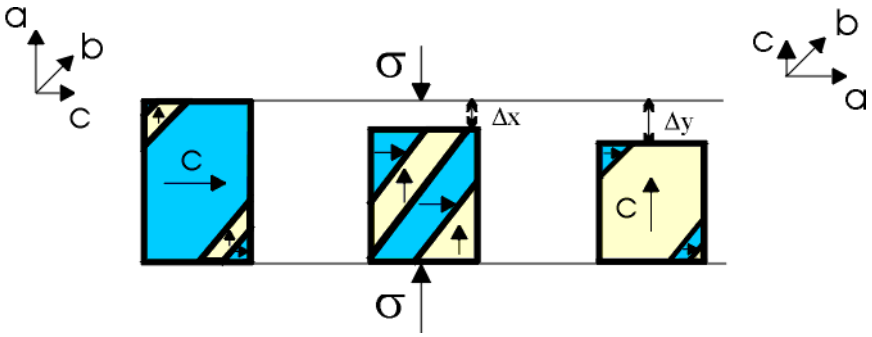

Fig. 8.7: Schematic diagram of stress induced reorientation of martensite in NiMnGa single crystal.

As a summary, the stress induced reorientation of martensite in ferromagnetic Ni-Mn-Ga single crystal is schematically outlined in Fig. 8.7. Initially, (Fig. 8.7a) the sample is mainly in one martensitic variant with *c* – axis perpendicular to the stress direction. Small fraction of second martensitic variant with *c* – axis parallel to the stress direction is also present in the sample. During the loading (Fig. 8.7b) martensitic variant with the *c* – axis parallel to the stress direction growths and corresponding change in length Δx is observed. In this stage two martensitic variants coexist. Finally, reorientation is finished (Fig. 8.7c) and the *c* – axis is now parallel to the stress direction, which is also the direction of the magnetization. The final change of the length of the sample is Δy (sample dimension is reduced in the direction of applied stress). After the unloading the sample contains small fraction of second martensitic variant.

8.1.4 Summary:

In-situ neutron diffraction studies of stress induced reorientation in NiMnGa single crystal were performed. Reorientation process in NiMnGa single crystal martensite was studied by following the changes in the intensities of two martensitic diffraction peaks $(002)_M \rightarrow (200)_M$. The change of martensite variant fraction is directly proportional to the measured macroscopic strain. This confirms that the strain is direct consequence of the structure reorientation or variant redistribution and no other microscopic mechanism takes place.

The obtained results show that during the stress-induced reorientation process only one twinning system is active and the reorientation is not totally completed even in the stress 20 times higher than mean stress needed for reorientation. During unloading there are small changes of martensitic reflections intensity. However, the changes are in the range of experimental error. Because of this observation it can not be concluded, that twin interfaces moves during the unloading of the sample.

8.2. Neutron diffraction studies of magnetic field induced strain in NiMnGa single crystal under constant stress

Magnetically controlled shape memory alloys are a new way to produce motion and force. If one wants to use the Ni_2MnGa as an actuator, a bias compression stress of suitable value must be applied to restore the shape of the crystal when magnetic field decreases. This bias stress is known to affect the maximum achievable actuation strains. The magnetic-field induced strains are related to the actually existing martensite variant microstructures in the specimen, which are sensitive to the bias load. The maximum strains are, in addition to the crystallography and lattice constants related to the actual twin microstructures, twinning stress and bias stress, detailed information on twinning stresses and variant microstructures existing under stress and magnetic field are missing due to the lack of reliable data. In addition, it has been found empirically that a compressive training prior the actuation (*e.g.* by the application of several compression cycles to different faces of the sample), is extremely beneficial for the magnetic actuation.

In this work, we have investigated microstructure evolutions in a Ni_2MnGa single crystal subjected simultaneously to a magnetic field and a mechanical force by *in-situ* neutron single crystal diffraction method. Results of dedicated experiments simulating conditions of a magneto-mechanic Ni_2MnGa single crystal actuator working under various bias stresses are discussed in section 8.2.2 and the effect of compressing training on magnetic actuation is discussed in section 8.2.3.

8.2.1 Experimental material

Single crystal of Ni49.7Mn29.3Ga21 magnetic shape memory alloy was used for *in situ* neutron diffraction experiment. Details about the single crystal characteristics (transformation temperatures, structure etc.) can be found in the previous chapter.

Neutron diffraction experiment was performed in ILL in Grenoble on the single crystal diffractometer D10 in two-axis configuration equipped with the horizontal cryomagnet (3.8 T) and 80x80 mm^2 two-dimensional detector. Measurements were performed at monochromatic wavelength λ = 1.26 Å. For the neutron in-situ diffraction experiments the small deformation set-up was prepared (Fig. 8.8).

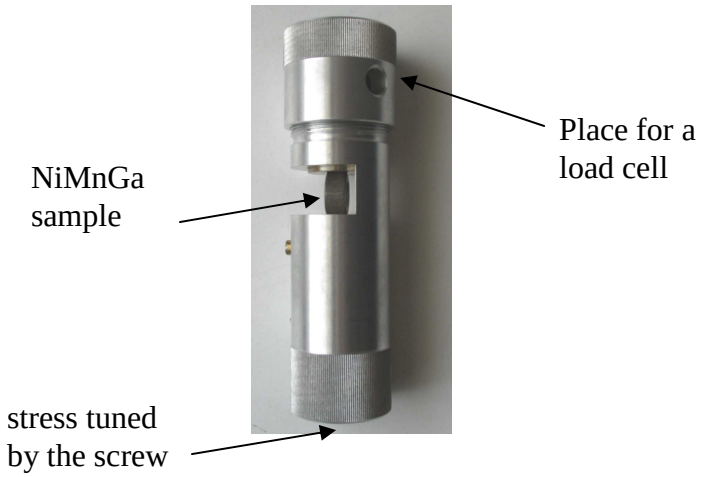

Fig. 8.8: Photo of deformation set-up.

The deformation set-up consists of cylindrically shaped part made from aluminium. The diameter of the cylinder was 3.4 mm and the length is 11.5 mm. The grips and spring were made from bronze. The spring is used to maintain the desired stress which is tuned by the screw from the bottom part of the deformation set-up. In the top part there is a place for a

small load cell that allows measuring the force. Materials used for the construction of this small deformation set-up are non-magnetic in order to prevent any unwanted effects when the magnetic field is applied. This small deformation set-up was mounted in a horizontal field cryomagnet. The sample was placed inside the deformation set-up under the constant stress value. The magnetic field and stress were applied in direction perpendicular to each other.

8.2.2 The magnetic field induced strain under different stress levels

The diffraction experiment consisted in the investigation of magnetic-field induced reorientation in Ni-Mn-Ga single crystal under different stress values (0 MPa, 0.9 MPa and 3 MPa). As common for any mechanical experiment on martensite single crystal [82], it is of key importance to have the initial microstructure in the sample well defined. In order to achieve that, the sample was deformed alternatively several times on two different faces denoted *B* and *G* in Fig. 8.9. Following such a simple training, the sample is assumed to consist mostly of one martensitic variant [82, 93] with short c-axis in the direction of the last compression direction. In the beginning of the experiment, the tetragonal *c*-axis of the crystal was always oriented in direction perpendicular to the magnetic field (applied in the martensitic direction $[100]_M$).

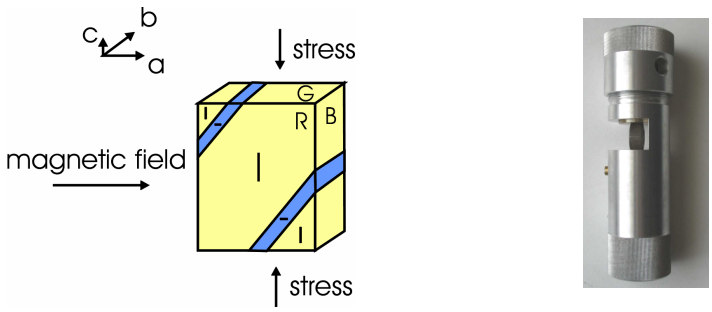

Fig. 8.9: Schematic view of the Ni-Mn-Ga single crystal sample existing mainly in the martensitic variant 1 (yellow) and small volume fraction of variant 3 (blue) together with the directions of applied magnetic field and compression stress applied by a spring in the miniature deformation rig.

Firstly, the experiment with magnetic actuation without stress was performed (Fig. 8.10). The microstructure changes during magnetic-field induced reorientation were investigated using the principles outlined in section 8.1.2. The peak intensity changes $(200)_M \rightarrow (002)_M$ and $(002)_M \rightarrow (200)_M$ were followed as an evidence for the martensite reorientation. Initially, the sample was mainly in the martensitic variant 1 (V1) that corresponds to the $(200)_M$ martensitic reflection in zero magnetic field (Fig. 8.10). Besides, the presence of the

martensitic reflection $(002)_M$ indicates a small volume fraction of another martensitic variant 3 (V3). The variant 2 $(020)_M$ was not detected with the help of the omega scan.

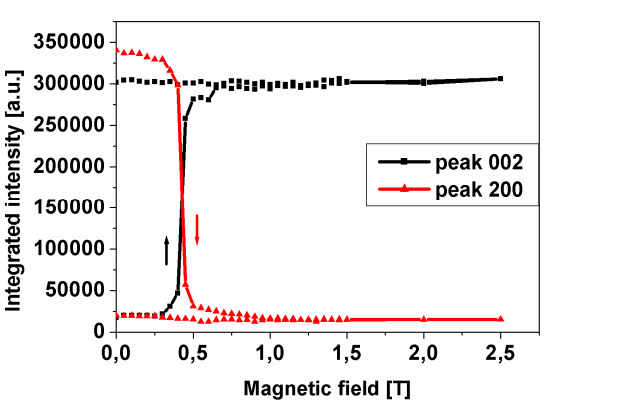

Fig. 8.10: Variation of the integrated intensity of diffraction peaks 200_M (V1) and 002_M (V3) with magnetic field (geometry shown in Fig. 8.9) measured by the in-situ neutron diffraction experiment under zero applied stress.

Figure 8.10 shows the sharp decrease of the $(200)_M$ martensitic reflection and the sharp increase of the $(002)_M$ martensitic reflection at the magnetic field value of 0.3 T. This indicates the onset of the magnetic-field induced reorientation. Since the $(200)_M$ never disappears completely, the martensite reorientation is not completed even at maximal magnetic field of 2.5 T which is well above magnetic saturation. It means that we did not get a true single crystal (single variant) of the martensite and the sample contains twin interfaces.
Fig. 8.11 shows a detail at low magnetic field. It is clearly seen that the intensity of the $(200)_M$ martensitic reflection slowly decreases from the start of the magnetic filed loading up to 0.3 T (Fig. 8.11b), where it starts to fall very quickly.

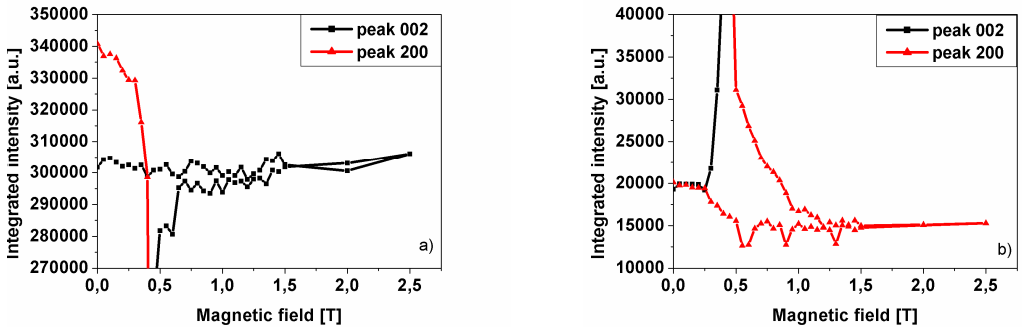

Fig. 8.11: Detailed views showing parts of figure 8.10.

This early decrease is attributed to the rotation of magnetization vector, since only the magnetic moments perpendicular to the scattering vector gives rise to the magnetic contribution, i.e. to the intensity of the $(200)_M$ reflection. The magnetic moments rotate from

the easy magnetization c-axis towards the direction of the increasing magnetic field prior the magnetically induced twin motion is activated. This agrees with the magnetic measurements performed on Ni-Mn-Ga single crystals [31, 58]. Observed jump in intensity is well correlated with the jump of magnetization observed at 0.25 T in [31]. This abrupt change in magnetization corresponds to the reorientation of martensite lattice, as a result of which the *c*-axis becomes aligned with the direction of magnetic field [31, 58]. Intensity of $(002)_M$ reflection, on the other hand, does not change remarkably prior the field of 0.25 T is reached (Fig. 8.11a), since the magnetic moments in this case are parallel to the scattering vector of $(002)_M$ reflection and there is thus no magnetic contribution.

The decrease of the magnetic field causes no significant changes in the intensity of both martensitic reflections down to the magnetic field of 0.5 T (Fig. 8.11b). Below this value, however, the intensity of the $(002)_M$ reflection stays constants but that of the $(200)_M$ reflection increases. A question is whether this small change should be ascribed to the changes of partial lattice orientation or magnetisation rotation. We believe this is not due to the lattice reorientations upon decrease of the magnetic field but due to the magnetic moment rotations back to the direction of easy magnetisation as the magnetic anisotropy prevails at low magnetic fields. This interpretation is also supported by the fact that the intensity of the $(002)_M$ martensitic reflection did not change significantly with the decrease of the magnetic field.

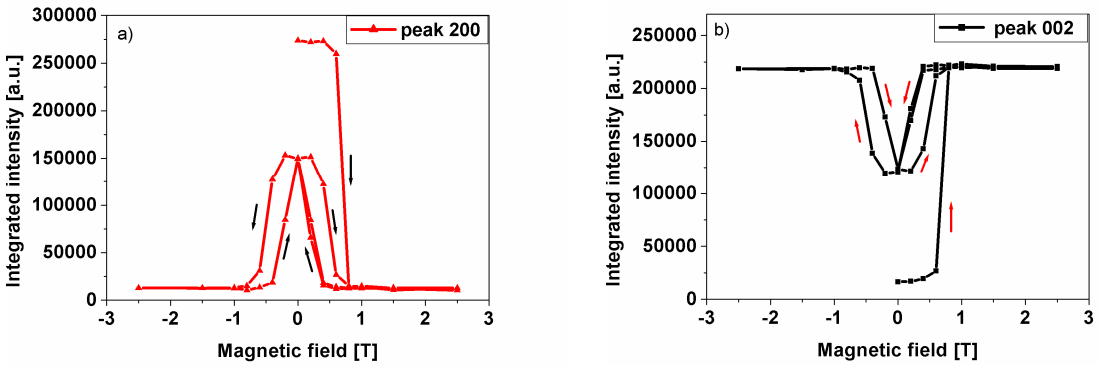

Fig. 8.12: Variation of the integrated intensity of diffraction peaks 200_M (V1) and 002_M (V3) with magnetic field (geometry shown in Fig. 8.9) under applied stress 0.9 MPa measured by the in-situ neutron diffraction experiment. Arrows show the test direction.

Figure 8.12 shows the neutron diffraction results obtained in the second experiment with the magnetic field induced reorientation under constant stress of 0.9 MPa. Initial state of the sample was same as in previous case – *i.e.* the sample was mainly in the martensitic variant 1, which corresponds to the large intensity of the $(200)_M$ martensitic reflection (Fig. 8.12a). The

minority variant 3 (martensitic reflection $(002)_M$ (Fig. 8.12b)) was also present. Magnetic field was applied in the same direction as for previous case, as shown in Fig. 8.9. Compared to the previous case, the martensite reorientation started at higher values of the applied magnetic field ~ 0.7 T. Again, the reorientation was never totally completed and the small volume fraction of the martensite variant 1 remained in the sample even at maximal magnetic field of 2.5 T (Fig. 8.13b). Upon decreasing the magnetic field under applied stress, the reverse reorientation occurred at magnetic field of 0.4 T due to the effect of the bias stress. The 0.9 MPa stress, however, was too small to reorient fully the martensite crystal back to the variant 1 (Fig. 8.13a). At zero magnetic field, the sample thus existed in the new microstructure state characterized by nearly equivalent volume fractions of martensitic variant 1 and 3 as can be inferred from the diffraction intensity (Fig. 8.12) and suggested schematically in figure 8.13c. When magnetic field of the opposite direction is applied, the variant 1 undergoes an analogical process of twinning reorientation to the martensitic variant 3 (Figs. 8.12, 8.13). Finally, the decrease of the magnetic field down to 0 T again leads to the same microstructure consisting of nearly equal volume fractions of the martensitic variants 1 and 3. As found in parallel magnetic strain measurement on this crystal, periodical changes of the magnetic field under 0.9 MPa bias stress bring about reversible strain changes of approximately 3 % similarly as in [31].

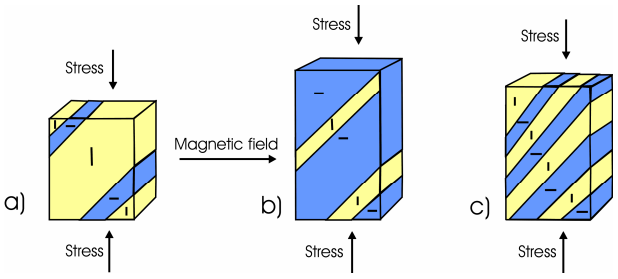

Fig. 8.13: Schematic drawing of the microstructure evolution during the magnetic field induced reorientation of the Ni-Mn-Ga single crystal under 0.9 MPa stress: a) Initial microstructure of the sample after multiple B-G training (see Fig. 8.15), variant microstructure after reorientation by magnetic field 2.5 T and c) microstructure consisting of mixture of variants 1 and 3 at magnetic field of 0 T (see Fig. 8.12)

Figure 8.14 shows the neutron diffraction results obtained in the third experiment with the magnetic field induced reorientation under constant compression stress of 3 MPa. The results are different again. In this case, there were only very small intensity changes of $(200)_M$ and $(002)_M$ martensitic reflections indicating that the reorientation of martensite lattice is small if any. The magnetic moments, however, rotated (as known from earlier magnetization

measurements [31]) towards the direction of the magnetic field, which gives rise to the minor intensity changes of the 200_M martensite reflection. However, very small but discernible change in the $(002)_M$ reflection suggests that small volume of the crystal underwent the reorientation at this level of stress, again in agreement with previous magnetic observation [31].

When applying magnetic field to the ferromagnetic Ni-Mn-Ga crystal, the two processes - rotation of the magnetic moments from the c-axis and the twin reorientation - compete. If it is energetically favourable to rotate the magnetic moments (the mechanical energy for the twinning is higher than the energy needed to rotate the magnetic moments), the moments rotate and no magnetic-field reorientation occurs. The mechanical energy due to applied bias stress must be added to the mechanical energy for the twinning [31, 94]. The applied bias stress 3MPa is, however, already too large for magnetic actuation, since the magnetic-field induced lattice reorientation was nearly completely suppressed as determined from the neutron diffraction results (Fig. 8.14).

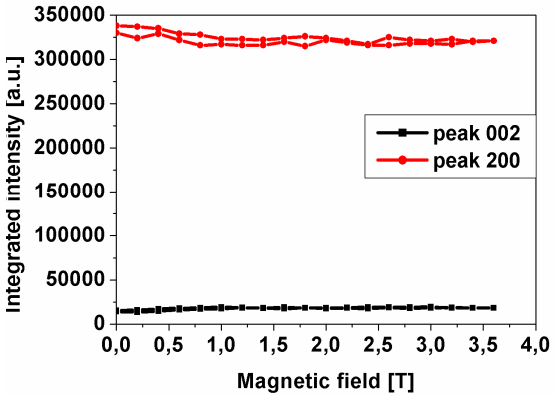

Fig. 8.14: Variation of the integrated intensity of diffraction peaks 200_M (V1) and 002_M (V3) with magnetic field (geometry shown in Fig. 8.9) measured by the in-situ neutron diffraction experiment under applied compression stress 3 MPa.

8.2.3. The effect of mechanical training on magnetomechanical actuation

In order to obtain the magnetic field induced strain in magnetic shape memory alloy single crystal, it is generally believed that three basic conditions must be fulfilled [31, 35, 95]. The material has to be ferromagnetic, the twin boundaries must be highly mobile and the magnetic anisotropy energy must be higher than the elastic energy needed for the twin boundary motion.

Based on our own experience with shape memory alloys and looking carefully through the literature reports, however, there seems to be another very important factor. An appropriate mechanical training done prior the magnetic actuation experiment on Ni-Mn-Ga single crystal

is beneficial for the actuation (larger strain and lower critical magnetic field) [58, 96, 97]. In this context, the experiments described in section 8.2.2 were all performed on samples trained by multiple successive compressive deformations applied on two different faces B and G of the cuboid sample (training B-G in Fig.8.15a).

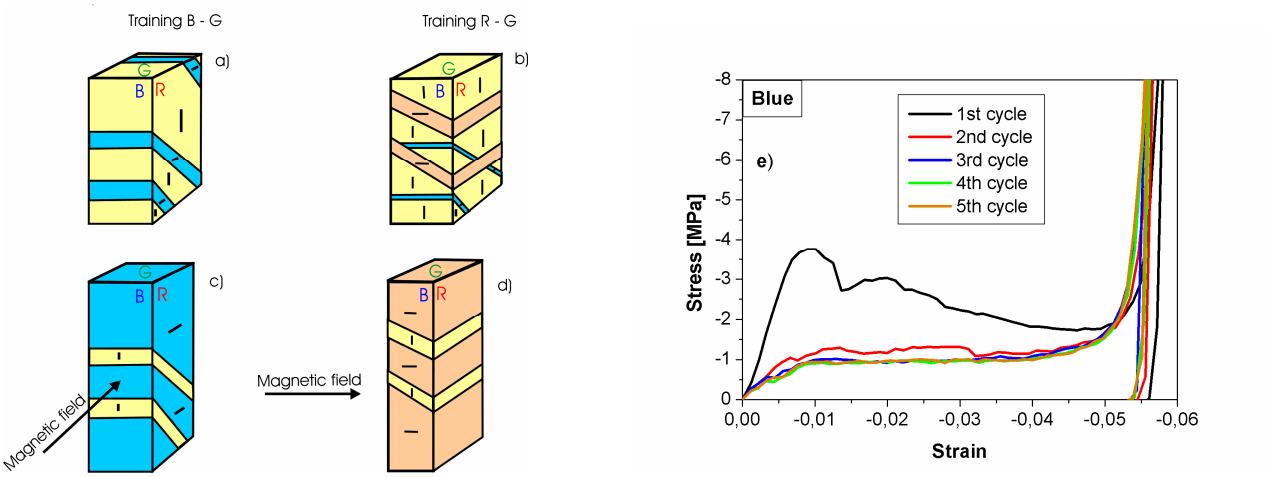

Fig. 8.15: Schematic drawing showing the microstructure of the Ni-Mn-Ga single crystal given the compressive training B-G (a, e) and R-G (b) the effect of the magnetic field applied in $[100]_M$ direction (c) and $[010]_M$ direction (d) on it. Stress-strain response of the crystal trained by multiple compression on faces B and G (e).

The twinning stress recorded during the training cycles (compression on face B in Fig. 8.15e right) significantly decreases with increasing number of training cycles. After the training, the magnetic field had always been applied perpendicularly to the compressive loading axis in the direction, where the deformation was before applied (along the direction B in Fig. 8.15c). Magnetic field induced reorientation was observed (Figs. 8.10-8.13) and crystal changed its shape as suggested in figures 8.15a, c.

On the other hand, if such trained crystal was magnetized along the third untrained direction, where the compressive deformation training was not applied (along the direction R in Fig. 8.15b), the reorientation process was not observed. This is apparently curious since the drastic difference between the crystal responses during the magnetic loading shown in Figures 8.10 and 8.16 is only due to the training. In fact, compared with the multiple compression in the B-G directions (Fig. 8.15a), the sample was given just 2 training cycles in R-G direction (Fig. 8.15b) in order to create the nuclei of the variant 2 (V2) observed as appearance of the $(002)_M$ reflection. This variant V2 was set to grow under magnetic field in the diffraction experiment. The sample was mounted to the holder and only the small stress of 0.2 MPa was applied only to hold it in place. The variant V2, however, although its nuclei were present in the sample prior the test (schematically shown in Fig. 8.15b and measured in Fig. 8.16), did

not grow and did not yield the strain as suggested in Fig. 8.15d under the increasing magnetic field. Only the magnetic moments rotation towards the direction of the magnetic field was observed (Fig. 8.16).

Why the reorientation did not occur in this last case can be explained based on the results of the neutron diffraction experiments. Recall that the sample is not martensite single crystal (there is also small volume fraction of second martensitic variant) prior the experiment and that the magnetic field induced reorientation strain appears only when the magnetic field is applied in the direction parallel to the crystallographic *c*-axis of this minor martensitic variant (see Fig. 8.9). This variant with *c*-axis parallel to the magnetic field grows and becomes the major variant at maximum field. If we apply the magnetic field along the direction R (Fig. 8.15b) along which the sample was not deformed before, the magnetic field is not oriented parallel to the *c*-axis of the minor martensitic variant and this is not thus expected to grow under the effect of magnetic field. Hence, new twinning system is needed which will reorient the major variant in the favourite martensite variant with the c-axis parallel to the magnetic field. The existing minor variant may even act as an obstacle for the magnetically driven reorientation process (increases the twinning stress).

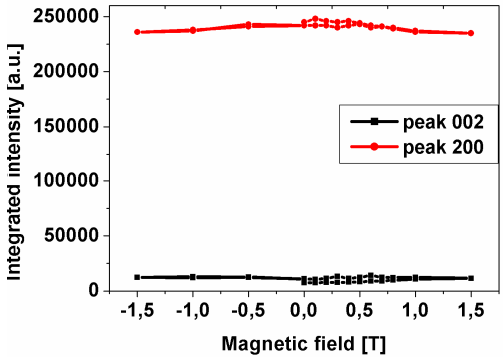

Fig. 8.16: Variation of the integrated intensity of diffraction peaks 200_M (V1) and 002_M (V2) with magnetic field applied along the third untrained direction $[010]_M$ (geometry shown in Fig. 8.15d) measured by the in-situ neutron diffraction experiment under applied stress 0.2 MPa.

It has been mentioned in the literature [96, 97] that the training is beneficial namely since it creates the nuclei (properly oriented minor variants) for the magnetically induced reorientation processes in the sample. This is probably true but it is only that? We succeeded to create the nuclei (evidenced by the existence of the variant 2 - 002_M reflection) only by the two R-G training cycles prior the last experiment but it did not help to achieve the magnetically induced reorientation (Fig. 8.16). More R-G training cycles to higher applied stresses might be necessary for that.

There is an analogy with the “superelastic training” of shape memory alloys. The upper plateau stress of superelastic SMA materials decreases with increasing number of superelastic deformation cycles and, as a consequence of this, a partial two way memory strain appears in successive stress free thermal cycles [98]. The two way memory phenomenon can be hardly ascribed solely to the effect of martensite nuclei as the nuclei are wiped out during transformation, there must be something else which stabilizes the trained transformation paths (internal stress, dislocations, ?). Similar argument can be put forward also for the training of Ni-Mn-Ga single crystals by successive compression deformations. The more training cycles is performed the easier is the subsequent magnetically induced reorientation along the trained reorientation path, *i.e.* the reorientation occurs at lower magnetic field and results in larger strain.

Presented results thus show that a substantial training is essential for the crystal to exhibit the magnetic-field induced variant reorientation. Training by just two cycles in the last experiment, although sufficient to create the nuclei of the minor variant destined to grow under the application of the magnetic field, was not sufficient to bring about magnetically induced reorientation and large strain (Fig. 8.16). There must be something else, in addition to the twin nuclei, which has been created during the compressive training, which assists the variant reorientation induced by the magnetic field applied along the proper crystal direction and prevents it, when the field is applied along the third improper (untrained) direction. The *in situ* neutron diffraction and electron microscopy experiments are now in progress in order to give the appropriate explanation of this feature.

8.2.4 Summary

A neutron diffraction single crystal method was applied to investigate the magnetic field driven twinning (variant reorientation) in NiMnGa martensite single crystal. It has been found that:

- ✧ Martensite variant reorientation by applying magnetic field to the stress free crystal is not completed even at 2.5 T.
- ✧ Diffraction experiments prove that recoverable strain about 3 % observed upon magnetic field cycling under external compression stress (< 3 MPa) is due to martensite variant reorientation process activated by magnetic field biased with external compression stress
- ✧ In order to achieve magnetic field induced cyclic reorientation in NiMnGa single crystal, mechanical training of a suitable twinning system is necessary

Conclusions:

A single crystal neutron diffraction method for inspection of the quality of martensite single crystal samples and for *in-situ* investigation of twinning processes in martensite single crystals was developed using two neutron diffractometers dedicated to single crystal diffraction - the three-circle single crystal diffractometer at NPI Řež near Prague and four-circle diffractometer D10 at ILL in Grenoble.

It was proven in experiments on CuAlNi model single crystals that this method can be used to detect and distinguish the presence of individual lattice correspondence martensite variants in prism sample as well as to follow the activity of the twinning processes during the deformation test on the martensite variant single crystal in *in situ* neutron diffraction experiments during mechanical loading. In order to follow these processes effectively the 2D detector has to be used.

It was found through combination of compression tests, *in situ* optical observation on the sample surface and *in situ* neutron diffraction experiment on 2H martensite single crystals, that two types of twinning mechanisms become activated during compression tests on CuAlNi 2H martensite single crystal samples. The compound twinning featuring highly mobile twins (1MPa twinning stress) and type II twining featuring the motion of interfaces at much higher stress(20MPa - 40MPa)

In unique compression experiments starting from cubic austenite crystal, the mechanism of the stress-induced martensitic transformation in CuAlNi single crystal was analyzed. It was found that the particles of monoclinic $\beta`_1$martensite firstly appear before the structure changes to ortorhombic 2H martensite. In fact, two 2H martensite variants (variant 5 and variant 6, which are compound type twins) appeared during compression. The volume fraction of the martensite variant 6 was significantly larger than that of the variant 5. Theoretical calculations, however, show that there no low energy interface exist between the austenite and 2H martensite which contains the compound type twinning. The neutron diffraction results nevertheless show that this is possible during the stress-induced martensite transformation, but firstly there has to be some amount of particles of the other martensitic phase ($\beta`_1$ martensite).

In the second part of the thesis the NiMnGa magnetic shape memory alloy was studied by single crystal neutron diffraction technique. The stress-induced reorientation of martensite was studied by following the changes in the intensities of two martensite reflections $(002)_M \rightarrow (002)_M$. The obtained results show that only one twinning process was activated during the reorientation of martensite and the reorientation is not totally completed even at stresses that are twenty times larger than the stress needed for the initiation of the reorientation of martensite. The presence of residual variant has important implication for MSME in such a way that no nucleation of the new variant is needed and the reorientation proceed only by the increase of the volume of the variant favorably oriented in the stress.

Magnetic field induced reorientation of martensite in NiMnGa single crystal under different stress levels was studied on four-circle single crystal diffractometer in ILL Grenoble. It has been found that: i) martensite variant reorientation is not completed by applying magnetic field as high as 2.5 T, ii) recoverable strain of about 3 % due to switching between two variant microstructures is observed upon cyclic application of magnetic field under external compression stress 0.9 MPa, iii) the magnetic field induced reorientation was nearly fully suppressed by the bias external stress of 3MPa and iv) mechanical training by successive compression deformation on two different faces of the cuboid Ni-Mn-Ga single crystal is essential to achieve the magnetic field induced cyclic reorientation.

Final note on future work

Single crystal neutron diffraction method presented in this thesis was successfully applied for the studies of deformation characteristics in shape memory single crystals. Using this method valuable and new information about the reorientation of martensite in CuAlNi and NiMnGa single crystals as well as new facts about the stress-induced martensitic transformation in CuAlNi single crystal SMAs were obtained. I would appreciate if the method is used further on in the laboratory and/or in the field. In a very brief summary, the success of the method in its application to SMA single crystals exposed to various external loads (temperature, stress, magnetic field..) is based on combination of unique features of neutron radiation (*e.g.* penetration deeply into the material), principles of detection the individual variants in martensitic structures and capabilities of 2D detection.

In near future, I am planning to perform dedicated experiments to better understand the significant effect of mechanical training on magnetic actuation with NiMnGa crystals. As an alternative to training, we are planning in collaboration with Ing. M. Landa from the Institute of Thermomechanics of the ASCR v.v.i., to investigate possible combined magnetic-ultrasonic actuation with NiMnGa and CoNiAl crystals. In addition, there is an ongoing collaboration work with HUT Helsinki focussed on the characterisation of the twinning processed in NiMnGa single crystal by *in situ* electron microscopy. Electron microscopy can yield information about the defects which may be created during the loading and consequently may affect the mobility of the twinning boundaries. Neutron diffraction can give us representative information about the presence of residual martensite variants and their possible evolution during cyclic deformations in bulk NiMnGa samples.

Disertant`s role in obtained results

Author's contribution to the results presented in the thesis is following:

- developing the single crystal neutron diffraction method for the detection of individual martensite variants and for *in situ* investigation of twinning processes in martensite single crystals
- preparation and carrying out *in situ* neutron diffraction experiments on the diffractometers dedicated to the single crystal diffraction - the three-circle single crystal diffractometer at NPI in Řež near Prague and four-circle diffractometer D10 at ILL in Grenoble
- modification of the deformation rig on the three-circle diffractometer at NPI in Řež for performing *in situ* single crystal deformation experiments
- performing deformation experiments on INSTRON deformation machine, microstructural observations by means of optical microscopy and magnetic measurements on NiMnGa single crystals
- performing the fitting and analysis of the data using PeakFit program
- active participating in physical interpretation of all results obtained by *in situ* neutron diffraction experiments

During my stay at Institute of Physics I have became author of the following scientific papers published in international journals and in proceedings of the international conferences:

1. **P. Molnar**, P. Sittner, V. Novak, J. Prokleska, V. Sechovsky, B. Ouladdiaf, S-P. Hannula, O. Heczko, In-situ neutron diffraction study of magnetic field induced martensite reorientation in Ni-Mn-Ga under constant stress, J. Phys. - Condes Matter 19 (2007), in press
2. **P. Molnar**, P. Sittner, V. Novak, P. Lukas, Twinning processes in CuAlNi martensite single crystals investigated by neutron single crystal diffraction method, Mater. Sci. Eng. A 2007, doi:10.1016/j.msea.2007.01.189
3. **P. Molnar**, O. Heczko, P. Sittner, P. Lukas, S.P. Hannula, Magnetic field induced strain and training process in NiMnGa single crystal, E-MRS Fall Meeting 2007, Warsaw, conference proceeding
4. **P. Molnar**, P. Sittner, P. Lukas, T.Cernoch, Neutron diffraction studies of deformation processes in single crystals shape memory alloys, EUROMAT 2005, 5-8 September 2005, Prague, conference proceeding

5. S.Ignacova, T.Cernoch, **P. Molnar**, V.Novak, Martensite-martensite transitions in Cu-based alloys-austenitization of single variant of martensite and indirect detwinnng, EUROMAT 2005, 5-8 September 2005, Prague, conference proceeding

Appendix 1:

Transformation matrices *U* for every lattice correspondence variant of orthorhombic martensite in CuAlNi single crystal.

Martensitic variant	Transformation matrix U
1	$\begin{pmatrix} \frac{b}{a_0} & 0 & 0 \\ 0 & \frac{a+c}{\sqrt{2}\,a_0} & \frac{a-c}{\sqrt{2}\,a_0} \\ 0 & \frac{a-c}{\sqrt{2}\,a_0} & \frac{a+c}{\sqrt{2}\,a_0} \end{pmatrix}$
2	$\begin{pmatrix} \frac{b}{a_0} & 0 & 0 \\ 0 & \frac{a+c}{\sqrt{2}\,a_0} & \frac{c-a}{\sqrt{2}\,a_0} \\ 0 & \frac{c-a}{\sqrt{2}\,a_0} & \frac{a+c}{\sqrt{2}\,a_0} \end{pmatrix}$
3	$\begin{pmatrix} \frac{a+c}{\sqrt{2}\,a_0} & 0 & \frac{a-c}{\sqrt{2}\,a_0} \\ 0 & \frac{b}{a_0} & 0 \\ \frac{a-c}{\sqrt{2}\,a_0} & 0 & \frac{a+c}{\sqrt{2}\,a_0} \end{pmatrix}$
4	$\begin{pmatrix} \frac{a+c}{\sqrt{2}\,a_0} & 0 & \frac{c-a}{\sqrt{2}\,a_0} \\ 0 & \frac{b}{a_0} & 0 \\ \frac{c-a}{\sqrt{2}\,a_0} & 0 & \frac{a+c}{\sqrt{2}\,a_0} \end{pmatrix}$
5	$\begin{pmatrix} \frac{a+c}{\sqrt{2}\,a_0} & \frac{a-c}{\sqrt{2}\,a_0} & 0 \\ \frac{a-c}{\sqrt{2}\,a_0} & \frac{a+c}{\sqrt{2}\,a_0} & 0 \\ 0 & 0 & \frac{b}{a_0} \end{pmatrix}$
6	$\begin{pmatrix} \frac{a+c}{\sqrt{2}\,a_0} & \frac{c-a}{\sqrt{2}\,a_0} & 0 \\ \frac{c-a}{\sqrt{2}\,a_0} & \frac{a+c}{\sqrt{2}\,a_0} & 0 \\ 0 & 0 & \frac{b}{a_0} \end{pmatrix}$

References

[1] M. Kohl, Shape memory microactuators, Springer, 2004.
[2] K. Otsuka and C.M. Wayman, Shape memory alloys, Cambridge university press, Cambridge, 1999.
[3] W.J. Buehler, J.W. Gilfrich, R.C Wiley, J. Appl. Phys. 34 (1963) 1475-1477.
[4] K. Bhattacharya, Microstructure of Martensite: Why It Forms and How It Gives Rise to the Shape-Memory Effect, Oxford University Press, USA, 2003.
[5] K. Otsuka, T. Kakeshita, Science and technology of shape memory alloys: New developments, MRS Bulletin, February (2002) 91-100.
[6] R.C. Smith, Smart material systems - Model development, SIAM Philadelphia, 2005.
[7] R. Stalmans, J. Van Humbeeck, L. Delaey, Thermomechanical cycling, two way memory and concomitant effects in Cu-Zn-Al alloys, Acta Metall. Mater. 40 (1992) 501-511.
[8] Z. Nishiyama, Martensitic Transformation, Academic Press, New York, 1978.
[9] L.S. Ramsdell, *Am. Mineralogist* 32 (1947) 64.
[10] K. Otsuka, T. Ohba, M. Tokonami, C.M. Wayman, New Description of long period stacking order structures of martensites in β-phase alloys, Scripta Metall. et Mat. 29 (1993) 1359-1364.
[11] T. Tadaki, M. Tokoro, K. Shimizu, Trans. Jpn. Inst. Metals 16 (1975) 285.
[12] J. Ye, M. Tokonami, K. Otsuka, Met. Trans., 21A (1990) 2669.
[13] http://sma.ims.tsukuba.ac.jp/html-e/index_e.html
[14] P.M. Kelly, L.R. Francis Rose, The martensitic transformation in ceramics – its role in transformation toughening, Progress in Mat. Science 47 (2002) 463-557.
[15] M.S. Wechsler, D.S. Lieberman, T.A. Read, On the Theory of the formation of martensite, Trans. AIME 197 (1953) 1503-1515.
[16] D.S. Lieberman, M.S. Wechsler, T.A. Read, Cubic to orthorhombic diffusionless phase change-experimental and theoretical studies of AuCd, J. App. Phys. 26 (1955) 473-484.
[17] http://www.aem.umn.edu/people/faculty/shield/hane/micro.twin.html
[18] S.Ichinose, Y. Funatsu, K. Otsuka, Type II deformation twinning in γ_1` martensite in CuAlNi alloy, Acta metal. 33 (1985) 1613-1620.
[19] J.M. Ball, R.D. James, Fine phase mixtures as minimizers of energy, Arch. Ration. Mech. Analysis 100 (1987) 13-52.
[20] K.F. Hane, T.W. Shield, Microstructure in a cubic to orthorhombic transition, J Elasticity 59 (2000) 267-318.
[21] K.F. Hane, T.W. Shield, Microstructure in a copper-aluminium-nickel shape-memory alloys, Proc. R. Soc. Lond. A 455 (1999) 3901-3915.
[22] L. Kaufmann, M. Cohen, Progr. Met. Phys. 7 (1985) 165-246.
[23] H. Warlimont, L. Delaey, R.V. Krishnan, H. Tas, J. Met. Sci. 9 (1974) 1545.
[24] V. Novák, J. Malimánek, N. Zárubová, Martensitic Transformations in Single Crystals of Cu-Al-Ni Induced by Tensile Stress, Mater. Sci. Eng. A191 (1995) 193-201.
[25] V. Novák, P. Sittner: Stability of the γ'_1 Phase in Cu-base Alloys, Journal de Physique, Colloque C5 , 7, (1998) 227.
[26] K. Ullakko, Magnetically controlled shape memory alloys: a new class of actuator materials, Journal of Materials Engineering and Performance 5 (1996) 405
[27] K. Ullakko, J.K. Huang, C. Kantner, R.C. O`Handley, V.V. Kokorin, Large magnetic-field-induced strains in Ni_2MnGa single crystals, Applied phys.lett. 69 (1996) 1966-1968.

[28] J. Koeda, Y. Nakamura, T. Fukuda, T. Kakeshita, T. Takeuchi, K. Kishio, Giants magnetostriction in Fe-Pd alloy single crystal exhibiting martensitic transformation, Trans. Mat. Res. Soc. Japan 26 (2001) 215.
[29] T. Kakeshita, T. Takeuchi, T. Fukuda, M. Tsujiguchi, T. Saburi, R. Oshima, S. Muto, Appl. Phys. Lett. 77 (2000) 1502-1504.
[30] O. Söderberg, A. Sozinov, Y. Ge, S.-P. Hannula, V.K. Lindroos, in: K.H.J. Buschow (Eds.), Handbook of magnetic materials, Elsevier B.V. 2006.
[31] O. Heczko, Magnetic shape memory effect and magnetization reversal, J. of Magnetism and Magnetic Materials 290-291 (2005) 787-794.
[32] H.E. Karaca, I. Karaman, B. Basaran, Y.I. Chumlyakov, H.J. Maier, Magnetic field and stress induced martensite reorientation in NiMnGa ferromagnetic shape memory alloy single crystals, Acta Mater. 54 (2006) 233-245.
[33] I. Karaman, H.E. Karaca, B. Basaran, D.C. Lagoudas, Y.I. Chumlyakov, H.J. Maier, Stress-assisted reversible magnetic field-induced phase transformation in Ni2MnGa magnetic shape memory alloys, Scripta Mater. 55 (2006) 403-406.
[34] J. Tellinen, I. Suorsa, A. Jääskeläinen, I. Aaltio, K. Ullakko, Basic properties of magnetic shape memory actuators, 8th international conference ACTUATOR 2002, Bremen, Germany, 10-12 June 2002.
[35] J. Enkovaara, A. Ayuela, A.T. Zayak, P. Entel, L. Nordstrom, M. Dube, J. Jalkanen, J. Impola, R.M. Nieminen Mater. Sci. Eng. A 378 (2004) 52-60.
[36] O. Heczko, L. Straka, N. Lanska, K. Ullakko, J. Enkovaara, Temperature dependence of magnetic anisotropy in Ni-Mn-Ga alloys exhibiting giant field-induced strain, J. App. Phys. 91 (2002) 82288230.
[37] O. Söderberg, Y. Ge, A. Sozinov, S.-P. Hannula, V.K. Lindroos, Recent breakthrough development of the magnetic shape memory effect in Ni-Mn-Ga alloys, Smart Mater. Struct. 14 (2005) S223-235.
[38] http://www.adaptamat.com/
[39] P.J. Webster, K.R.A. Ziebeck, S.L. Town, M.S. Peak, Magnetic order and phase transformation in Ni_2MnGa alloy, Phil. Mag. B 49 (1984) 295
[40] V.A. Chernenko, E. Cesari, V.V. Kokorin, I.N. Vitenko, The development of new ferromagnetic shape memory alloys in Ni-MnGa system, Scripta mett. et mater. 33 (1995) 1239-1244.
[41] P.J. Brown, A.Y. Bargawi, J. Crangle, K.-U. Neumann, K.R.A. Ziebeck, Direct observation of a band Jahn-Teler effect in the martensitic phase transition of Ni_2MnGa, J. Phys. - Condes. Mat. 11 (1999) 4715-4722.
[42] Y. Ge, O. Söderberg, N. Lanska, A. Sozinov, K. Ullakko, V.K. Lindroos, Crystal structure of three Ni-Mn-Ga alloys in powder and bulk materials, Journal de Phys. IV 112 (2003) 921.
[43] M. Kreissl, T. Kanomata, M. Matsumoto, K.-U. Neumann, B. Ouladdiaf, T. Stephens, K.R.A. Ziebeck, The influence of atomic order and residual strain on the magnetic and structural properties of Ni_2MnGa, J. of Magnetism and Magnetic Materials 272-276 (2004) 2033.
[44] V.V. Martynov, V.V. Kokorin, The crystal structure of thermally and stress-induced phase transformations in single crystalline Ni-Mn-Ga alloys, Journal de Phys. III 2 (1992) 739
[45] V.A. Chernenko, C. Segui, E. Cesari, J. Pons, V.V. Kokorin, Sequence of martensitic transformations in Ni-Mn-Ga alloys, Phys. Rew. B 57 (1998) 2659-2662.
[46] J. Pons, V.A. Chernenko, R. Santamarta, E. Cesari, crystal structure of martensitic phases in Ni-Mn-Ga shape memory alloys, Acta Mater. 48 (2000) 3027-3038.
[47] K.F. Hane, T.W. Shield, Symmetry and microstructure in martensite, Phil. Mag. A 78 (1998) 1215-1252.

[48] P.J. Brown, J. Crangle, T. Kanomata, M. Matsumoto, K.-U. Neumann, B. Ouladdiaf, K.R.A. Ziebeck, The crystal structure and phase transitions in the magnetic shape memory compound Ni_2MnGa, Journal of Phys. Cond. Matter 14 (2002) 10159-10171.
[49] L. Mañosa, A. Gonzalez-Comas, E. Obrado, A. Planes, Premartensitic phase transformation in the Ni_2MnGa shape memory alloy, Mater. Sci. Eng. A 273-275 (1999) 329-332.
[50] N. Lanska, O. Söderberg, A. Sozinov, Y. Ge, K. Ullakko, V.K. Lindroos, Composition and temperature dependence of the crystal structure of Ni-Mn-Ga alloys, J. App. Phys. 95 (2004) 8074-8078.
[51] P. Weiss, L`hypothese du champ moleculaire et de la propriete ferromagnetique, Journal de Physique theoretique et appliquee 4 (1907) 661.
[52] Ch. Kittel, Uvod do fyziky pevnych latek, Academia, Praha, 1985.
[53] Y. Ge, O. Heczko, O. Söderberg, S.-P. Hannula, V.K. Lindroos, Investigation of magnetic domains in Ni-Mn-Ga alloys with a scanning electron microscope, Smart Mat. Struct. 14 (2005) S211-S215.
[54] Y. Ge, The crystal and magnetic microstructure of Ni-Mn-Ga alloys, Doctoral thesis, HUT, Helsinki, 2007.
[55] B. Kiefer, D.C. Lagoudas, Magnetic field-induced martensitic variant reorientation in magnetic shape memory alloys, Phil. Mag. 85 (2005) 4289-4322.
[56] B.D. Cullity, Introduction to magnetic materials, Addision-Wesley publishing company, 1972, p. 211
[57] R. Tickle, R.D. James, Magnetic and magnetomechanical properties of Ni_2MnGa, J. of Magnetism and Magnetic Materials 195 (1999) 627-638.
[58] O. Heczko, A. Sozinov, K. Ullakko, Giant field-induced reversible strain in magnetic shape memory NiMnGa alloy, IEEE Trans. Magn. 36 (2000) 3266
[59] A. A. Likhachev, K. Ullakko, Magnetic-field-controlled twin boundaries motionn and giant magneto-mechanical effects in Ni-Mn-Ga shape memory alloys, Phys. Lett. A 275, (2000) 142-151.
[60] O. Heczko, L. Straka, Temperature dependence and temperature limits of magnetic shape memory effect, J. Appl. Phys. 94 (2003) 7139-7143.
[61] N. Glavatska, G. Mogylny, I. Glavatsky, A. Tyshchenko, O. Söderberg, V.K. Lindroos, Temperature dependence of magnetic shape-memory effect and martensitic structure of NiMnGa alloy, Mat. Sc. Forum 394-395 (2002) 537.
[62] P.J. Brown, in: G. Kostorz (Eds.), Treatise on materials science and technology 15, Neutron scattering, edited by Academic Press, New York, 1979, pp. 69.
[63] T.F. Koetzle, Single crystal neutron diffraction, Internal report BNL-68112, Argonne National Laboratory, Argonne, IL, USA
[64] Ch. Barrett, Structure of metals, McGraw-Hill, New York, 1966.
[65] V. Valvoda, M. Polcarova, P. Lukac, Zaklady strukturni analyzy, Karolinum, Praha, 1992, pp. 132.
[66] W. Massa, Crystal structure determination, Springer, Berlin, 2004, pp. 29.
[67] http://www.isis.rl.ac.uk/TrainingCourse/
[68] C. Giacovazzo, H.L. Monaco, G. Artioli, D. Viterbo, G. Ferraris, G. Gilli, G. Zanotti, M. Catti, Fundamentals of Crystallography, Oxford university press, 2002, pp.178.
[69] L.A. Aslanov, G.V. Fetisov, Crystallographic instrumentation, IUCr Monographs on Crystallography, Oxford, 1998.
[70] M. Schlenker, in: J. Baruchel, J.-L. Hodeau, M.S. Lehmann, J.-R. Regnard, C. Schlenker (Eds.), Neutron and Synchrotron radiation for condensed matter studies, Vol.1, 1993, pp. 154.
[71] W. Prandl, in: H. Dachs (Eds.), Neutron diffraction, Springer-Verlag, 1978, pp. 113.

[72] J. Rossat-Mignod, in: K. Sköld and D.L. Price (Eds.), Neutron Scattering, Academic press, Orlando, 1987, pp. 73.
[73] G.E. Bacon, Neutron Diffraction, Clarendon press, Oxford, 1975, pp. 203.
[74] P.J. Webster, Heusler alloys, Contemp. Phys. 10 (1969) 559-577.
[75] P.J. Webster, K.R.A. Ziebeck, S.L. Town, M.S. Peak, Magnetic order and phase transformation in Ni_2MnGa, Philosophical magazine B 49, (1984) 295-310.
[76] U.W. Arndt, B.T.M. Willis, Single crystal diffractometry, Cambridge University Press, 1966, pp. 37.
[77] J. Schweizer, in: J. Baruchel, J.-L. Hodeau, M.S. Lehmann, J.-R. Regnard, C. Schlenker (Eds.), Neutron and Synchrotron radiation for condensed matter studies, Vol.2, 1994, pp. 104.
[78] G. McIntyre, in: J. Baruchel, J.-L. Hodeau, M.S. Lehmann, J.-R. Regnard, C. Schlenker Neutron and Synchrotron radiation for condensed matter studies, Vol.1, 1993, pp. 182.
[79] W. R. Busing, H. A. Levy, Angle calculations for 3- and 4-circle X-ray and neutron diffractometers, Acta Cryst. 22 (1967) 457-464.
[80] H.R. Trebin, Quasicrystals: Structure and physical properties, Wiley-VCH, 2003, pp. 9.
[81] http://people.ccmr.cornell.edu/~mseugrad/dsclab.html
[82] V. Novak, P. Sittner, S. Ignacova, T. Cernoch, Transformation behavior of prism shaped shape memory alloy single crystals, Mater. Sci.Eng. A 438-440 (2006) 755-762.
[83] P. Sedlak, H. Seiner, M. Landa, V. Novak, P. Sittner, Ll. Mañosa, Elastic constants of bcc austenite and 2H orthorhombic martensite in CuAlNi shape memory alloy, Acta mater. 53 (2005) 3643-3661.
[84] S. Ignacova, T. Cernoch, V. Novak, P. Sittner, The reorientation of the 2H martensite phase in Cu–Al–Mn shape memory single crystal alloy, Mater. Sci. Eng. A doi:10.1016/j.msea.2007.02.163
[85] K. Otsuka, C.M. Wayman, K. Nakai, H. Sakamoto, K. Shimizu, Superelasticity effects and stress-induced martensitic transformation in Cu-Al-Ni alloys, Acta Metall. 24 (1976) 207-226.
[86] K. Otsuka, H. Sakamoto, K. Shimizu, Successive stress-induced martensitic transformations and associated transformation pseudoelasticity in Cu-Al-Ni alloys, Acta Metall. 27 (1979) 585-601.
[87] P. Sittner, private communication
[88] L. Straka, V. Novak, M. Landa, O. Heczko, Acoustic emission of Ni-Mn-Ga magnetic shape memory alloy in different straining modes, Mater. Sci. Eng A 374 (2004) 263-269.
[89] L. Straka, O. Heczko, V. Novak, N. Lanska, J. Phys. IV 113 (2003) 911.
[90] P.J. Brown, B. Dennis, J. Crangle, T. Kanomata, M. Matsumoto, K-U. Neumann, L.M. Justham, K. R. A. Ziebeck, J. Phys. - Condes. Matter 16 (2004) 65-75.
[91] Y. Ge, O. Heczko, O. Söderberg V. K. Lindroos, S-P Hannula, Direct optical observation of magnetic domains in Ni-Mn-Ga martensite, Appl. Phys. Lett. 89 (2006) 082502-082525.
[92] A. Malla, M. J. Dapino, T. A. Lograsso, D. L. Schlagel, J. Appl. Phys. 99, (2006) 063903-063912.
[93] P. Molnar, P. Sittner, V. Novak, P. Lukas, Mater. Sci. Eng A, (2007) doi:10.1016/j.msea.2007.01.189
[94] L. Straka, O. Heczko, IEEE Trans. Mag. 39 (2003) 3402.
[95] T. Kakeshita, T. Fukuda, T. Takeuchi, Mater. Sci. Eng A 438–440 (2006) 12–17.
[96] A. Sozinov, A.A. Likhachev, N. Lanska, O. Söderberg, K. Ullako, V.K. Lindroos, Mater. Sci. Eng A 378 (2004) 399-402.
[97] N. Glavatska, I. Glavatskiy, G. Mogylny, S. Danilkin, D. Hohlwein, O. Soderberg, V. Lindroos, A. Beskrovnij, J. Phys. IV 112 (2003) 963.
[98] Sittner P, Takakura M, Tokuda M, Scripta Metallurgica 32 (1995) 2073-2079.